Impact Wear Mechanisms of DLC Coating

Mohd Fadzli Bin ABDOLLAH

Impact Wear Mechanisms of DLC Coating

Mohd Fadzli Bin ABDOLLAH

Advisor:
Professor Noritsugu UMEHARA

A dissertation submitted to the Department of Mechanical Science and Engineering, Graduate School of Engineering, Nagoya University

In partial fulfillment of the requirements for the degree of Doctor of Engineering

2011

Acknowledgements

Foremost, I would like to express my sincere gratitude to my advisor Prof. Noritsugu UMEHARA for the continuous support of my Doctoral study and research, for his patience, motivation, enthusiasm, and immense knowledge. His guidance helped me in all the time of research and writing of this dissertation. I could not have imagined having a better advisor and mentor for my study.

Besides my advisor, I would like to thank the rest of my dissertation committee: Prof. Nobutada OHNO, Prof. Kenji FUKUZAWA and Assoc. Prof. Hiroyuki KOUSAKA for their encouragement and insightful comments.

My sincere thanks to those who made this dissertation possible: Dr. Takayuki TOKOROYAMA and Mr. Shinko SENDA from Nagoya University. I also wish to thank Mr. Naruhiko INAYOSHI, Mr. Nobuyuki MIYAMOTO and Mr. Tsuyoshi AKAO from DENSO Corporation.

It is honor for me to thank the scholarship from Universiti Teknikal Malaysia Melaka (UTeM) for the financial support, including the cost of living and tuition fees during my Doctoral study in Nagoya University.

Special thanks extended to my research partner, Mr. Yuto YAMAGUCHI for the stimulating discussions. I have further to thank my colleagues from the Advanced Materials and Manufacturing Laboratory for their support, encouragement, help, and for all the fun we have had in the last three years. To my study leave officer, Mrs. Siti Salwah Binti Ahmad from UTeM, many thanks for her great help in difficult times.

I would like to give my special thanks to my parents, Abdollah Bin Baba and Rosnah Binti Hasim, no words can describe my gratitude towards you. Both of you have been the pillar of strength in my life. In you, I learned about empathy, conscience, filiality and forgiveness. Thank you for your unlimited love, care and support even at all times. To my siblings, it's fortunate to be with you. My dearest sisters, Hendon Binti Abdollah, Siti Zaleha Binti Abdollah, Siti Aisah Binti Abdollah, Saripah Binti Abdollah, Siti Zubaidah Binti Abdollah, Siti Rosilah Binti Abdollah

and Siti Khairiah Binti Abdollah, for their love and encouragement. My dear brother, Mohd Isa Bin Abdollah, for their kindness and source of motivation.

Last but not least, to my buddies, those who are still working on their Doctoral study in Japan, Faiz Redza Bin Ramli, Nor Azmmi Bin Masripan, Mohd Khairi Bin Mohamed Nor, Ahmad Anas Bin Yusof and Mohd Rizal Bin Alkahari, my sincere thanks for your constant support for all the ups and downs, joy and sadness, laughter and tears. Many years have passed and our friendship is still blooming, and I hope our friendship will remain the same in the coming years. Many thanks to all Malaysia students in Nagoya and many others who are not listed here for their friendship and hospitability.

Abstract

Diamond-like carbon (DLC) films have been explored in the past due to their highly attractive properties, such as high hardness; low friction coefficient; chemical inertness and electrical insulation; optical transparency and smoothness; and biological compatibility. In previous studies, most of the impact wear mechanisms of DLC coatings are concerned with the fracture process in the coating due to the crack propagation under severe wear conditions. However, no reports discuss about how the impact wear mechanisms of the DLC coatings act under mild wear conditions. Under impact, it is well known that plastic deformation should occur prior to the impact wear. So, the first objective of this study is to identify the most significant impact parameter that controls the deformation of DLC coating. After cyclic impacts, though under mild wear conditions, it believes that impact wear should be occurring by the phase transformation of DLC coating. Therefore, the second objective is to clarify the impact wear mechanisms of DLC coating based on its phase transformation. Finally, in order to distinguish more clearly between the plastic deformation and impact wear of DLC coating as well as to predict its transition points, a deformation-wear transition map has been proposed.

In this present study, DLC films were deposited on the tungsten high speed steel (SKH2) substrate using physical vapor deposition (PVD) method. The impact test was performed by using a horizontal impact tester for more than 10^2 impact cycles with a frequency of 10 Hz, and a drop-weight impact tester for low impact cycles. The DLC coated SKH2 disc was repeatedly impacted by a chromium molybdenum steel (SCM420) pin. The 90^o inclination of impact tests were performed at room temperature under lubricated conditions. Prior to the impact test, both disc and pin were cleaned using acetone in an ultrasonic bath. The maximum normal impact load was obtained from the graph of normal impact load vs. time, generated by a load cell. Besides, the contact impulse was determined from the area below this graph. As for the absorbed energy, this can be determined using a high speed camera.

From the experimental analysis, there is no unique relationship between the residual impact crater volume/depth of DLC coating and contact impulse. The highest coefficient of determination R^2 for both the V_r and h_r (R^2_{hr} = 0.9362 and R^2_{Vr} = 0.9076) obtained from the response of maximum normal impact load. Besides, there is an experimental error in the case of absorbed energy due to the microslip effect. Furthermore, the impact phenomenon in this study can be considered as the quasi-static indentation, where load is a governing parameter, because the impact velocity is very low. By comparing with the analytical solutions, it is easier to predict the residual impact crater volume/depth by static indentation analysis. Therefore, from these reasons, it can be concluded that the residual impact crater volume/depth is more affected by maximum normal impact load than absorbed energy.

From Raman spectroscopy analysis, it has been suggested that there is pressure-induced graphitization since the impact testing was performed at the room temperature. The phase transformation of wear debris and transfer layer from sp^3 to sp^2 induced graphitization process. However, the sp^3 fractions of DLC coating on the crater surface are significantly increased with impact cycles as it is evidently shown by decreasing I_D/I_G ratio approximately from 0.63 (as-deposited) to 0.47 (after 10^5 impact cycles), accompanied by a widening of full-width at half maximum of G peak $FWHM_G$ (approximately from 179 cm^{-1} to 192 cm^{-1}) with impact cycles. Besides the hardness reaches approximately to 21 GPa that is higher than as-deposited (17.14 GPa) after several impact cycles. This suggests the size of the larger sp^2 clusters is reduced due to the mechanical crush of the larger sp^2 clusters. Since the impact test was performed under atmospheric conditions, oxidation of iron with the environment also occurs in the wear debris and transfer layer, where two predominant peaks of magnetite (Fe_3O_4) and hematitie (α-Fe_2O_3) are observed from its Raman spectrum.

For a given material and controlled variables (pin radius, coating thickness, substrate material, environmental conditions and so on), the proposed deformation-wear transition map of DLC coating apparently shows that the maximum normal impact load and impact cycles influence this transition. This empirical-based transition map, which presents deformation and wear data in a graphical manner, is able to provide a more global picture of how DLC coating behaves under cyclic impacts systematically. Three main transition zones that graphically distinguish

between the plastic deformation and impact wear of DLC coating were identified: (i) Plastic deformation of the substrate, (ii) suppression of plastic deformation of the substrate and (iii) wear of the DLC coating. Beyond the elastic limit, the DLC coating only follows the plastic deformation of the substrate until several impact cycles. Then, a suppression of plastic deformation of the substrate is taking place due to the decreasing contact pressure with impact cycles to the yield point. The hardness of the DLC coating on the crater surface is also increases after numerous impacts and no wear has been observed within these two zones. Wear of the DLC coating becomes dominant when the critical limit of maximum normal impact load and impact cycles is exceeded. Experimental observations show that this wear is associated with some degradation of the DLC coating. This includes the phase transformation of the wear debris/transfer layer and propagation of radial cracks in the DLC film as well as the formation of transfer layer on the counterpart material, which may attribute to the adhesive wear.

論　文　内　容　の　要　旨

ダイヤモンドライクカーボン膜(DLC膜)は、高硬質で表面あらさが小さく、耐摩耗性が期待でき、かつ密着性にも優れるためエンジンバルブやカムへの適用が試みられている。しかし、固体が繰り返し接触する衝撃摩耗は金属において研究は進んでいるが、DLC膜においては摩耗の基本特性及び摩耗メカニズムは不明である。特に、DLC膜の繰り返し衝撃接触における膜の破壊や剥離のメカニズムについては検討されているが、実用上重要な、DLC膜の脆性破壊を伴わない衝突条件下での摩耗については、摩耗の基本特性及びメカニズム共に不明である。

本研究では、物理蒸着法で高速度工具鋼（SKH2）ディスクに成膜した水素含有DLC膜と、クロムモリブデン鋼（SCM420）ピンの衝突角90°において、試作した装置により室温での油中衝撃摩耗実験を行い、DLCを成膜した高速度工具鋼ディスクの変形及び摩耗特性を明らかにし、詳細な表面観察及び分析から摩耗メカニズムを明らかにした。具体的には、DLCを成膜した高速度工具鋼の塑性変形を含む摩耗に及ぼす最大衝突荷重、衝突エネルギー及び力積の影響を明らかにした。また、DLC膜の繰り返し衝突下におけるDLC膜の衝突摩耗痕及び相手ピンへの移着物の構造分析を行い、DLC膜の構造変化に伴う摩耗メカニズムを提案した。さらに、DLC膜の塑性変形と摩耗を分離評価する方法を提案し、DLC膜の塑性変形と摩耗メカニズムが、最大衝突荷重と衝突繰り返し数により遷移することを、DLC膜の変形-摩耗形態遷移図で表せることを明らかにした。

第１章「緒論」

耐衝撃摩耗のために期待されるDLC膜の応用例として、エンジンバルブ及びカムの使用条件を解説した。DLC膜の材料特性、すべり摩擦における摩擦摩耗特性の従来の研究を紹介した。金属及びDLC膜の衝撃摩耗の従来の研究を紹介し、DLC膜の衝撃摩耗に関して、脆性破壊が発生する大

きな衝突荷重下でのDLC膜の破壊に関する従来研究はあるが、低荷重下での衝撃摩耗におけるDLC膜の摩耗特性及びその摩耗メカニズムの研究成果がほとんど無いことを述べた。これらの調査内容に基づき本研究で、DLC膜の塑性変形を含む摩耗特性に及ぼす最大衝突荷重などの力学的因子の影響の解明、繰り返し衝突に伴うDLC膜及び相手面の移着膜の構造変化の詳細な観察による摩耗メカニズムの検討、並びに塑性変形と摩耗を分離分析し、DLC膜の変形-摩耗形態遷移図の提案を行う背景を述べた。

第2章「繰り返し衝突における最大衝突荷重、衝突吸収エネルギー及び力積のDLC膜の変形を含む摩耗に及ぼす影響」

物理蒸着法で高速度工具鋼（SKH2）ディスクに成膜した水素含有DLC膜と、クロムモリブデン鋼（SCM420）ピンの衝突角90°における室温での油中衝撃摩耗実験を行い、繰り返し衝突後に残留したDLC膜の摩耗痕の深さ及び体積に及ぼす最大衝突荷重、衝突吸収エネルギー及び力積の影響を明らかにした。最大衝突荷重、衝突吸収エネルギー及び力積は、DLC膜ディスク試験片下のロードセルによる荷重の時間応答及びピンの高速度カメラによる衝突・反発速度の観察結果から算出した。DLC膜の厚さは3.0 ・mであり、潤滑油として灯油を滴下した。最大衝突荷重は200～550Nであり、衝突時間は0.2 ms程度である。

その結果、10^2回の衝突においてDLC成膜した高速度工具鋼の摩耗痕の深さ及び体積は、最大衝撃荷重と衝突吸収エネルギーに強く依存するが、力積には依存しないことが明らかになった。また、DLCを成膜した場合と成膜しない場合の摩耗痕深さを比較したところ、ほぼ同じであり、これより本実験においては高速度工具鋼ディスクの塑性変形がそのままDLC膜表面の摩耗深さとなっていることが明らかになった。更に、実験結果を解析結果と比較した結果、DLC膜の摩耗痕の深さと体積は最大衝撃荷重を最大荷重とする押し込みによる値とほぼ同じであり推定可能である事、一方衝撃吸収エネルギーからの推定は困難であることが明らかとなった。

第3章「繰り返し衝突におけるDLC膜の構造変化」

DLC膜は、sp^2及びsp^3構造が混在しているが、すべり摩擦においてsp^2及びsp^3構造の割合が変化し、sp^2構造が豊富なDLCが相手面に移着し摩擦摩耗特性に影響を及ぼす報告がある。本研究の繰り返し衝突下においてもDLC膜の構造変化が重要と考えられる。そこで、DLC膜の前章と同じ実験において、摩耗痕及び相手面への移着物のラマン分光分析を行い繰り返し衝撃試験におけるDLC膜の構造変化を明らかにした。

その結果、10^2回から10^5回の衝突繰り返し数の増加と伴にDLC膜からの摩耗粒子と相手面の移着物はsp^2構造が豊富な構造に変化し、一方、DLC膜の摩耗痕ではsp^3構造が豊富な構造に変化したことが明らかとなった。さらに、DLC膜の摩耗痕硬さは、17GPaから21ＧPaに増加したことも明らかになった。また、クロムモリブデン鋼の移着物はDLCだけでなく酸化鉄が観察された。本結果より、DLC膜の衝撃摩耗メカニズムに、DLC膜の構造変化が重要であることが明らかになった。

第4章「繰り返し衝突におけるDLC膜の変形-摩耗形態遷移図」

第２章においてDLC膜の繰り返し衝突において高速度工具鋼基板の塑性変形が生じていることが明らかになった。そこで、前章までと同じ実験において、DLC膜の摩耗と基板の変形をDLC膜の断面を詳細に観察する事で、分離評価し、繰り返し衝突におけるDLC膜の変形と摩耗形態を最大衝突荷重と衝突繰り返し数を変化させDLC膜の変形-摩耗形態遷移図を作成し検討した。具体的には、DLC膜の繰り返し衝突後の摩耗痕の断面観察から、DLC膜の厚さの減少量を測定し、それを摩耗深さとした。また、DLC膜の繰り返し衝突後の表面の摩耗痕深さから、DLC膜の摩耗深さを減じた差を基板の塑性変形深さとした。

その結果、衝突繰り返し数が10^2回程度までは基板の塑性変形深さが摩耗痕深さの大部分であるが、その後、基板の塑性変形は停止し、DLC膜の摩耗が始まることが明らかとなった。すなわち、DLC膜の主となる変形と摩耗の遷移は衝突繰り返し数の増加に伴い、１）基板の塑性変形、

２）基板の塑性変形停止及び３）DLC膜の摩耗へと遷移した。また、この変形と摩耗形態の遷移は、最大衝突荷重の増加に伴い、少ない衝突繰り返し数で生じる事が明らかとなった。これらの結果と第３章のDLC膜の構造変化の結果を総合する事で、DLC膜の衝撃摩耗メカニズムは、繰り返し衝突によるsp^2が豊富な相への構造変化と、機械的特性の劣化した構造変化層のクロムモリブデン鋼ピンへの凝着である事が提案された。

第5章「結論」

以上の各章で得られた知見をまとめている。

以上、本論文では、物理蒸着法で高速度工具鋼（SKH2）に成膜した水素含有DLC膜と、クロムモリブデン鋼（SCM420）ピンの衝突角90°における室温油中衝撃摩耗実験を行い、DLC膜の変形及び摩耗特性を明らかにし、摩耗メカニズムを明らかにした。具体的には、DLCを成膜した高速度工具鋼ディスクの繰り返し衝突後の塑性変形量と摩耗量を詳細な断面観察から分離分析する方法を提案し、最大衝突荷重と衝突繰り返し数の増加に伴うDLC膜の塑性変形と摩耗を評価した。また、DLC膜の繰り返し衝突下におけるDLC膜の衝突摩耗痕及び相手ピンの移着物の構造分析を行い、DLC膜の構造変化を伴う摩耗メカニズムを提案した。

Abbreviation

α-Fe_2O_3	Hematite
a-C	Hydrogen free diamond-like carbon
a-C:H	Hydrogenated diamond-like carbon
AFM	Atomic force microscopy
Cr-DLC	Chromium diamond-like carbon
CVD	Chemical vapor deposition
DLC	Diamond-like carbon
EDS	Energy dispersive x-ray spectroscopy
Fe	Iron
Fe_3O_4	Magnetite
FE-SEM	Field emission scanning electron microscopy
FIB	Focused ion beam
$FWHM_G$	Full-width at half maximum of G peak
GFRP	Glass fiber reinforced polymer
H	Hydrogen
I_D/I_G	Raman intensity ratio = Intensity ratio of D peak to G peak
ISE	Indentation size effect
MSIB	Mass selected ion beam
PACVD	Plasma assisted chemical vapor deposition
PLD	Pulsed laser deposition
PVD	Physical vapor deposition
RH	Relative humidity
SCM420	Chromium molybdenum steel
SKH2	Tungsten high speed steel
ta-C	Tetrahedral amorphous carbon
ta-C:H	Hydrogenated tetrahedral amorphous carbon
W-DLC	Tungsten diamond-like carbon

Table of contents

List of Figures

Figure no.

List of Tables

Table no.

Chapter 1

Introduction

1.1 Industrial needs of DLC coatings

1.1.1 Plunger of diesel fuel injection

For modern environmentally friendly cars we need engines with low emissions and with reduced fuel consumption. On the other hand, we would like to have a fun driving experience and we want to buy a car at the lowest price possible. Gasoline and diesel fuel injection systems provide the basis for the car manufacturer to fulfill these targets. The gasoline direct injection system sprays the exact needed quantity of fuel directly into the cylinder of the engine. It allows a higher compression and a more efficient combustion process and can be flexibly adjusted for economical as well as sportive driving. Furthermore, direct gasoline injection reduces pollutant emissions to levels that will meet the even tougher US laws of the future. Diesel engines have a higher degree of efficiency in their use of the fuel energy. In Europe, more than 40% of all new cars are equipped with a diesel engine, including high class cars. High-pressure injection systems with pressures up to 200 MPa give the best results for combustion [1].

In direct injection diesel engine applications, a fuel injector is a precision device that must meter the quantity of fuel required for each cycle of engine and must develop the high pressure necessary to inject the fuel into the combustion chamber at the correct instant of the engine operating cycle. Many fuel systems presently used in direct injection diesel engines utilize a hydraulically actuated and/or electronically controlled fuel injector to pressurize the fuel charge to obtain the desired fuel spray pattern and fuel volume into the combustion chamber at the precise moment. These hydraulically actuated and/or electronically controlled fuel injectors often use very compact and high precision moveable components to achieve the prescribed delivery of fuel at the desired time and for the desired duration.

As a result of the compact nature of many fuel injector components together with the harsher environment, the stresses and forces present within an operating fuel injector are often concentrated on such smaller components. Reduction of contact

area of the smaller components, which spread out the higher contact forces and stresses, increases adhesive and abrasive wear at the contact surfaces, such as the nozzle tip and check interface. In addition, fuel injectors and fuel injector components require superior harness characteristic and lubricity characteristics to combat the higher contact stress. The maximum contact pressure approximately 1.5 GPa is located at the tip point as shown in Fig. 1.1. Ignition occurs in a diesel engine by injecting fuel into the air charge, which has been heated by compression to a temperature greater than the ignition point of the fuel or about 538°C.

Therefore, the disclosed thin film diamond-like carbon (DLC) coatings for fuel injector components such as fuel injector needles (was patented on April, 2004 [2]) are particularly useful in highly loaded, marginally lubricated fuel injection system applications where component wear (both sliding and impact type) are typically encountered. The thin film minimized abrasive and adhesive wear.

However, the complex interaction between many coating types, contact combination, operating temperature, contact geometry and load and etc. indicate that the DLC coating require extensive future research to provide optimum combination for different applications especially under mild wear conditions.

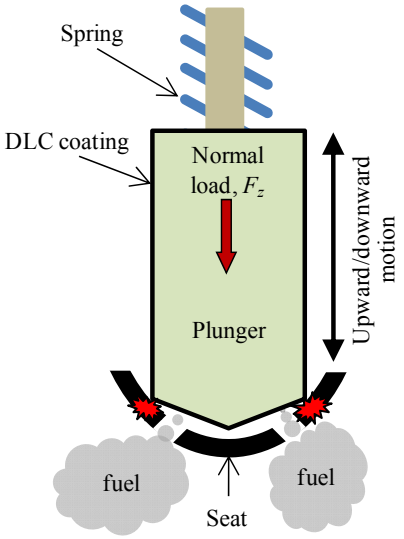

Fig. 1.1 Schematic illustration of the DLC coated plunger inside the barrel of diesel fuel injection and its impact process when the fuel is injected directly into the cylinder.

1.1.2 Bucket of engine valve train

The valve train is the engine component that controls the timing of the inlet and exhaust valves. Many systems have been employed for controlling valve timing and designs have commonly used the application of cams with a combination of pushrods, rocker-arms and/or lifters in a variety of configurations.

The valve opening and closing sequence for all chambers is controlled from the valve train by the relative rotational position of the individual cams. In bucket-type valve trains (bucket is also known as tappet), valves are actuated directly. No transmission mechanism is required between valve and camshaft. The cam stroke is transmitted directly to the valve via the bottom of the bucket. As the camshaft rotates, the eccentricity of an individual cam's shape brings it into contact with the bucket surface, where the two surfaces are in both sliding and rolling contact. The cam's continued rotation causes depression of the bucket, compression of the valve spring, and depression of the valve stem, opening the valve. As the camshaft rotation continues, the contact passes the most eccentric point of the cam after which momentum and the force of the valve-spring return the valve train components to their initial state. During a typical camshaft cycle there are a number of forces applied to the cam–bucket contact that influence the tribology of the system, which gave a maximum contact pressure of approximately 445 MPa at the temperature of 105^{o}C [3]. The forces at the point of contact vary in magnitude depending on the point in the cycle, the lubrication regime and the steady-state camshaft rotational speed. It is the impact loading that is of interest in this study. It is common for the travel of the valve-stem to be limited by the complete closing of the valve in order to avoid unnecessary friction losses. The force of keeping the spring compressed is borne by the valve-stem and valve-seat. The limited valve-stem movement also causes separation of the cam and tappet surfaces for approximately 55% of the cycle. At the point where the cam rotation brings the cam and bucket back into contact, the load from the compressed spring is transferred from valve-stem and valve-seat to the cam–bucket contact, as shown in Fig. 1.2 (b).

In order to protect the top surface of bucket from continuous wear due to the cyclic contacts with the camshaft, DLC coatings can potentially be used to provide a low friction and low wear surface to the upper face of the bucket. According to

Kano [4], the tetrahedral amorphous carbon (ta-C) coated cam follower of the bucket type has been applied to gasoline engines from autumn 2006 for the first time in the world.

Even though an alternative solution by using the DLC coatings has practically applied in the industry, nobody knows how the impact wear mechanisms of the DLC coating acts in low-load regime. This requires an extensive future research.

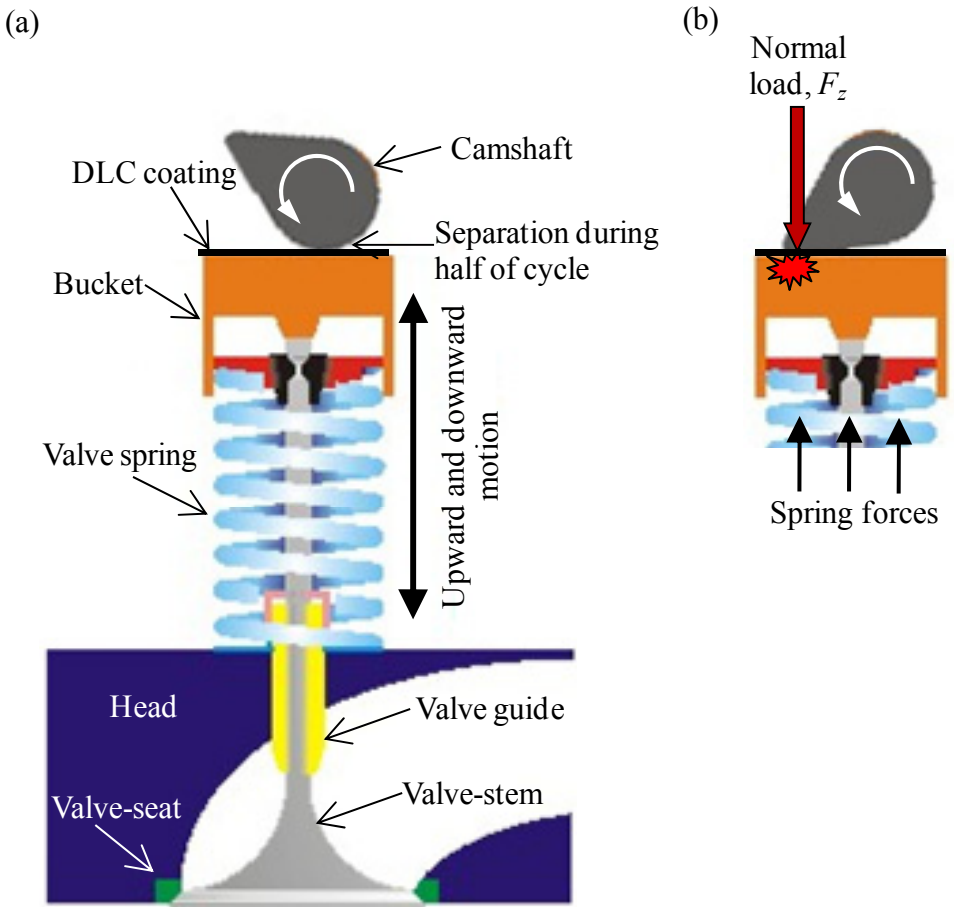

Fig. 1.2 Schematic illustration of the future DLC coated bucket-type valve train and its impact process during cam rotational cycle. (a) Completed closing of valve during the combustion stroke and (b) Valve opened during the intake and exhaust stroke. Half of the illustration is from [5].

1.2 DLC coatings

Carbon is one of the commonest elements throughout the universe. In the nature carbon is found as diamond, graphite and amorphous carbon. The name of DLC was first coined by Aisenberg in 1971 to describe the hard carbon films that he prepared by direct deposition from low energy carbon ion beams [6]. Now, DLC is the name commonly accepted for hard carbon coatings which have similar mechanical, optical, electrical and chemical properties to natural diamond, but which do not have a dominant crystalline lattice structure.

DLC films have received much attention over recent years and been under intensive research since the middle of 1980s [7]. Besides, DLC owing to the broad range of applications where they can offer tribological benefits. DLC is a generic term that is used to describe a range of different amorphous carbon films whose properties range considerably depending on deposition conditions and method. DLC films are thin, usually in the region of 1–4μm in thickness and have wide ranging properties. The main factor that controls their properties is the proportion of sp^2 (graphitically-bonded) to sp^3 (diamond-bonded) carbon atoms but additional factors such as the presence of silicon, hydrogen, nitrogen and metal dopants, the use of interlayers to promote adhesion and tailor residual stress levels, the surface roughness and interaction with lubricants are also key to their ultimate performance. DLC is not simply a single solution to a tribological problem as the range of mechanical properties and the potential for different tribochemical reactions with these films is vast. DLC films include hydrogenated DLC (a-C:H), hydrogenated tetrahedral amorphous carbon (ta-C:H); hydrogen free DLC (a-C); tetrahedral amorphous carbon (ta-C); and those containing dopants of either silicon or metal such as Si-DLC and Me-DLC, respectively. These materials depict the following valuable properties: Resistance to wear as the cause of a very high hardness; low friction coefficient; chemical inertness and electrical insulation; optical transparency and smoothness; and biological compatibility.

1.2.1 Structure and deposition of DLC coatings

Carbon has three different types of bonding configurations, namely sp^3, sp^2 and sp^1. The bonding configuration of carbon atom in diamond, DLC and graphite are illustrated in Fig. 1.3 [8]. In diamond, carbon has four sp^3 hybridized orbitals. These sp^3 orbitals contribute to the formation of four equal carbon-carbon bonds with adjacent atoms, which produces the tetrahedral structure of diamond. This covalently bonded tetrahedral structure is the origin of the superior properties of diamond, like high hardness and high thermal conductivity. Graphite has three trigonally directed sp^2 hybrid orbitals, which lie in plane. Each carbon atom in plane is bonded to three other carbon atoms with strong covalent bonds. The layers of carbon atoms are attracted to each other by weak Van der Walls forces producing the layered structure of graphite. The layers can cleave easily, which accounts for the typical low friction property of graphite [9-10]. The DLC films have a mixed sp^3/sp^2 structure with different proportions of sp^3 and sp^2 bonds depending on the deposition techniques and deposition parameters used. The structure is claimed to consist of sp^2 bonded clusters embedded in an amorphous sp^3 bonded carbon matrix [11-12]. So the term "diamond-like" emphasizes a set of properties akin to diamond and, at the same time implies the absence of crystalline diamond order [13].

Basically, a-C:H is an amorphous network composed of carbon and hydrogen. The properties of these coatings depend strongly on the hydrogen content and the sp^3/sp^2 content, which in turn, depend on the deposition process and its parameters [14]. The hydrogen is important for obtaining a wide optical gap and high electrical resistivity and stabilizing the diamond structure by maintaining the sp^3 hybridization configuration [15]. For a-C films, hydrogen is generally treated as an impurity. The hydrogen-free amorphous carbon, which is highly sp^3 bonded, is known as ta-C. The compositions of DLC can be displayed on a ternary phase diagram of sp^3 ratio, sp^2 ratio and hydrogen content of the film, as shown in Fig. 1.4 [16].

DLC coatings are formed when ionized and decomposed hydrocarbon or carbon species hit the surface with energies ranging from several tens of eV to 200 eV [17]. All methods for the deposition of DLC films are non-equilibrium processes characterized by the interaction of energetic ions with the surface of the

growing films. The methods can be divided into chemical vapor deposition (CVD) and physical vapor deposition (PVD) techniques. The CVD techniques, such as d.c. plasma and radio frequency (r.f.) plasma assisted CVD; and PVD techniques, like sputter deposition, ion-plating techniques and ion beam techniques can be used for depositing the a-C:H coatings. The PVD techniques, such as magnetron sputtering, mass selected ion beam (MSIB), cathodic arc and laser plasma deposition can be used for a-C and ta-C coatings [16],[18-19]. DLC coatings can be deposited at temperatures that are below 200°C [20] to 325°C [15]. This property makes it possible to deposit DLC coatings on most relevant engineering materials, including polymers.

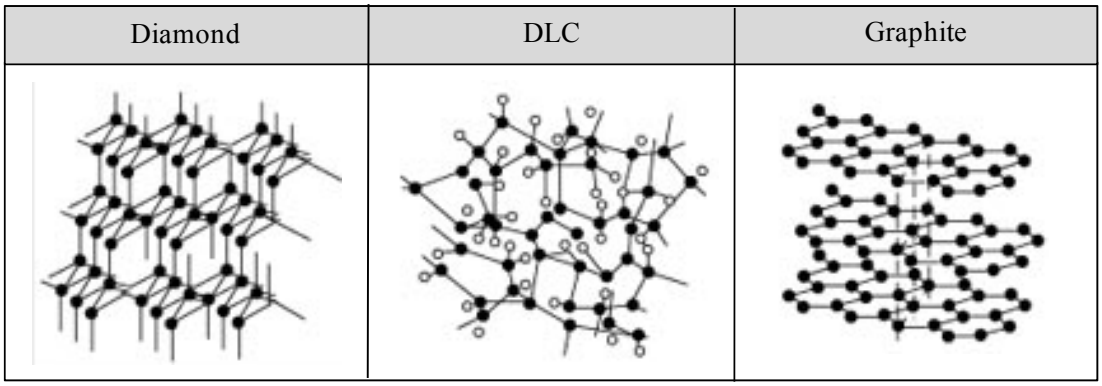

Fig. 1.3 The bonding configuration and typical Raman spectrum of diamond, DLC and graphite [8].

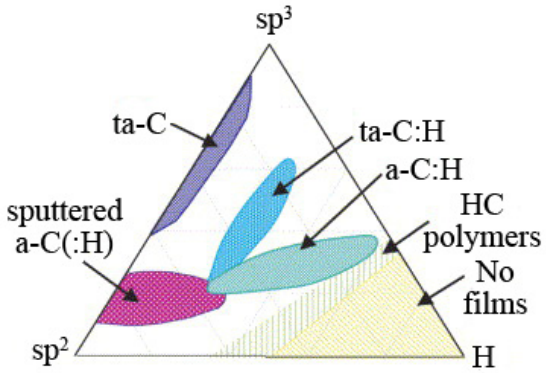

Fig. 1.4 Ternary phase diagram of sp^2, sp^3, and hydrogen contents of various forms of DLC [16].

1.2.2 Tribological properties of DLC coatings for sliding contact

The tribological behaviour of DLC is strongly influenced by the film deposition conditions, the tribological conditions and especially the atmosphere during operation. The fundamental characteristics of the a-C:H coatings and ta-C coatings are represented in Table 1.1 [21].

The pulsed laser deposition (PLD) a-C films have a coefficient of friction less than 0.1 in vacuum and 0.03 in dry nitrogen [22]. Voevodin et al. [23], Huang et al. [24] and Eskusson et al. [25] studied a-C coatings prepared by a PLD technique. Voevodin et al. [23] showed the formation of graphite-like transfer layer during sliding friction. The sp^3 to sp^2 phase transformation was observed after several thousands of sliding cycles. Besides, Erdemir et al. [26] also discovered the same phenomenon on pin wear surface after a long sliding distance against a-C:H coating produced by Ion Beam Deposition. The surface graphitization was found to be responsible for low friction in humid air, and for high friction in vacuum. In addition, Huang et al. [24] showed that the G-peak width and the intensity ratio (I_D/I_G) of DLC film were found to be sensitive to the structural changes induced by the change of the deposition temperature. The total sp^3 fraction in the DLC film remains almost constant at a temperature less than 200^oC and shows a sharp decrease at a temperature greater than 200^oC. Eskusson et al. [25] suggested that laser irradiation intensity has noticeable influence on the structure and hybridization of carbon atoms deposited. At higher irradiation intensities, the graphitization of the amorphous films was observed. The a-C films deposited by cathodic vacuum arc, were found to give coefficient of friction values in the range of 0.04 to 0.18 in ambient atmospheres [20].

The properties of DLC films can be changed or tailored by different techniques. Alloying the DLC structures can be used to inhibit the triboactivity of the a-C:H coatings. Different alloying techniques may also be used to reduce the internal stresses of the DLC coatings. Alloying a-C:H films with different metals generally reduces the compressive stresses to values below 1 GPa. The tribological of metal-alloyed a-C:H films has been explained by a combination of ceramic-like properties (high hardness) and polymer-like properties (high elasticity, low surface energy) [27].

The a-C:H and ta-C coatings showed some variation in tribological performance in the different tests carried out. In dry sliding conditions, the wear of the ta-C coating was lower compared to the a-C:H coating, which was due to the high hardness and high stability of the ta-C film. On the other hand, wear of the counterpart materials against ta-C coating was about one order of magnitude higher compared to that of the a-C:H coating. However, the coefficient of friction of ta-C coating in dry air reached high values compared to a-C:H carbon coating [28-31]. The a-C:H coating suffered from catastrophic wear in water soon after the beginning of the test and the coating could not survive under water lubrication [31-32]. Conversely, the ta-C performed well with water lubrication, since no measurable wear could be detected. The pin wear rates increased against both a-C:H and ta-C coatings. However, the coefficient of friction is significantly lower, particularly for the ta-C coating. Furthermore, the wear and the coefficient of friction of both a-C:H and ta-C coatings decreased when oil lubrication was applied, even though the additives used in the oils [31-32]. This shows that a-C:H and ta-C coatings have excellent performance in oil-lubricated conditions. Considering the utilization of DLC films in practical components, it is suggested that the a-C:H and particularly the ta-C coating can be used not only in dry conditions, but also in boundary lubricated conditions for providing safe operation in demanding operating conditions. However, the oil lubrication prevented the formation of the tribolayer on the pin wear surface in the same manner as the water lubrication, which increased the pin wear to some extent. Fig. 1.5 and Fig. 1.6 summarize the tribological properties of DLC coating in dry, water- and oil-lubricated conditions [31].

Table 1.1 The fundamental characteristics of a-C:H and ta-C films [21].

Coating	**Deposition parameters**			**Coating properties**			
	U_B V	*p* pa	Temp. °C	H-content %	sp^3 bonding %	Hardness GPa	Young`s Modulus GPa
a-C:H	-550	5.5	100	26-33	70	14±1	129±5
ta-C	-	3×10^{-4}	60	<1	60[a]	15±18	445±57

[a]Koshiken et al. [33]

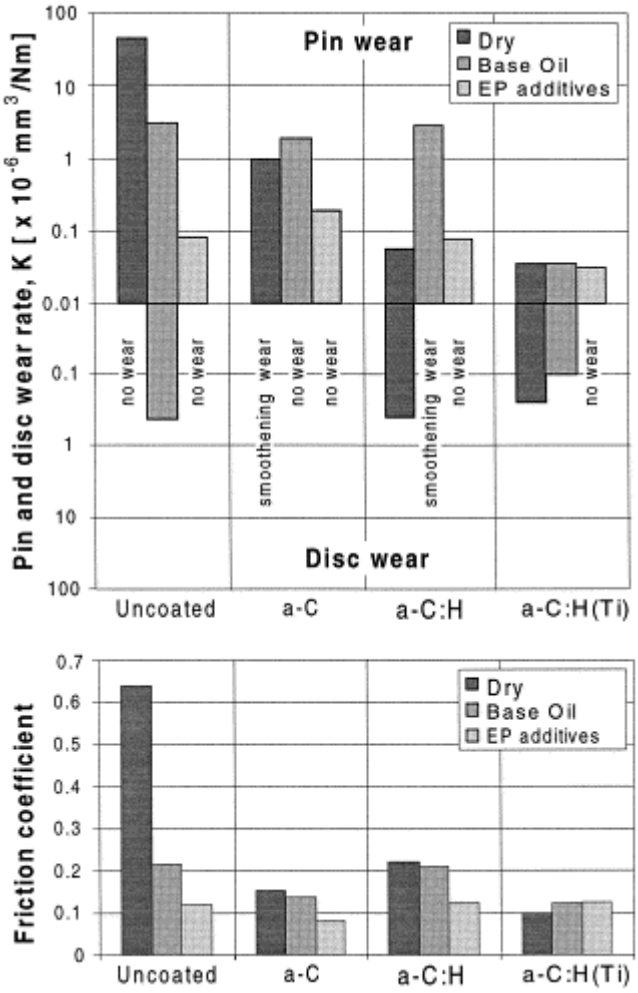

Fig. 1.5 The friction coefficient values, the wear rates of the steel pins and the wear rates of the uncoated, a-C, a-C:H and a-C:H(Ti)-coated substrates in dry (50% RH) and oil-lubricated tests with mineral base oil and mineral oil with EP additives. The normal force was 10 N and the sliding velocity 0.004 ms^{-1} [31].

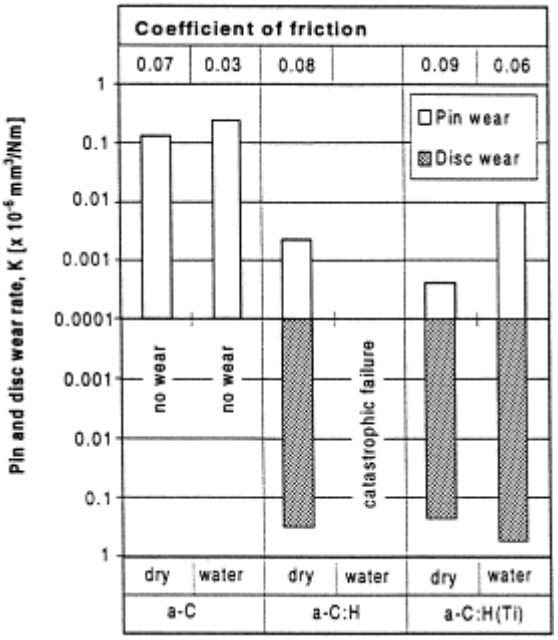

Fig. 1.6 The friction coefficient values, the wear rates of the alumina pins and the wear rates of a-C, a-C:H and a-C:H(Ti)-coated substrates in dry (50% RH) and water-lubricated test. The normal force was 5 N and the sliding velocity 0.004 ms^{-1} [31].

1.3 Impact wear

Impact wear can be defined as wear of a solid surface due to repetitive exposure to dynamic contact by another solid body [34]. Some researchers investigated impact wear of metals and DLC coatings as described in the following section.

1.3.1 Impact wear of metals

For metal impact pairs, the behavior of impact wear involves elastic and plastic deformation when impact loading or impact energy is high and/or fatigue accompanied by wear debris release due to crack formation [35-36]. If oxygen is present and the wearing material can be oxidized then a corrosive or oxidative wear mechanism can also take place. The mechanisms of impact wear are illustrated schematically in Fig. 1.7 [35].

In general, impact wear of metals is dependent on the formation of deformed layers, particularly when wear by fatigue or crack formation is predominant [37]. In such cases, subsurface cracks extend parallel to the surface in a manner very similar to `delamination` wear. The material through which the cracks propagate is very often plastically deformed and work-hardened as a result of contact stresses during impact [37]. Spallation and wear by crack formation can also occur in relatively brittle materials [38]. Therefore, the presence of surface plastic deformation, in some cases, is not essential to this form of wear.

The type of material sustaining impact wear has a strong effect on the wear mechanism. Metals are prone to an oxidative form of impact wear while ceramics wear by cracking and spalling. Polymers tend to wear by plastic deformation, fatigue cracking or by chemical attack from hot compressed layers of oxygen and pollutants at the moment of impact.

Sufficient hardness of the impacted component is necessary to prevent rapid wear or extrusion of material from the contact by plastic deformation. In most situations this condition can be fulfilled by assuring an adequate hardness and then wear is controlled by other material characteristics. For example, wear by spalling or crack formation is controlled by brittleness and microstructure. The use of materials with low concentrations of inclusions and material flaws would suppress impact wear

by crack formation. Brittleness favors rapid crack growth and the formation of very large spalls or even macroscopic fracture of the component [38] while crack initiation is facilitated by inclusions [37].

Lubricants are useful in controlling impact wear in applications where they can be reasonably applied and providing that the lubricant does not cause chemical attack on the contacting surfaces. Hydrodynamic squeeze films can separate contacting surfaces for the duration of impact and the absence of sliding ensures that contact temperature rises are relatively small so that lubrication by adsorbed films is feasible. The basic limitation of lubricants, however, is their inability to significantly reduce the contact stresses during impact and wear is therefore only partially suppressed.

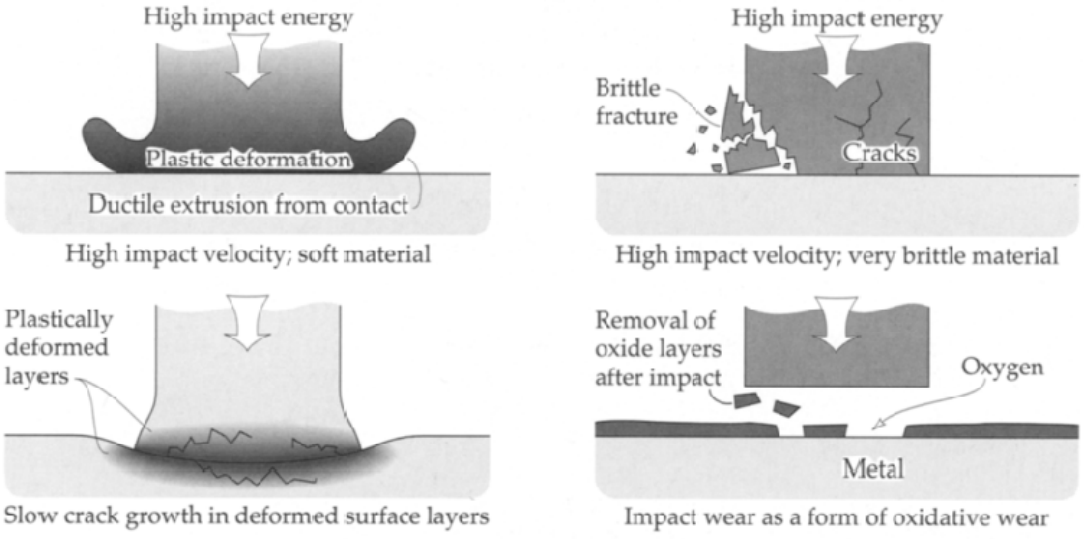

Fig. 1.7 Schematic illustrations of the mechanisms of impact wear [35].

1.3.2 Impact wear of DLC coatings

According to the previous studies [1],[39-40], impact wear mechanisms of the DLC coating are concerned with the fracture process in the coating due to the crack propagation under severe wear conditions. All the repetitive impacts used in these studies involve either only normal loading [1],[40] or under combined normal and tangential loading [39]. However, no reports discuss about the tribological properties of DLC coating under impact conditions.

Treutler [1] found two types of failure modes of DLC coating under repeated impacts. He also found that the endurance limit of DLC coating depending on the impact load and impact cycles. The first mode is the interface failure, in which the coating loses adhesion to the substrate due to shear and tensile stress. Cracks may start from defects at the interface and sometimes cause catastrophic failure with delamination of rather big flakes of the coating. Normally, the wear starts at the edges of the spherical calotte (where the maximum of the shear stress is located) (Fig. 1.8). However, even with the best coatings, the second failure mode can be found if the load is high enough. The second mode is wear and fatigue of the coating or, in other words, the cohesive failure mode. It normally consists of a continuous removal of the coating, starting from the middle of the spherical calotte. The fatigue occurs due to periodical stress loads and shows micro cracks within the coating.

Three different types of DLC coatings under a non-lubricated repetitive inclined impact test were studied by Zanoria and Seitzman [39]. One is tungsten diamond-like carbon (W-DLC) and the other two are chromium diamond-like carbon (Cr-DLC) made from different deposition recipes. The typical wear events that lead to failure of the coating, characterized by exposure of the substrate, are (i) formation of partial ring cracks at the trailing edge of the impact crater, (ii) thinning of the top coating due to sliding wear, (iii) formation of through-thickness shear cracks in the top layer, (iv) delamination of the top layer from the interlayer, (v) formation of through-thickness cracks in the interlayer, (vi) delamination of the interlayer from the substrate. In the high-load regime, as shown in Fig. 1.9, the poor fracture resistance of both the top layer and interlayer causes the very low impact wear life of the W-DLC coating relative to that of the Cr-DLCs. The superior wear life of the Cr-

DLC2 compared to that of the Cr-DLC1 coating is attributed primarily to the high resistance of the top coating to shear-induced fracture. In the low-load regime, as shown in Fig. 1.10, in which shear cracks were not observed, the poor wear life of the W-DLC coating relative to the Cr-DLCs is attributed mainly to the low fracture resistance of the interlayer. In contrast, the interlayer of the Cr-DLC coatings have adequate fracture strength to temporarily provide secondary protection to the substrate after the top coating has been delaminated.

Ledrappier et al. [40] focused on the spalling phenomena of DLC coatings, obtained by plasma assisted chemical vapor deposition (PACVD), under repeated impact conditions. Spalling may lead to a catastrophic failure. The spalls slowly grow and coalesce as a function of number of impacts and applied normal load. The mechanism responsible for this spallation phenomenon was due to the blister failure on DLC coatings. Some hypotheses for this unusual behavior are proposed in reference to the film mechanical properties and residual stresses level. The blister may be considered as the result of a classical buckling phenomenon. Once the first small buckle is obtained, the size of the formed buckle remains stable. No further growth is observed. Blisters may eventually interact with each other and coalesce later on. Due to the repeated impacts, buckles undergo cyclic loadings that may induce failure and spall formation. This slow blistering evolution is illustrated on Fig. 1.11. For thicker films, an interfacial delamination occurred rather than a film buckling but required high compressive stress level. The buckle formation and stability then directly depend on the film thickness and residual stress level in the coating.

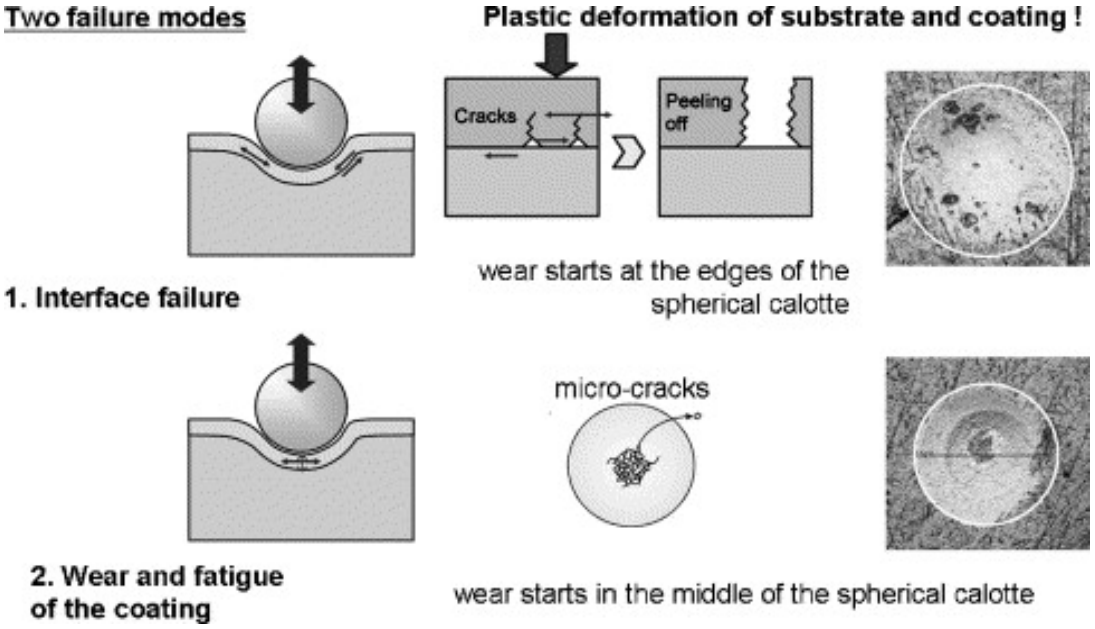

Fig. 1.8 Failure modes of DLC coatings under repeated impact test [1].

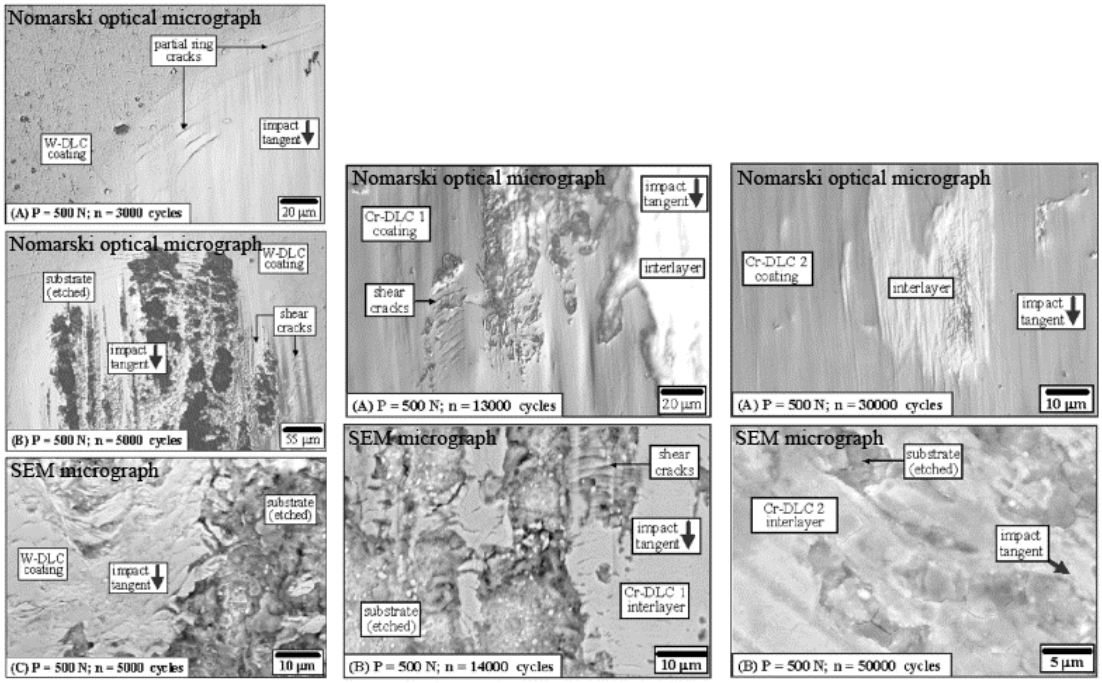

Fig. 1.9 Wear of (a) W-DLC (b) Cr-DLC1 and (c) Cr-DLC2 coating in the high-load regime [39].

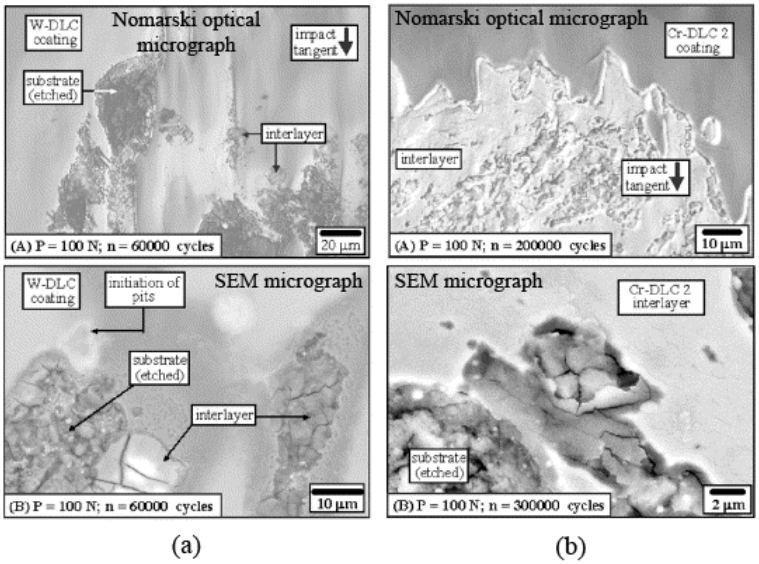

Fig. 1.10 Wear of (a) W-DLC and (b) Cr-DLC2 coating in the low-load regime [39].

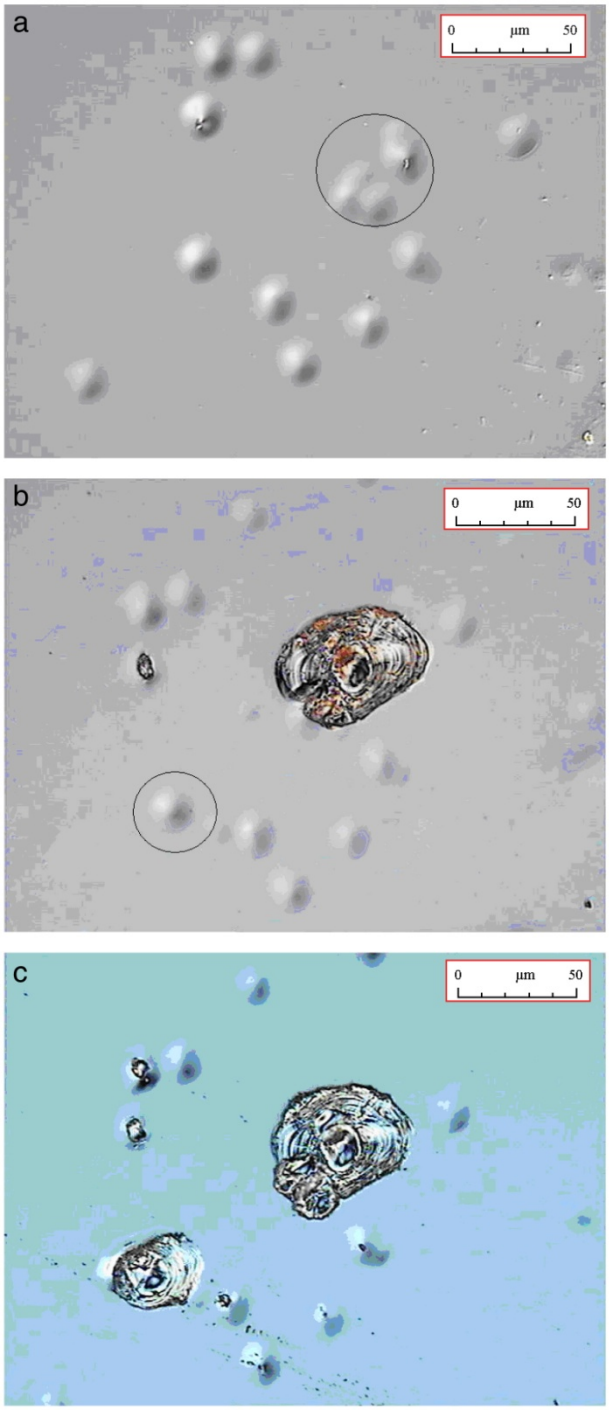

Fig. 1.11 Evolution of the formed blister as a function of the number of cycles for a DLC coating at 120 N impact load. a) After 2 x 10^6 impact cycles b) after 3 x 10^6 impact cycles and c) after 7 x 10^6 impact cycles [40].

1.4 Purposes of this study

According to the previous studies that have been described in Section 1.3.1, impact wear mechanisms of DLC coatings are concerned with the fracture process in the coating due to the crack propagation under severe wear conditions. Besides, nobody will use the DLC under this condition that may lead to a catastrophic failure and should be avoided in most industrial cases. However, no reports discuss about how the impact wear mechanisms of DLC coatings acts under mild wear conditions. Under impact, it is well known that plastic deformation should occur prior to the impact wear. So, the first objective of this study is to identify the most significant impact parameter that controls the deformation of DLC coating. After cyclic impacts, though under mild wear conditions, it believes that impact wear should be occurring by the phase transformation of DLC coating. Therefore, the second objective is to clarify the impact wear mechanisms of DLC coating based on its phase transformation. Finally, in order to distinguish more clearly between the plastic deformation and impact wear of DLC coating as well as to predict its transition points, a deformation-wear transition map is proposed.

In summary, the objectives of this study are as follows:

(a) To identify the governing impact parameter from the viewpoint of mechanical aspects that affects the most on the deformation of DLC coating.

(a) To investigate the phase transformation of DLC coating under cyclic impact loading.

(b) To propose a deformation-wear transition map of DLC coating under cyclic impact loading.

1.5 Outline of dissertation

This dissertation specially describes the impact wear properties of DLC coating, in terms of its wear mechanisms under cyclic impacts, up to 10^5 impact cycles. There are five chapters and briefly outlined as in Fig. 1.12. The following chapters of this dissertation are as follows:

Chapter 1 is an introduction to the industrial needs and its global issues especially under impact applications. Even though an alternative solution by using DLC coatings has practically applied in the industry, the DLC coatings still require extensive future research to provide optimum combination for different applications especially under mild wear conditions. In addition to the tribological properties of DLC coating for sliding contact, this chapter also describes the differences between impact wear of metals and DLC coatings under severe wear conditions based on the previous studies. Furthermore, the purposes of this study also clearly stated.

Under impact, it is well known that plastic deformation should be occurred prior to the impact wear. Therefore, Chapter 2 aims to identify the most significant impact parameter that controls the deformation of DLC coating. The impact parameters only limited to the mechanical aspects such as maximum normal impact load, absorbed energy and contact impulse. Apart from the experimental results, an analytical approximation of the residual impact crater volume/depth and absorbed energy for assigned maximum normal impact load is presented.

After cyclic impacts, though under mild wear conditions, it believes that impact wear should be occurring by the phase transformation of DLC coating. Therefore, Chapter 3 is meant to clarify the impact wear mechanisms of DLC coating under cyclic impact loading based on its phase transformation. In this chapter, Raman spectroscopy is used to investigate the phase transformation of DLC coating. The relationship between the Raman properties (such as I_D/I_G ratio, $FWHM_G$ and G peak frequency) with the sp^2 and sp^3 content in the DLC coating on the crater surface, wear debris as well as in the transfer layer play an important role in achieving the objective of this chapter.

Additionally, in order to distinguish more clearly between the plastic deformation and impact wear of the DLC coating as well as to predict its transition points, Chapter 4 proposes a deformation-wear transition map of DLC coating under

cyclic impact loading based on empirical approach. This chapter goes on to describe the role that transition map plays in predicting the transition of deformation to wear of the DLC coating during impact systematically for future design purposes.

Chapter 5 concludes the major findings of this work and their context in current research.

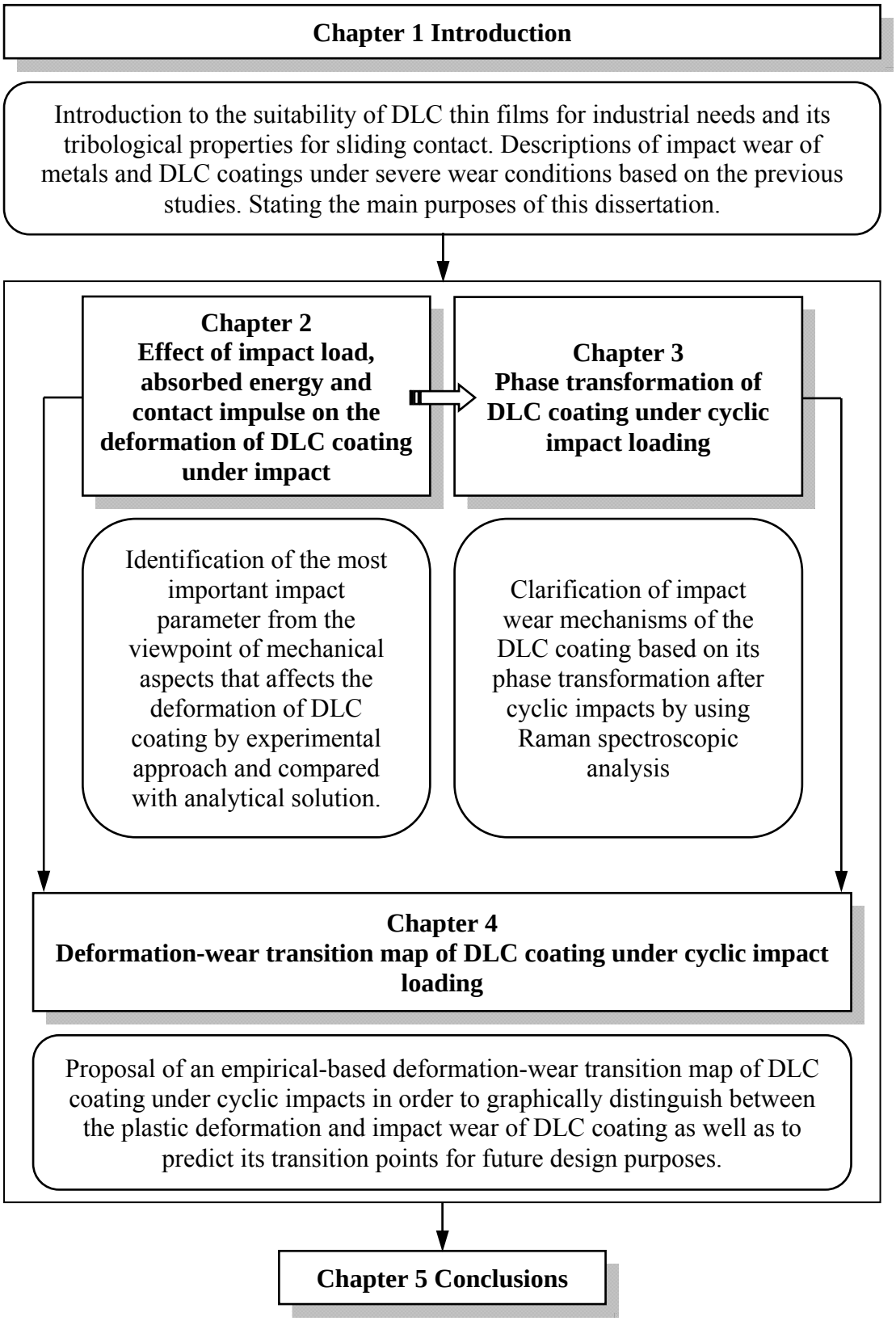

Fig. 1.12 Outline of dissertation.

References

[1] C.P.O. Treutler, Industrial use of plasma deposited coatings for components of automotive fuel injection systems, Surf. Coat. Technol. 200 (2005) 1969-1975.

[2] C.Q. Dam, M.C. Long, S.F. Shafer, J.E. Tomaseski, Thin film coating for fuel injector components, US 6,715,693 B1, (2004).

[3] S.V. Johnson, S.V. Hainsworth, Effects of DLC coatings on wear in automotive applications, Surf. Eng. 21 (2005) 67-71.

[4] M. Kano, DLC coating technology applied to sliding parts of automotive engine, N. Diam. Front. Carbon Technol. 16 (2006) 201-210.

[5] http://www.memphisracing.com/vb/showthread.php?1383-All-motor-engine-buildup-Part-1-updated-6-23-04, Online Article, Access on Mei (2011).

[6] J. Angus, Diamond-like hydrocarbon and carbon films, in Diamond and diamond like films and coatings, NewYork, (1991) 173.

[7] K. Holmberg, A. Matthews, Coatings Tribology - Properties, Techniques and Applications in Surface Engineering. Tribology series 28, Elsevier Science B.V., Amsterdam, The Netherlands, (1994).

[8] http://techon.nikkeibp.co.jp/article/HONSHI_LEAF/20050528/105217/, Online article, Access on April (2009). (In Japanese).

[9] A.G. Guy, Essentials of Materials Science, McGraw-Hill, Inc., New York, USA, (1976).

[10] B. Bhushan, Principles and Applications of Tribology, John Wiley & Sons, Inc, New York, USA, (1999).

[11] B. Dischler, Bonding and hydrogen incorporation in a-C:H studied by infrared spectroscopy, in: P. Koidl, P. Oelhafen (Eds.), EMRS Symposia Proceedings, Volume XVII, Amorphous Hydrogenated Carbon Films, France, Les Éditions de Physique, (1987) 189–201.

[12] J. Robertson, Mechanical properties and structure of diamond-like carbon, Diam. Relat. Mater. 1, (1992) 397–406.

[13] B.X. lam, Diamond-like carbon coatings for tribological applications, Sci. Technol. Dev. 11 (2008) 100-108.

[14] R. Hauert, An overview on the tribological behavior of diamond-like carbon in technical and medical applications, Tribol. Int. 37 (2004) 991-1003.

[15] C. Donnet, A. Grill, Friction control of diamond-like carbon coatings, Surf. Coat. Technol. 94–95 (1997) 456–462.

[16] J. Robertson, Deposition and properties of diamond-like carbons, Mater. Res. Soc. Symp. Proc. 555 (1999) 12.

[17] J.C. Angus, Categorisation of dense hydrocarbon films, in: P. Koidl, P. Oelhafen (Eds.), EMRS Symposia Proceedings, Volume XVII, Amorphous Hydrogenated Carbon Films, France, Les Éditions de Physique, (1987) 179–87.

[18] W. Weissmantel, Preparation, structure and properties of hard coatings on the basis of i-C and i-BN, in: K.J. Klabunde (Eds.). Thin Films from Free Atoms and Particles, Academic Press Inc. Florida, USA, (1985) 153–201.

[19] S. Neuville, A. Matthews, Hard carbon coatings: the way forward, MRS Bulletin, September (1997) 22–26.

[20] C. Donnet, Tribology of solid lubricant coatings, Condenced Matter News, 4, 6 (1995) 9–24.

[21] H. Ronkainen, Tribological properties of hydrogenated and hydrogen-free diamond-like carbon coatings, VTT Publ. (2001) 1-52.

[22] A. Grill, Tribology of diamond like carbon and related materials: an updated review, Surf. Coat. Technol. 94–95 (1997) 507–513.

[23] A.A. Voevodin, A.W. Phelps, J.S. Zabinski, M.S. Donley, Friction induced phase transformation of pulsed laser deposited diamond-like carbon, Diam. Relat. Mater. 5 (1996) 1264–1269.

[24] S.M. Huang, Z. Sun, Y.F. Lu, M.H. Hong, Ultraviolet and visible Raman spectroscopy characterization of diamond-like carbon film growth by pulsed laser deposition, Appl. Phys. A, 74 (2002) 519-523.

[25] J. Eskusson, R. Jaaniso, E. Lust, Diamond-like phase formation in an amorphous carbon films prepared by periodic pulsed laser deposition and laser irradiation method, Appl. Surf. Sci. 255 (2009) 7104-7108.

[26] A. Erdemir, F.A. Nichols, X.Z. Pan, R. Wei, P. Wilbur, Friction and wear performance of ion-beam-deposited diamond-like carbon films on steel substrates, Diam. Relat. Mater. 3 (1993) 119-125.

[27] C. Donnet, Recent progress on the tribology of doped diamond-like and carbon alloy coatings: a review. Surf. Coat. Technol. 100-101 (1998) 180-186.

[28] H. Ronkainen, J. Koskinen, J. Likonen, S. Varjus, J. Vihersalo, Characterization of wear surfaces in dry sliding of steel and alumina on hydrogenated and hydrogen-free carbon films, Diam. Relat. Mater. 3 (1994) 1329-1336.

[29] H. Ronkainen, S. Varjus, J. Koskinen, K. Holmberg, Friction and wear performance of a-C:H films in a wide normal load and sliding velocity range. Tribologia, Finnish J. Tribol. 18 (1999) 3-12.

[30] H. Ronkainen, S. Varjus, J. Koskinen, K. Holmberg, Differentiating the tribological performance of hydrogenated and hydrogen-free DLC coatings, Wear, 249 (2001) 260-266.

[31] H. Ronkainen, S. Varjus, K. Holmberg, Friction and wear properties in dry, water- and oil-lubricated DLC against alumina and DLC against steel contacts, Wear, 222 (1998) 120-128.

[32] K. Holmberg, H. Ronkainen, A. Matthews, Tribology of thin coatings, Ceram. Int. 26 (2000) 787-795.

[33] J. Koskinen, J.P. Hirvonen, J. Keränen, Relaxation of sp^3 bonds in hydrogen-free carbon films during growth, in: S.R.P. Silva, J. Robertson, W. Milne, G.A.J. Amaratunga (Eds.), Amorphous Carbon: State of the Art. Singapore, World Scientifitic Publishing Co. Ltd. Cambridge, UK, (1998) 46-56.

[34] G.W. Stachowiak, A.W. Batchelor, Engineering Tribology, Elsevier, Burlington, USA, (2005).

[35] P.A. Engel, Impact Wear of Materials, Elsevier, Amsterdam, (1976).

[36] P.A. Engel, Percussive Impact Wear, Tribol. Int. 11 (1978) 169-176.

[37] S.L. Rice, The role of microstructure in the impact wear of two aluminum alloys, Wear, 54 (1979) 291-301.

[38] K.J. Swick, G.W. Stachowiak, A.W. Batchelor, Mechanism of wear of rotary-percussive drilling bits and the effect of rock type on wear, Tribol. Int. 25 (1992) 83-88.

[39] E.S. Zanoria, L.E. Seitzman, Characterization of thin metallurgical coating systems by repetitive inclined impact test in dry condition, Surf. Coat. Technol. 182 (2004) 161-170.

[40] F. Ledrappier, C. Langlade, Y. Gachon, B. Vannes, Blistering and spalling of thin hard coatings submitted to repeated impacts, Surf. Coat. Technol. 202 (2008) 1789-1796.

Chapter 2

Effect of impact load, absorbed energy and contact impulse on the deformation of DLC coating under impact

2.1 Introduction

Recently, the requirements for measuring dynamic responses have become severe and vary amongst many industrial and research applications, such as material testing, model analysis, and crash testing [41]. Surface degradation often occurs due to these dynamic responses. This phenomenon also appears in the DLC coating.

Zhu et al. [42], showed that applied kinetic energy, absorbed and transformed to plastic deformation energy, has a strong relationship to the CrN-Cu coating failure. Therefore, the energy relationship is a more suitable index than the load relationship, for indicating the damage resistance of coatings.

According to Robinson and Davies [43], the differences in impactor mass, used for the differently sized specimens, did not significantly affect impact performance. The damage size, of the glass fiber reinforced polymer (GFRP) solid laminate, was also shown to correlate to the absorbed energy. Besides, the agreement of the damage size curve versus the peak contact force is very good if the behavior of the plates is in the quasi static process. However, as perforation is approached, the damage size and peak force both tend to plateau and so a cluster of data points at higher peak contact force.

Many other studies have reported the failure of thin coatings during impact by a cyclic loading system [40],[44-49]. The majority of repetitive impact testing, which appear in the above studies, are conducted either with loads normal to the surface or a combination of normal and tangential loadings.

However, no reports describe how much the maximum normal impact load and absorbed energy affects the volume/depth of the impact crater. Other than these two dynamic factors, another interesting parameter, which should be taken into account, is the contact impulse. For that reason, the main goal of this chapter is to find the

most important impact parameter, which affects the residual impact crater volume/depth of DLC coating, by using a self-developed impact tester. In the present work, the possible governing impact parameters are only limited to the maximum normal impact load, absorbed energy; as well as the additional parameter of contact impulse. The influence of impactor mass was also considered.

2.2 Experimental method

2.2.1 Materials

The tungsten high speed steel (SKH2) disc was used as a substrate, whilst a chromium molybdenum steel (SCM420) pin, was used as an impactor. The diameter of the disc and the pin were 10 mm and 2 mm, respectively (as shown in Fig. 2.1). All DLC films were deposited onto the SKH2 substrate using a PVD method; where tungsten (W) was used as an interlayer material. The film thickness h_c is approximately 2.97 μm. The average surface roughness R_a of the as-deposited DLC coating is approximately 18.63 nm, which was measured by atomic force microscopy (AFM). Material properties are listed in Table 2.1.

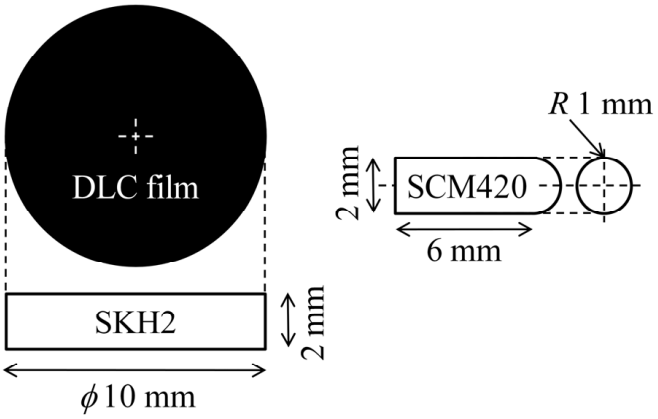

Fig. 2.1 Dimensions of the DLC coated disc and the SCM420 pin.

Table 2.1 Material properties of the DLC, SKH2 substrate and SCM420 pin.

Properties	DLC	SKH2	SCM420
Young modulus E, GPa	251	378	295
Poisson's ratio v	0.3	0.3	0.3
[a]Hardness H, GPa	17.14	9.80	7.43
[b]Yield strength Y, GPa	6.12	3.50	2.65

[a]From the nanoindentation test.
[b]$Y = H/2.8$.

2.2.2 Impact testing

The impact test was performed using a self-developed impact tester, as shown in Fig. 2.2. Horizontal impact tester was used for more than 10^2 impact cycles with a frequency of 10 Hz.

The impact test rig was designed to impact a DLC coated disc with a SCM420 pin for numerous impacts. The total impactor masses *m* were 115.4 g and 171.5 g, respectively. Prior to the impact test, both disc and pin were cleaned using acetone in an ultrasonic bath. The disc was repeatedly impacted at 400 impact cycles, with a 90° inclination. All impact tests were conducted at room temperature. Kerosene was used as a lubricant. Several different normal impact loads were applied to the DLC coated disc via a spring system. The applied load was observed by a load cell. The absorbed energy was determined using a high speed camera. As for the contact impulse and maximum normal impact load, this can be obtained from the graph generated by a load cell. The contact impulse is determined from the area below the graph of normal impact load with time as shown in Fig. 2.3. In addition, three dimensional (3D) topography measurements were performed to obtain quantitative data on the residual impact crater volume/depth of DLC coating, using an AFM. The cross section of DLC coating on the SKH2 substrate was prepared using a focused ion beam (FIB) and observed by field emission scanning electron microscopy (FE-SEM). The affected area on the SCM420 pin surface was analyzed using energy dispersive x-ray spectroscopy (EDS).

In this impact test, the maximum normal impact load and contact impulse are constant for each impact cycle, whilst the absorbed energy was obtained for only one impact cycle. It is very difficult to get an accumulative absorbed energy for multi-impacts. As demonstrated in the experimental work [50], a single loading and subsequent cyclic loadings formed an identical residual radii and depths of crater under the same contact loads. In this study, only a small difference of impact crater volume/depth of DLC coating has been observed between a single loading and subsequent cyclic loadings under low maximum normal impact load. Furthermore, by increasing the maximum normal impact load, a threshold of the residual impact

crater volume/depth to remain constant with impact cycles is much faster[†]. For this reason, the analytical solutions were performed for one impact cycle.

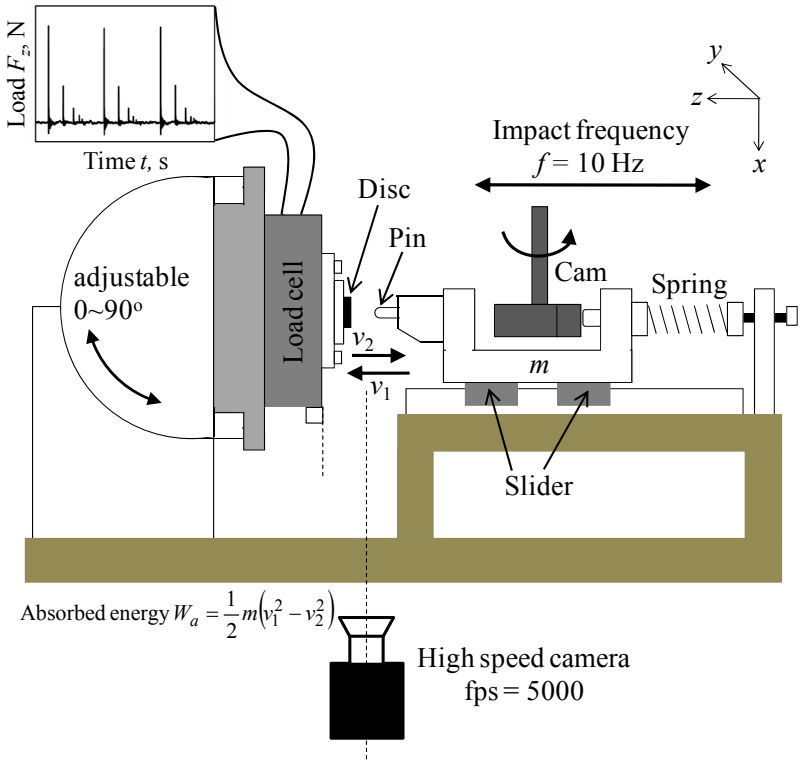

Fig. 2.2 Schematic illustration of the repeated impact tester.

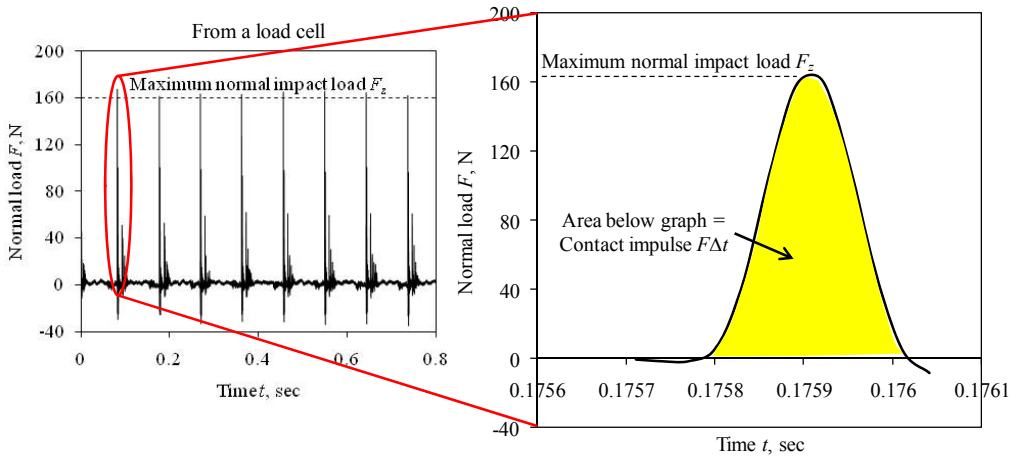

Fig. 2.3 Area below the graph of F vs. t, which generated by a load cell, is similar to the contact impulse $F\Delta t$.

[†] Further explanations are in Section 4.3.1

2.2.3 Residual impact crater volume/depth

The raw data collected included the measurements of the residual impact crater volume and its depth/radius. The depth h_r and radius a_r of the residual impact crater of the DLC coating were measured directly from a cross-sectional AFM topography image. The cross-sectional image, parallel to the y-axis, was taken at the center of impact crater, as shown in Fig. 2.4. In order to calculate the residual impact crater volume, raw data from the AFM was exported to Origin 8.1. An illustration of how the residual impact crater volume was calculated is shown in Fig. 2.4. The raw data of x-axis were discrete to n cross-sections with the thickness of Δx. The surface area A of each cross-section was determined using the integration method function in Origin 8.1. The residual impact crater volume V_r is determined using the following equation:

$$V_r = \sum_{j=1}^{n-1} (A)_j \times \Delta x \tag{2.1}$$

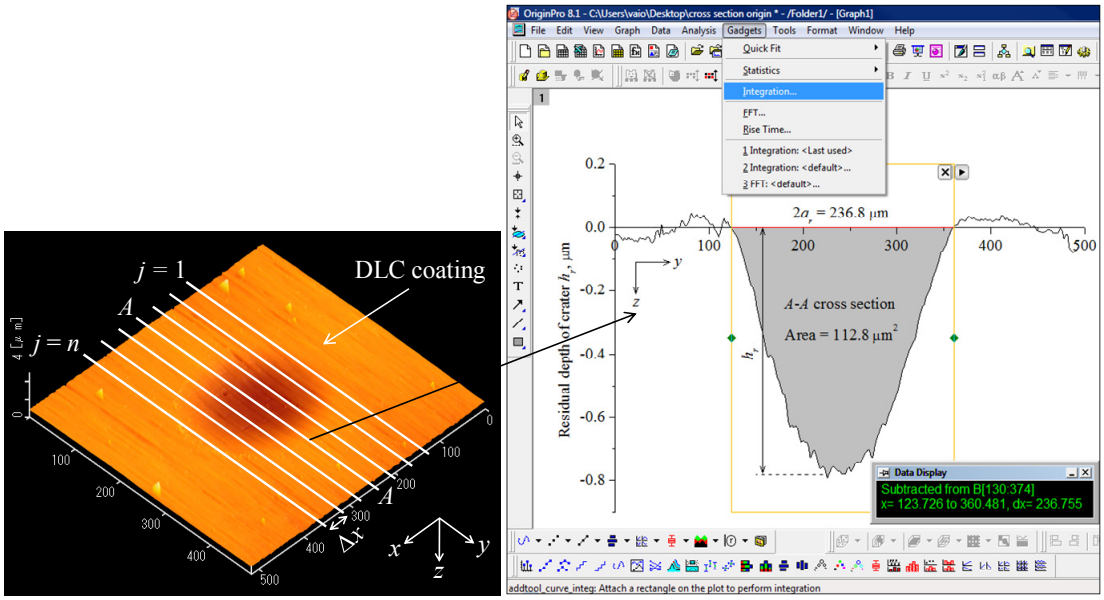

(a) (b)

Fig. 2.4 (a) Discretions of x-axis of an impact crater to n cross sections, with the thickness of Δx, and (b) determination of each surface area (A-A cross section) using the integration function in Origin 8.1.

2.3 Theoretical background

The absorbed energy is calculated using the following equation:

$$W_a = \frac{1}{2} m(v_1 - v_2)(v_1 + v_2) \tag{2.2}$$

where m is the impactor mass, v_1 is the velocity before impact, and v_2 is the velocity after impact.

The change in the momentum of the pin, and the impulse $\int F_z dt$ acting on the load cell, are equal; according to the law of conservation of momentum, if other forces can be ignored [41]. This is expressed as:

$$\int F_z dt = m(v_1 - v_2) \tag{2.3}$$

Because of the velocity after impact v_2 is in an opposite direction to the velocity before impact v_1, the Eq. (2.3) becomes:

$$\int F_z dt = m(v_1 + v_2) \tag{2.4}$$

The relationship between the maximum normal impact load, absorbed energy, and contact impulse, is given by substituting Eq. (2.4) into (2.2), which yields:

$$W_a = 1/2 \cdot (v_1 - v_2) \int F_z dt = 1/2 \cdot (v_1 - v_2) F_z \Delta t \tag{2.5}$$

In the case of the normal impact, where a target deforms plastically, most of the initial kinetic energy W_1 is dissipated as plastic work W_p in the target, with small amounts being restored by elastic forces to the kinetic energy of the rebounding projectile W_2. Besides, one possible source of this energy loss appears to lie in the dissipation of energy in the specimen, in the form of elastic vibrations W_v occasioned by the transient nature of the collision [51]. An expression of these energies can be shown as follows:

$$W_1 = W_2 + W_v + W_p \tag{2.6}$$

$$W_a = W_1 - W_2 = W_v + W_p \tag{2.7}$$

The estimation of the W_v was theoretically derived by Hutchings [52]. It is assumed that the contact pressure, acting over the area of contact, is constant, then:

$$W_v = \frac{\beta(1+v_d)}{\rho_d C_d^{\,3}} \cdot \left(\frac{1-v_d^{\,2}}{1-2v_d} \right)^{1/2} F_z^{\,2} \omega_d \alpha \tag{2.8}$$

where

$$C_d = \left(\frac{E_d}{\rho_d} \right)^{1/2} \tag{2.9}$$

$$\omega_d = \frac{2\omega}{1+e} \tag{2.10}$$

$$e = \left(\frac{W_2}{W_1} \right)^{1/2} \tag{2.11}$$

$$\omega = \frac{\pi}{2t} \tag{2.12}$$

v_d is Poisson's ratio for the substrate; ρ_d and E_d are its density and Young modulus, respectively. F_z is the maximum normal impact load, e is the coefficient of restitution, and t is the loading time, obtained from the graph of load-time relationships. β is a dimensionless quantity dependent only on Poisson's ratio [49]. For v = 0.25, β = 0.537 and for v = 0.3, β = 0.415. The variation of α with e has been computed numerically by Hutchings [49]. The reason why the material properties of the substrate were used in the theoretical analysis, instead of the film properties, will be described later in Section 2.4.2.

The process of impact may be divided into three parts [50]. (i) When the impactor, with a radius of R, first strikes the flat surface, an elastic deformation takes place until the mean pressure developed is sufficient to cause plastic deformation of the flat surface to a maximum height h_{max}. (ii) Plastic deformation of the flat surface now occurs accompanied by a building up of further elastic stresses in both the impactor and the flat surface. (iii) There is now a release of elastic stresses in the impactor and the flat surface surrounding the impaction, as a result of which rebound occurs to a residual depth h_r, as shown in Fig. 2.5, where the $r_r > R$.

Consider the normal contact between a rigid sphere and an elastic-perfectly plastic substrate. If the maximum pressure at the contact centre generated by the

contact load is below than $1.6Y_d$; where Y_d is the yield strength of the substrate, the contact is purely elastic and the problem can be described by the well-known Hertz theory [53].

The contact radius a_y, contact displacement h_y, contact load F_y, contact volume V_y and the mean contact pressure p_y at the elastic limit can be determined using the following equation:

$$a_y = \left(\frac{3F_y R}{4E}\right)^{1/3} = \frac{1.6Y_d \pi R}{2E} \tag{2.13}$$

$$h_y = \frac{a_y}{R} \tag{2.14}$$

$$F_y = \frac{4Ea_y^{\,3}}{3R} = \frac{(1.6Y_d)^3 \pi^3 R^2}{6E} \tag{2.15}$$

$$V_y = \frac{\pi a_y^{\,4}}{4R} \tag{2.16}$$

$$p_y = \frac{4Ea_y}{3\pi R} = \frac{2}{3}(1.6Y_d) \tag{2.17}$$

where

$$\frac{1}{E} = \frac{1-\nu_p^{\,2}}{E_p} + \frac{1-\nu_d^{\,2}}{E_d} \tag{2.18}$$

ν_p and E_p are Poisson's ratio and Young modulus of the pin, respectively.

When the contact load exceeds the maximum elastic contact load, plastic deformation is developed and the contact pressure is no longer to follow the Hertzian pressure distribution. Theoretically, the expression for the contact pressure beyond the elastic limit was developed by Johnson [53]:

$$p_{ep} = \frac{2Y_d}{3}\left[2 + \ln\left(\frac{E}{3Y_d R}\right) + \ln a_{ep}\right] \tag{2.19}$$

where

$$a_{ep} = \left(\frac{3F_z R}{4E} \right)^{1/3} \tag{2.20}$$

Besides, the impact crater volume under elastic-plastic contact, V_{ep} is calculated as follows:

$$V_{ep} = \frac{\pi a_{ep}^{\ 4}}{4R} \tag{2.21}$$

The initial mean contact pressure, under rebound conditions, p_r is to be the same as the mean contact pressure at the end of the loading process, p_{ep}, thus:

$$p_r = p_{ep} \tag{2.22}$$

The residual depth of crater after the contact load is completely removed thus is given by [53]:

$$h_r = h_{\max} - h^* = \frac{a^2}{R} - \left(\frac{9\pi F_z p_r}{6E^2} \right)^{1/2} \tag{2.23}$$

From geometrical considerations, the residual impact crater volume may be written as [50]:

$$V_r = \frac{\pi a_r^{\ 4}}{4r_r} \tag{2.24}$$

where

$$r_r = \frac{a_r^{\ 2} + h_r^{\ 2}}{2h_r} \tag{2.25}$$

$$a_r = a_{ep} \tag{2.26}$$

Then, the work done as plastic deformation energy W_p is defined as the total energy under elastic W_y, elastic-plastic deformation W_{ep} and the energy of rebound W_r:

$$W_p = W_y + W_{ep} - W_r \tag{2.27}$$

$$= \int_0^{V_y} p_y dV + \int_{V_y}^{V_{\max}} p_{ep} dV - \int_{V_r}^{V_{ep}} p_r dV \tag{2.28}$$

By combining Eqs. (2.13) – (2.28), thus:

$$W_p = \frac{4EV}{3\pi R}\left(\frac{4rV}{\pi}\right)^{1/4}\Bigg|_0^{V_y} + \frac{2Y_d V}{3}\left(2 + \ln\frac{E}{3Y_d R} + \ln\frac{4rV}{\pi}\right)\Bigg|_{V_y}^{V_{ep}} - \frac{2Y_d V}{3}\left(2 + \ln\frac{E}{3Y_d R} + \ln\frac{4rV}{\pi}\right)\Bigg|_{Vr}^{V_{ep}} \tag{2.29}$$

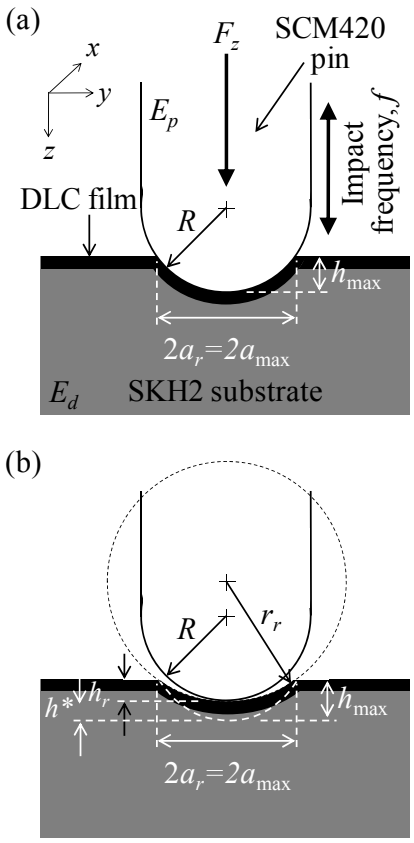

Fig. 2.5 (a) Profile of contact surface during impacting at the maximum normal impact load F_z, and (b) the remaining permanent impact crater at the end of impact.

2.4 Results and discussion

2.4.1 Morphology observations of impacted DLC coating.

A cross-sectional observation of an impact crater on the DLC coating at the higher maximum normal impact load (Fig. 2.6), reveals that no cracks or film exfoliation has occurred within the DLC film. The relative ratio of the difference in non-impacted and impacted thicknesses of DLC film to its original thickness $\Delta h_c/h_c$, is approximately 1/50, and nearly zero. Furthermore, the EDS maps, as shown in Fig. 2.7, shows that the dark area of the affected SCM420 pin surface not comes from the carbon element. This indicates no transfer layer from the DLC coating to the pin is observed. These results apparently show that the residual impact crater volume and its depth are not due to real material loss, but mainly due to plastic deformation.

At the higher maximum normal impact load, where the light impactor was used, it obviously shows that microslip has occurred. The pin, where attached to the light impactor, has shifted tangentially by a small amount, during impact (indicated by the larger a_x as compared to a_y, as shown in Fig. 2.8). This tangential movement is usually caused by an elastic deformation of the supporting structures [30].

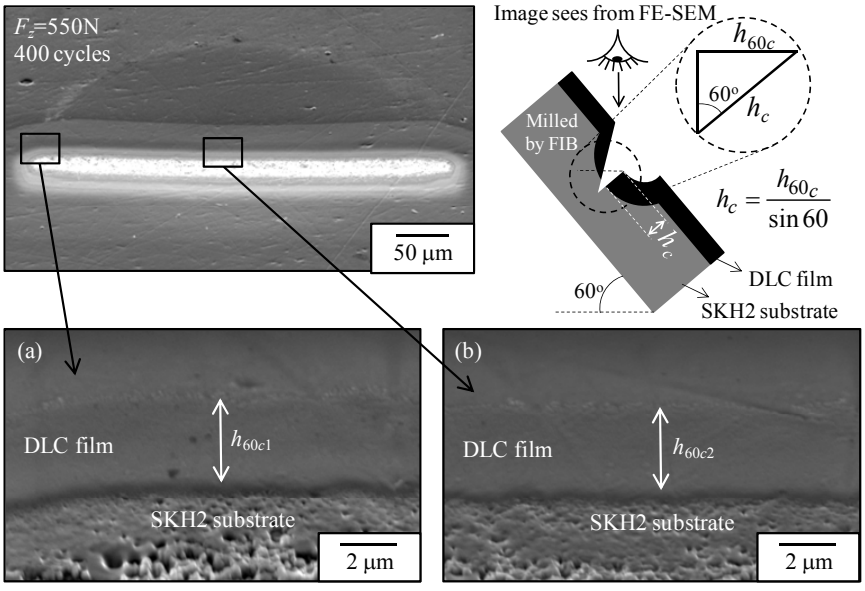

Fig. 2.6 FE-SEM cross-sectional view of the FIB-milled DLC coating on the SKH2 substrate (tilted at 60°); where (a) h_{60c1} is the non-impacted film thickness, and (b) h_{60c2} is the impacted film thickness.

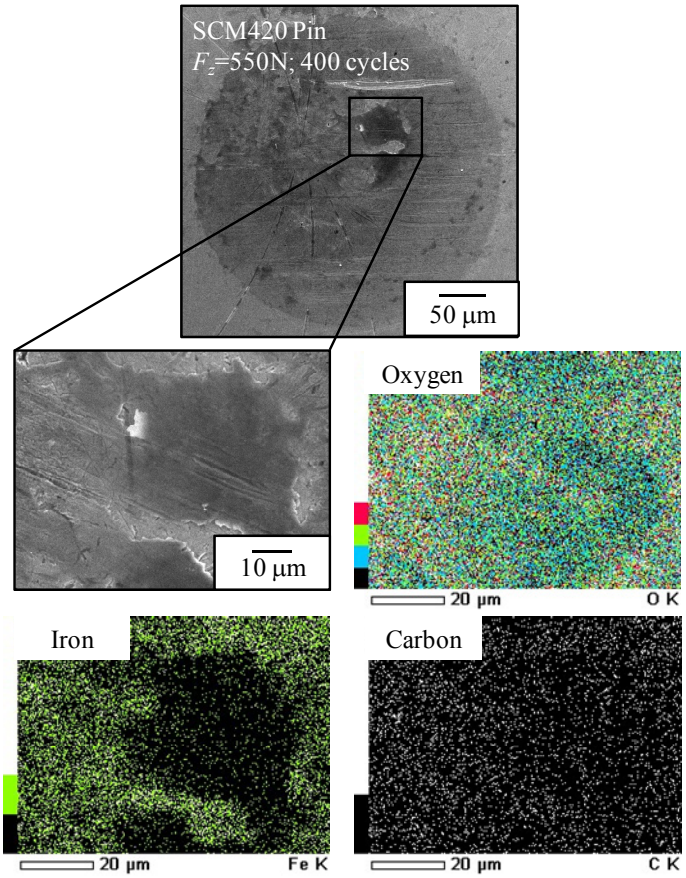

Fig. 2.7 EDS maps of the affected area on the SCM420 pin surface.

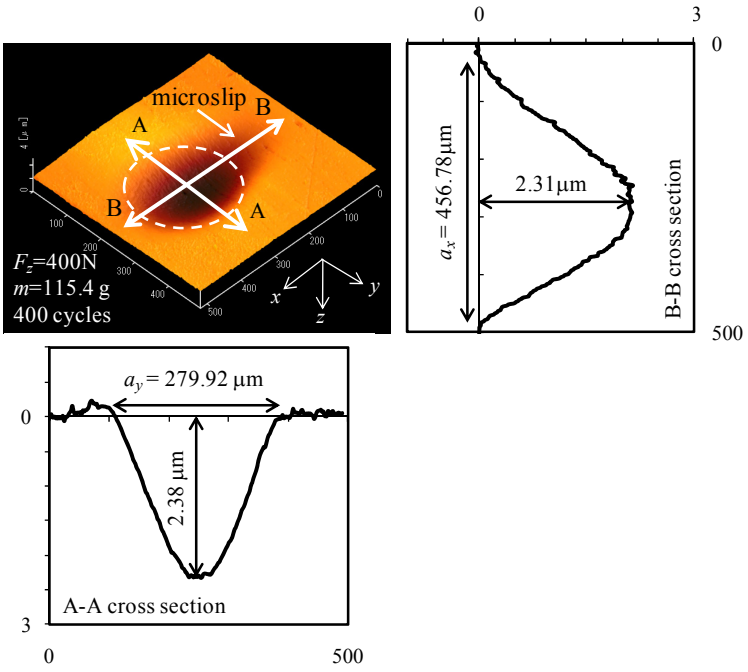

Fig. 2.8 The biggest difference between a_x and a_y is caused by the effects of microslip.

2.4.2 Effect the thin film on the substrate

In this study, the DLC film is very thin and the ratio of film thickness to pin radius h_c/R is approximately 0.003. From the finite element analysis by Michler and Blank [47], thin films with a ratio of h_c/R<0.01 have no effect on the load bearing capacity of the surface. Besides, the deformation of an elastic-perfect plastic substrate, is not supposed to be altered by the presence of a thin film, which itself, simply follows the deformation of the substrate at the interface. This is in accordance with this study, where the residual depth of the impact crater, with or without a DLC coating, shares the same line and formed a good relationship with the maximum normal impact load, as shown in Fig. 2.9. Additionally, the residual depth of impaction is less than the film thickness, as shown in Fig. 2.10. As stated by Begley et al. [48], a thin film does not play a significant role, when the depth of the affected area is less than approximately five times the thickness of the film. The strain in the film is governed by the surface strain in the substrate. Therefore, in this study, the material properties of the film could be ignored (i.e.: $E_{\text{film}} = E_{\text{substrate}} = E_d$) in order to calculate the theoretical values.

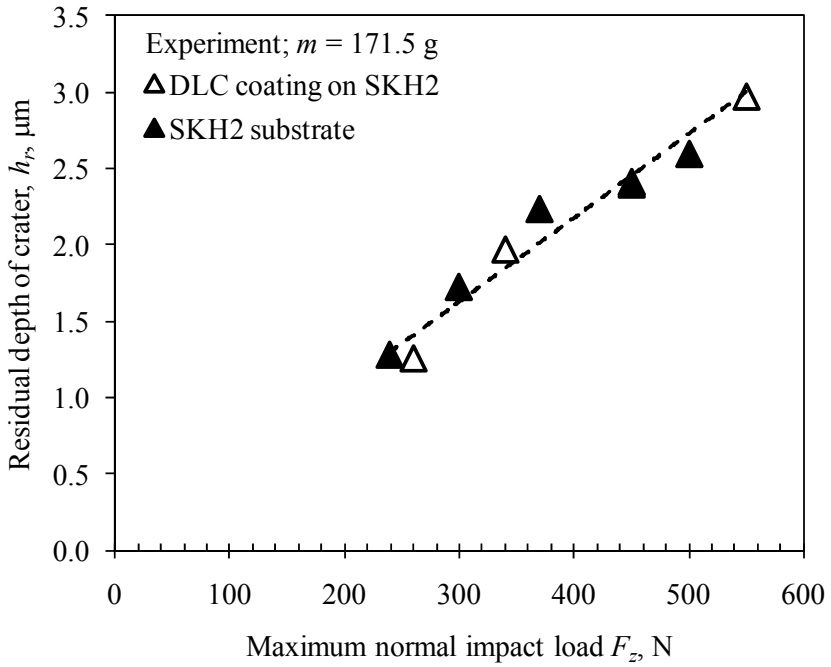

Fig. 2.9 The residual depth of crater, with or without DLC coating on the SKH2 substrate after impact at 400 cycles.

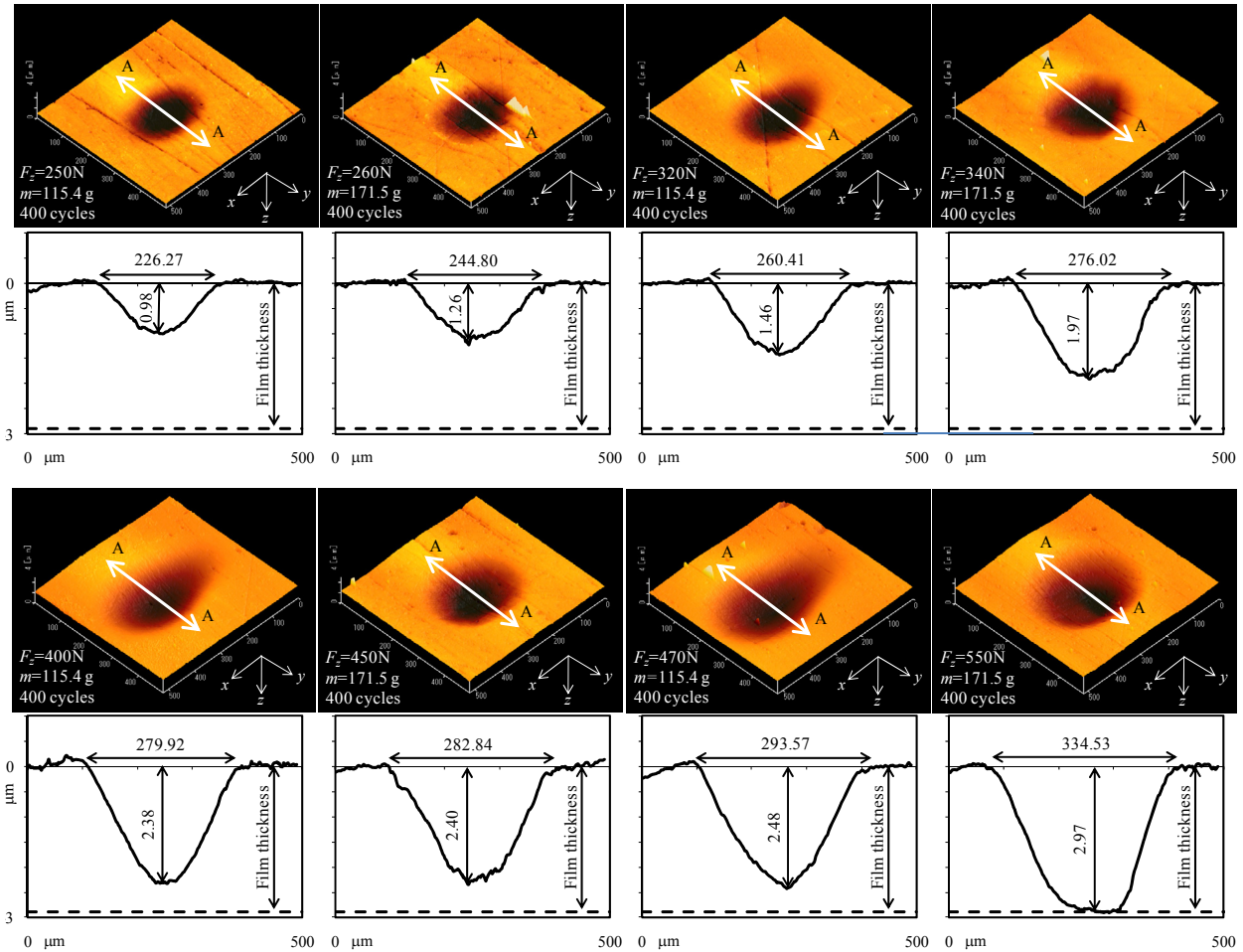

Fig. 2.10 AFM observations of the residual impact crater of DLC coating on the SKH2 substrate and its cross sectional profile (A-A cross section). All conditions show $h_r < 5h_c$.

2.4.3 Experimental relationship of the residual impact crater volume/depth with a maximum normal impact load, absorbed energy and the contact impulse.

Figure 2.11 shows how the residual impact crater volume/depth of DLC coating, varies with maximum normal impact load, absorbed energy, and the contact impulse. The implication of the contact impulse to the residual impact crater volume/depth of DLC coating is apparently not very good because there is no unique relationship between them. It seems like there are two different curves being plotted together, as illustrated in Fig. 2.11 (c). This means that the contact impulse did not have a significant effect on the residual impact crater volume/depth of DLC coating. At first thought, this poor relationship might be dependent on impactor mass. However, a good agreement is obtained from the responses of maximum normal impact load and absorbed energy regardless of impactor mass (Fig. 2.11 (a) and (b)). Thus, Eq. (2.5) suggests that this discrepancy is due to the total difference of impact velocity (v_1-v_2).

The coefficient of determination R^2 is a statistical measure of how well a regression line approximates real data points. The R^2 values range from 0 to 1. The higher the R^2 the more effective one variable is at forecasting another. If the R^2 is 0 then one variable has nothing in common with the other. The closer its R^2 value is to 1, the greater the ability of that model to predict a trend. Even though a good agreement is obtained from the responses of maximum normal impact load and absorbed energy, both R^2 (for the V_r and h_r) from the response of maximum normal impact load (R^2_{hr} = 0.9362 and R^2_{Vr} = 0.9076) is higher than that from the response of absorbed energy (R^2_{hr} = 0.7945 and R^2_{Vr} = 0.8779). This indicates that the residual impact crater volume/depth is more affected by maximum normal impact load than absorbed energy as R^2 value.

In this experiment, absorbed energy can also be a governing parameter even if R^2 value is less than maximum normal impact load. However, there is an experimental error in the case of absorbed energy. This is due to the microslip effect, where the light impactor was used, as described previously. More absorbed energy is needed if there is a sliding effect. From Fig. 2.11 (b), a cluster of data points (indicates by a low R^2 value) from the relationship between absorbed energy and

residual impact crater depth can also be seen. The absorbed energy, where the light impactor was used, is larger than as should be.

On the basis of physics, if this phenomenon is done by a quasi-static indentation, load is a governing parameter. But if this phenomenon is governed by the energy conservation law, absorbed energy should be significant. According to Zhang et al. [54], the impact loading at speeds lower than 3.5 ms^{-1} resulted in global deformation and failure processes similar to the static indentation experiment. Besides, the experimental results coincided approximately with those the analytical results by static indentation analysis (later will discuss in Section 2.44). Therefore, it is believes that the impact phenomenon in this study is a physical phenomenon in which can be same as the quasi-static indentation because the impact velocity is very low (in this study the maximum impact velocity is approximately 0.3 ms^{-1}).

By considering the physical meaning of a quasi-static indentation and the experimental error in the case of absorbed energy in addition to R^2 value, it is worth to choose the maximum normal impact load as an important parameter that affects the most on the residual impact crater volume/depth of DLC coating.

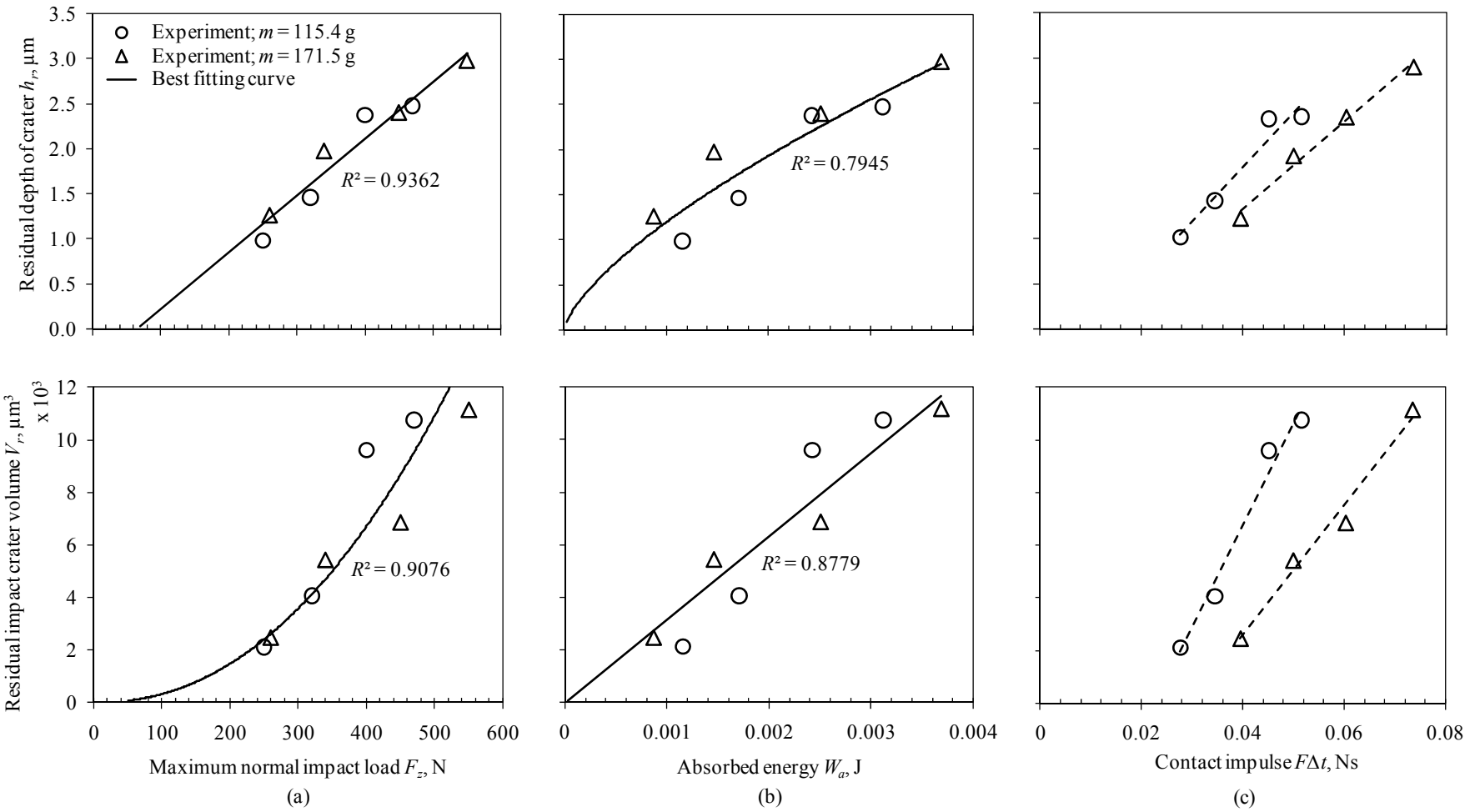

Fig. 2.11 Experimental relationship between the residual impact crater volume/depth of DLC coating and the maximum normal impact load, absorbed energy, as well as the contact impulse. The solid line indicates the best fitting curve from regression analysis.

2.4.4 Comparison of experimental results and analytical solutions

The elastic vibrational energy is calculated from Eq. (2.8). Table 2.2, presents the fraction λ_v of the initial kinetic energy, dissipated in the form of elastic vibrations and is typically only a few per cent, approximately 0.02% - 0.07% of the W_1. For that reason, it is proposed that the dissipation of energy, in the form of elastic vibrations, becomes negligible and the loss of energy is mainly from the W_p.

Table 2.2 Fraction of vibrational energy W_v to the initial kinetic energy W_1.

m (g)	W_1 (J)	W_v (J)	λ_v (%)
115.4	0.0018	3.64E-07	0.019
171.5	0.0013	3.85E-07	0.029
115.4	0.0026	6.53E-07	0.025
171.5	0.0020	6.68E-07	0.034
115.4	0.0036	9.96E-07	0.028
171.5	0.0031	1.46E-06	0.048
115.4	0.0045	1.46E-06	0.032
171.5	0.0042	2.85E-06	0.068

For the normal impact, with maximum normal impact load F_z, one can determine h_r and a_r from Eqs. (2.23) and (2.26) and then use Eqs. (2.24) and (2.29) to calculate the V_r and W_p. This W_p can be expressed from Eq. (2.7) as an absorbed energy W_a, where the elastic vibrations become negligible. These calculated values are plotted in the same axis of the experimental graphs of residual impact crater volume/depth of DLC coating, against maximum normal impact load and absorbed energy.

A comparison of the calculated and experimental results is shown in Fig. 2.12. It is seen that the agreement between the residual impact crater volume/depth of DLC

coating against maximum normal impact load, is reasonably good. However, the agreement for the absorbed energy is poor, where the experimental values are approximately 3 times larger than the calculated values. From this comparison, it is easier to predict the residual impact crater volume/depth by static indentation analysis (F_z). However, it is difficult to predict these values by energy approach (W_a). This means that it is does not need to consider about the absorbed energy.

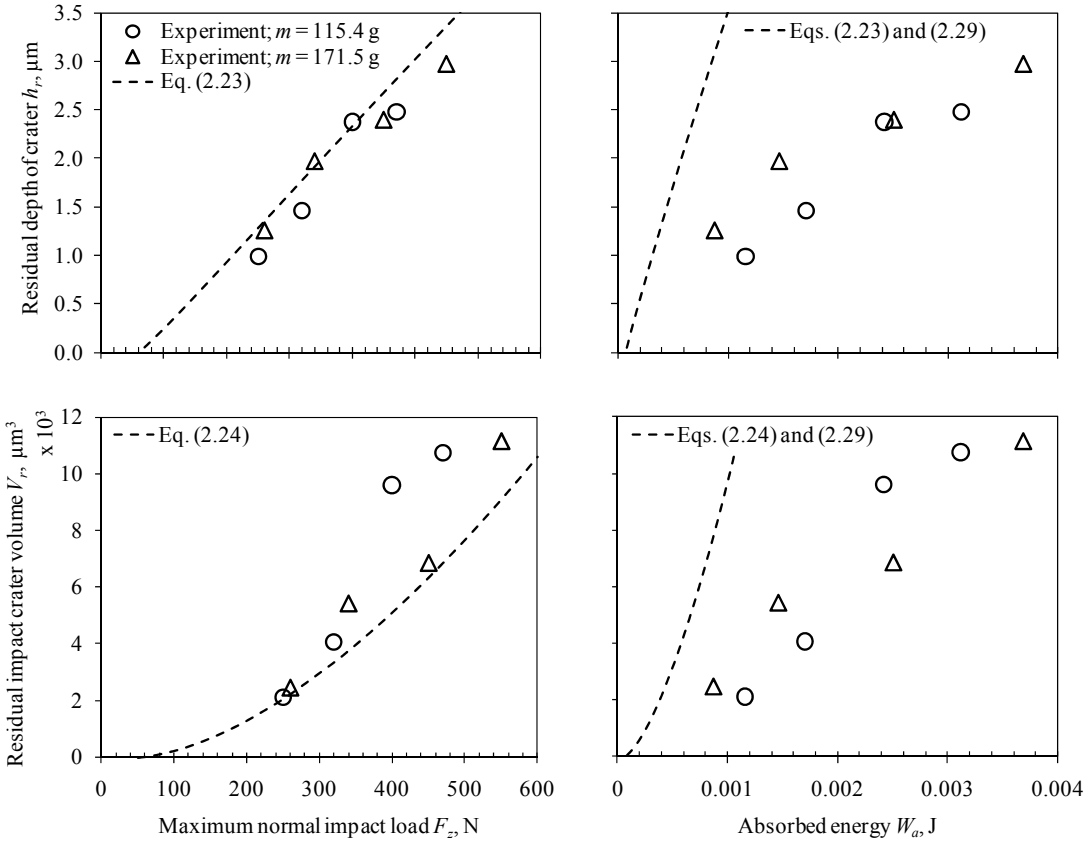

Fig. 2.12 Experimental and analytical comparison of the residual impact crater volume/depth of DLC coating, as a function of maximum normal impact load and absorbed energy.

2.5 Conclusions

The impact test was performed to evaluate the significance of maximum normal impact load, absorbed energy, and contact impulse, on the residual impact crater volume/depth of DLC coating. The following main results were obtained:

(a) From the experimental analysis, there is no unique relationship between the residual impact crater volume/depth of DLC coating and contact impulse. This means that the contact impulse did not have a significant effect on the residual impact crater volume/depth of DLC coating. However, the residual impact crater volume/depth of DLC coating is dependent on maximum normal impact load and absorbed energy, regardless of impactor mass. Even though a good agreement is obtained from the responses of maximum normal impact load and absorbed energy, both R^2 (for the V_r and h_r relationship) from the response of maximum normal impact load (R^2_{hr} = 0.9362 and R^2_{Vr} = 0.9076) is higher than that from the response of absorbed energy (R^2_{hr} = 0.7945 and R^2_{Vr} = 0.8779). Besides, there is an experimental error in the case of absorbed energy due to the microslip effect. Furthermore, the impact phenomenon in this study can be considered as the quasi-static indentation, where load is a governing parameter, because the impact velocity is very low. From these reasons, it can be concluded that the residual impact crater volume/depth is more affected by maximum normal impact load than absorbed energy.

(a) From the comparison between the experimental and analytical solution, residual impact crater volume/depth could be predicted by static indentation analysis (F_z). However, it is difficult to predict these values by energy approach (W_a). This means that it is does not need to consider about the absorbed energy.

References

[41] Y. Fujii, H. Fujimoto, Design note: Proposal for an impulse response evaluation method for force transducers, Meas. Sci. Technol. 10 (1999) 31-33.

[42] X. Zhu, H. Dou, Z. Ban, Y. Liu, J. He, Repeated impact test for characterization of hard coatings, Surf. Coat. Technol. 201 (2007) 5493-5497.

[43] P. Robinson, G.A.O. Davies, Impactor mass and specimen geometry effects in low velocity impact of laminated composites, Int. J. Impact Eng. 12 (1992) 189-207.

[44] S.D.A. Lawes, S.V. Hainsworth, M.E. Fitzpatrick, Impact wear testing of diamond-like carbon films for engine valve-tappet surfaces, Wear, 268 (2010) 1303-1308.

[45] E.S. Zanoria, L.E. Seitzman, Characterization of thin metallurgical coating systems by repetitive inclined impact test in dry condition, Surf. Coat. Technol. 182 (2004) 161-170.

[46] J.C.A. Batisca, C. Godoy, A. Matthews, Impact testing of duplex and non-duplex (Ti,Al)N and Cr-N PVD coatings, Surf. Coat. Technol. 163-164 (2003) 353-361.

[47] J. Michler, E. Blank, Analysis of coating fracture and substrate plasticity induced by spherical indentors: diamond and diamond-like carbon layers on steel substrates, Thin Solid Film, 381 (2001) 119-134.

[48] M.R. Begley, A.G. Evans, J.W. Hutchinson, Spherical impression of thin elastic films on elastic-plastic substrates, Int. J. Solids and Struct. 36 (1999) 2773-2788.

[49] O. Knotek, B. Bosserhoff, A. Schrey, A new technique for testing the impact load of thin films: the coating impact test, Surf. Coat. Technol. 54-55 (1992) 102-107.

[50] D. Tabor, A simple theory of static and dynamic hardness, Proc. R. Soc. A: Math. Phys. Eng. Sci. 192 (1948) 247-274.

[51] S.C. Hunter, Energy absorbed by elastic waves during impact, J. Mech. Phys. Solids, 5 (1957) 162-171.

[52] I.M. Hutchings, Energy absorbed by elastic waves during plastic impact, J. Phys. D: Appl. Phys. 12 (1979) 1819-1824.

[53] K.L. Johnson, Contact Mechanics, Cambridge University Press, Cambridge, (1985).

[54] J. Y. Zhang, T. X. Yu, J. K. Kim, Static indentation and impact behavior of reformed bamboo/aluminium laminated composites, Compos. Struct. 50 (2000) 207-216.

Chapter 3

Phase transformation of DLC coating under cyclic impact loading

3.1 Introduction

Generally, phase transformation of DLC may involve a change in the structure itself either from sp^2 to sp^3 or vice versa. The DLC is a disordered mixture of carbon atoms with sp^2 and sp^3 hybridizations [55]. The sp^3 hybrids confer diamond-like properties like high hardness, high density, chemical inertness, etc., while sp^2 hybrids control the electronic and optical properties because the π states lie closest to the Fermi level [56].

The phase transformation of DLC coating due to sliding has been performed extensively for a decade [57-63]. However, there is still a lack of information about how the structure will change by repetitive impacts.

Liao et al. [59] reported that as the number of the sliding cycles or the load is increasing, the tribological properties decrease due to the graphitization of DLC films within a wear track. Liu et al. [60] showed with evidence that the transfer layer contained a fine distribution of graphite nano-particles in a distorted diamond-like structure. Besides, a graphitization process took place within the wear track region of the coatings probably due to thermal and strain effects from the repeated friction. A year later, Liu and Meletis [61] said that the transformation of DLC to graphite-like may also be facilitated by shear stresses existing in the surface layer. However, Zhou et al. [62] suggested that the structural transformation of DLC coatings within the wear tracks was mainly due to the formation of a compact wear debris layer rather than a frictional heating effect. In addition, according to Sanchez-Lopez et al. [63], evidence of extended graphite layer formation was not observed in the transfer film of DLC after friction test.

The main goal of this chapter is to discuss the changes in the structure of the DLC coating by applying different maximum normal impact loads under repetitive impacts.

3.2 Experimental method

All materials and impact testing procedures are same as in the Section 2.2, excluding a high speed camera. 70 N, 160 N and 240 N of maximum normal impact load were chosen and the impact test was performed under 10^2~10^5 impact cycles.

The bonding structures of DLC coating on the crater surface, wear debris as well as transfer layer on the pin were studied using Raman spectroscopic analysis and assisted by EDS, AFM and FE-SEM observations.

Additionally, the nanoindentation test was performed at the surface of impact crater on the DLC coating for each maximum normal impact load and impact cycle. Testing load is 500 μN. The mean value was assumed to be hardness of DLC coating on the crater surface.

3.2.1 Raman spectroscopy analysis

Raman spectroscopy is the best way to obtain the detailed bonding structures of the DLC films [63]. The Raman spectrum of carbon films offers valuable information about the atomic bonds and level structure of the molecule. Especially in the nanostructured carbon thin films range Raman spectra has a great importance for define the structure of this kind of films. For example, magnetic disks for information storage are protected with a thin layer of semi-ordered DLC film. The most common method of testing the integrity of these films is to simulate the disk drive's start-up/shut-down procedure many times over the course of 2~4 days and determine the degree of wear. Raman spectroscopy gives much faster, non-destructive analysis. In addition, Raman analysis can be performed at room temperature and offers high spatial resolution (<1 μm).

The DLC films show common features in their Raman spectrum in the 800-2000 cm^{-1} region. The so called G and D peaks, which lie at approximately 1550 cm^{-1} and at 1370 cm^{-1}, respectively, for visible excitation and the T-peak at approximately 1060 cm^{-1} which is visible only with UV excitation. The G peak is due to the bond stretching of all pears of sp^2 atoms in both rings and chains. The D peak is due to the breathing modes of sp^2 atoms in rings. The T peak is due to the C-C sp^3 vibrations.

In this present work, Raman scattering of DLC coating was performed in the visible light range. While Raman cannot provide an exhaustive analysis of the film structure, correlations between Raman intensities and band positions can provide insight into the atomic structure of the films. The intensity vs. frequency spectrum was presented. The frequency was plotted relative to the laser frequency, so the frequency scale represents the Raman shift and was acquired over the range of 500–2000 cm^{-1}.

3.3 Results and discussion

3.3.1 Phase transformation of DLC coating on the crater surface

The Raman spectra shown in Fig. 3.1, which were taken from the surface layer of impact craters, exhibit a broad asymmetric peak in the range 1400–1700 cm^{-1} and centered at approximately 1550 cm^{-1}. This confirms that the coatings are amorphous carbon as reported by other researcher [62].

In order to obtain quantitative information about the sp^3 content in the coatings, Raman spectra are considered a combination of D and G peaks by the Gaussian curves. The carbon peak is characterized by a large G peak close to 1550 cm^{-1} with a broad peak shoulder close to 1370 cm^{-1}. In the case of the amorphous carbon, "G" does not just mean graphite. The G mode arises from the stretching of any pair of sp^2 sites, whether in rings or chains. The D mode is the breathing mode of sp^2 sites in rings not chains [65]. The atomic bond structure of the coatings is characterized by I_D/I_G ratio and $FWHM_G$ values.

Some investigators have reported that the sp^3 content can be estimated from the variation of the I_D/I_G ratio with the sp^3 fractions [66-68]. A smaller value of the I_D/I_G ratio will correspond to higher sp^3 content and amorphization.

Further analysis of the structural changes in the DLC coating on the crater surfaces with impact cycles, is summarized in Fig. 3.2. Based on the graph's trend, the I_D/I_G ratio decreases with the increasing number of impact cycles, accompanied by a widening of $FWHM_G$, which correlates well to a higher sp^3 content with the increase of amorphization. This also suggests that the mechanical impact will destroy the larger resulting sp^2 clusters, which may be reduced in their organization in the larger stacks of sp^2 dense planes; therefore, no longer show any breathing modes.

According to Tamor and Vassell [64], the hardness of amorphous carbon films increases with an increasing $FWHM_G$. In addition, the hardness of the films is dependent on the sp^3/sp^2 ratios of the carbon bonding and the films with higher sp^3 should give higher hardness values [69]. From the graph in Fig. 3.2 (a) and (b), it is expected that the hardness of DLC coating on the crater surface also increases with the impact cycles and is pronouncedly harder than that of the as-deposited. Therefore,

Fig. 3.3 demonstrates that the hardness of DLC coating on the crater surface is increases with impact cycles regardless of maximum normal impact loads.

The increase in sp^3 content and hardness can be correlated to the reduction of surface roughness [69-70]. This is in accordance with this study, where the surface of impact crater is also smoother at the large impact cycles as shown in Fig. 3.4. The observation is taken from the centre of the impact crater after 10^2 and 10^5 impact cycles, for each maximum normal impact load. The rougher the surface, the more energy that has been dissipated during the plastic deformation and the more significant the indentation size effect (ISE) will be. This can be a cause of random scattering in hardness values, and their consequential decrease.

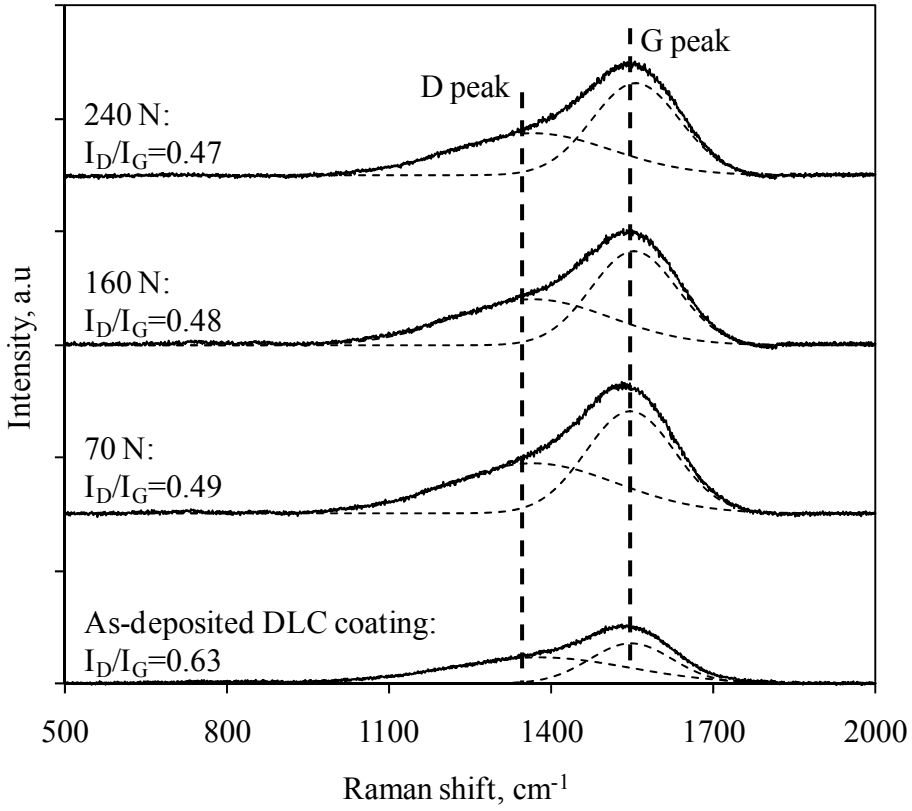

Fig. 3.1 Raman spectra of the DLC coating on the craters surface after 10^5 impact cycles under different maximum normal impact loads.

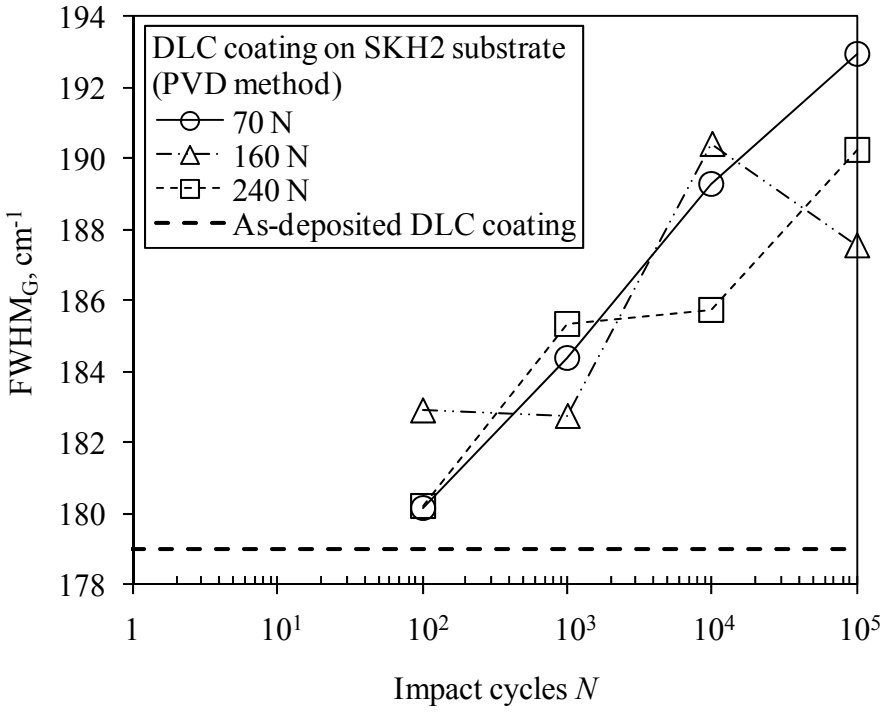

(a)

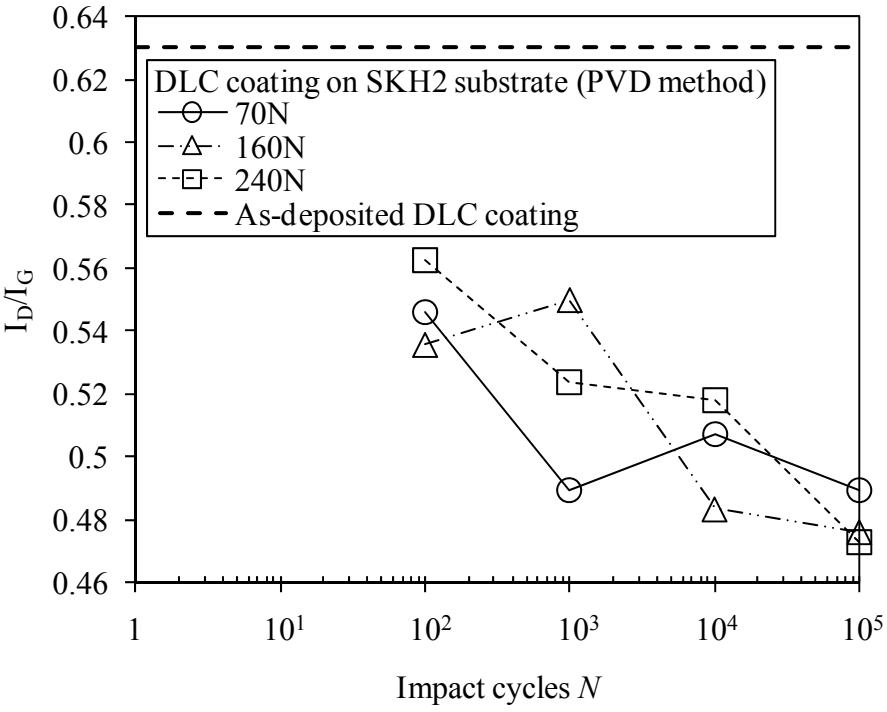

(b)

Fig. 3.2 Variation of (a) $FWHM_G$, and
(b) Raman intensity ratio I_D/I_G with impact cycles.

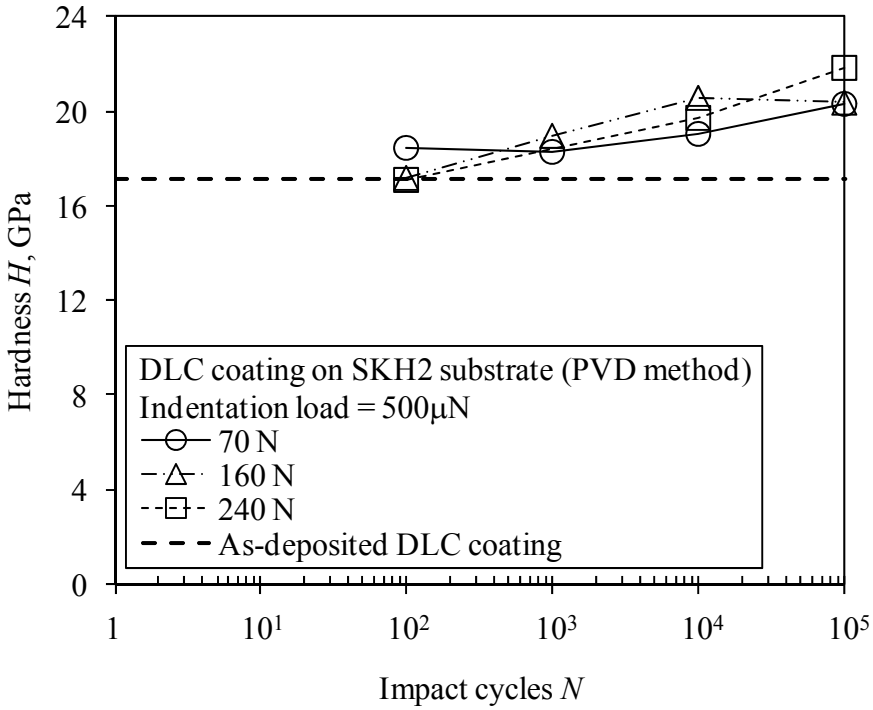

Fig. 3.3 Nanoindentation test at the surface of impact craters with respects to impact cycles.

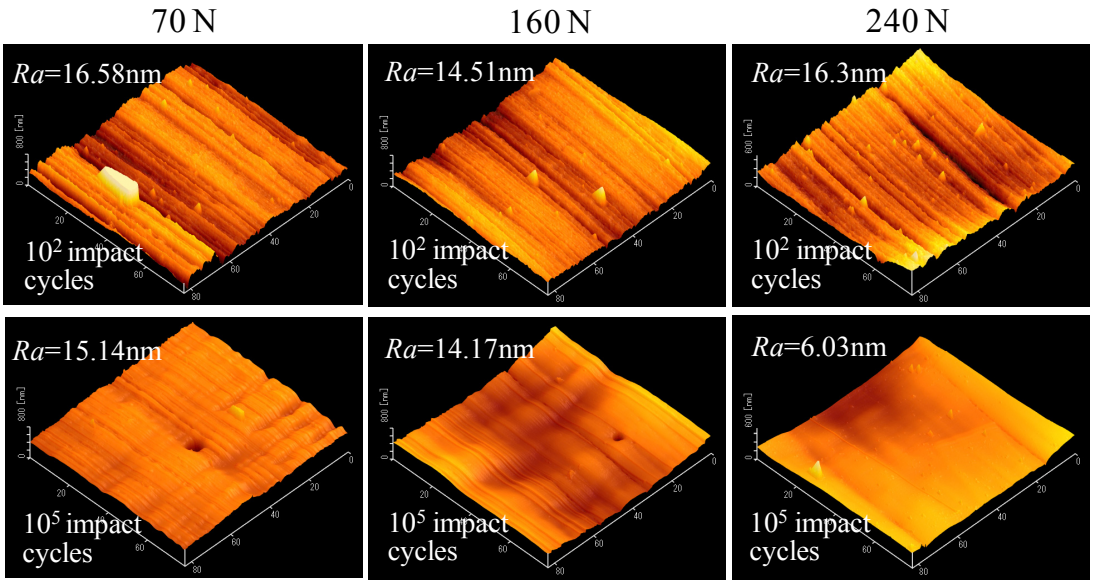

Fig. 3.4 AFM topography images at the surface of impact craters and its arithmetic average of surface roughness *Ra* under different maximum normal impact loads and impact cycles.

3.3.2 Phase transformation of wear debris and transfer layer

Fig. 3.5 (a) shows the affected area on SCM420 pins examined from the FE-SEM micrographs after numerous impacts under different maximum normal impact loads. The FE-SEM examination of affected areas revealed the transfer of material from the DLC coating surface to the mating SCM420 pin. Even after cleaning the pins ultrasonically in acetone to remove the loose particles and excess oil distributed on its surface, it was observed that an adherent layer still existed, as indicated by the dark contrasting material in the FE-SEM micrographs. The micrograph of the as-received SCM420 pin is shown in Fig. 3.5 (b) for comparison. The black areas show a transfer layer and verification by EDS analysis as shown in Fig. 3.9, where the elemental composition of the carbon element is slightly increased compared to the as-received.

The Raman spectra of the transfer layer at different impact cycles under 240 N of maximum normal impact load are summarized in Fig. 3.6. In the case of the continuous presence of oil lubricant, the generated debris have been combined to oil and removed progressively by its evacuation outside the impact crater, hence, no wear debris is observed inside it. However, some of the wear debris has transferred to the counterpart material as a transfer layer. Therefore, the Raman spectra of wear debris were only obtained from the debris on the edge of the impact crater as shown in Fig. 3.7. The FE-SEM micrograph of the wear debris is shown in Fig. 3.8.

A reasonable fit of the data for the Raman spectra of the transfer layer and wear debris could not be obtained using a single Gaussian line shape, and it was necessary to include in the fit a second and third Lorentzian centered at about 680 cm^{-1} and 1317 cm^{-1}, respectively. However, the broad peak at about 1350 cm^{-1}, which is probably due to the disordered graphite (D peak), overlapped with the α-Fe_2O_3 peak at 1317 cm^{-1}. Thus, the D peak is not clearly visible in Fig. 3.6 and Fig. 3.7. The ratio intensity of the α-Fe_2O_3 peak (namely F peak) to the G peak (I_F/I_G) of the wear debris at maximum normal impact loads of 70 N, 160 N and 240 N is about 0.78, 0.88, and 0.92, respectively. This implies that the amount of the disordered graphite phase (D peak) is slightly increased.

It is proven as shown in the Raman spectra taken from the wear debris that the G peak has shifted to a higher frequency compared to as-deposited. It begins at a 160 N maximum normal impact load. Therefore, it means that the sp^2 bonding fraction increases, partial tetrahedral bonds have been broken and have transformed to trigonal bonds [71]. With the increasing of the maximum normal impact load, the decrease in the $FWHM_G$ indicated the removal of a bond angle disorder and the increasing dominance crystallites [71]. From the analysis above, the sp^2 coordinated carbon becomes gradually dominant with the increasing maximum normal impact load and causes phase transformation from sp^3 to sp^2, which would induce graphitization.

There would be a sufficient temperature rise during impact. This could be due to the fact that some of the lost energy goes into heating up the impacted surface. High temperature can promote the transformation of the thermodynamically meta-stable bonding structure (sp^3) into the more stable graphite-like structure (sp^2). However, in this study, the rise of temperature is believes not as high as a graphitization temperature of DLC approximately 300^{o}C [72] since the impact test was performed at room temperature. According to Zhou et al. [62] and Haque et al. [73], the graphitization temperature decreases when contact pressure increases. The contact pressure exerted by the counter body on the DLC coating is not just only corresponding to the applied maximum normal impact load. A high contact pressure may also be developed by the presence of oil lubricant on the contact surface of the DLC coating. It was shown both theoretically and experimentally by Christensen [74] that the maximum contact pressure was significantly larger than the corresponding ones produced under Hertzian, dry contact impacts. A small increase in load will produce a large increase in maximum pressure. For this reason, it seems that graphitization occur at a high contact pressure due to low graphitization temperature during impact.

As mentioned earlier, the transfer layer mainly comes from the wear debris. Therefore, it is expected that the graphitization is also occurred in the transfer layer due to a small shift of G peak, as shown in Fig. 3.6. However a widening of its $FWHM_G$ after 10^5 impact cycles at the maximum normal impact load of 240 N

suggest the size of the larger sp^2 clusters is reduced due to the mechanical crush of the larger sp^2 clusters.

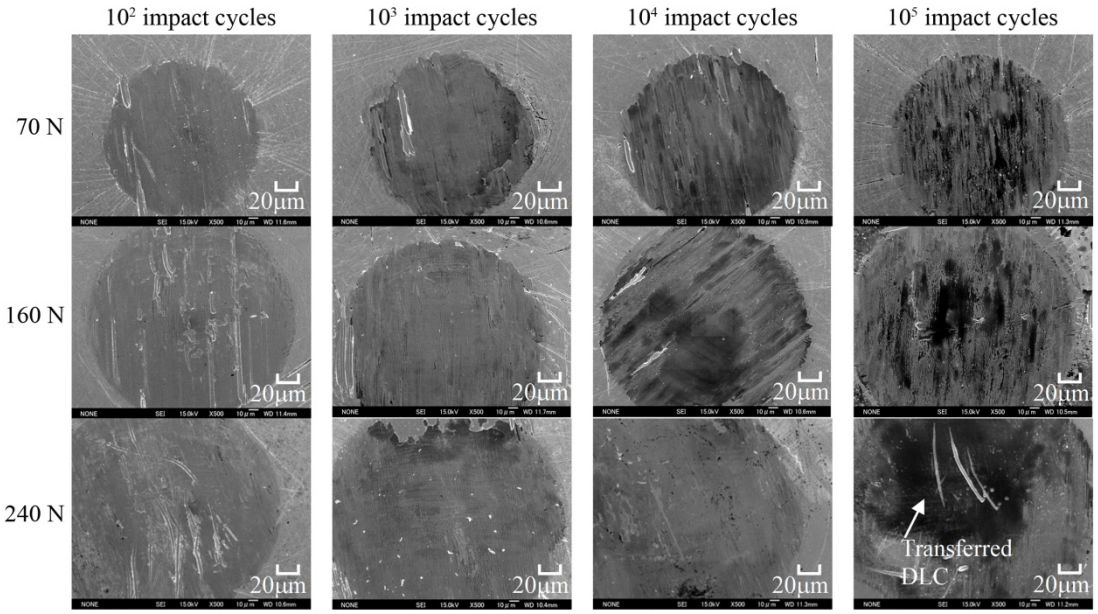

(a)

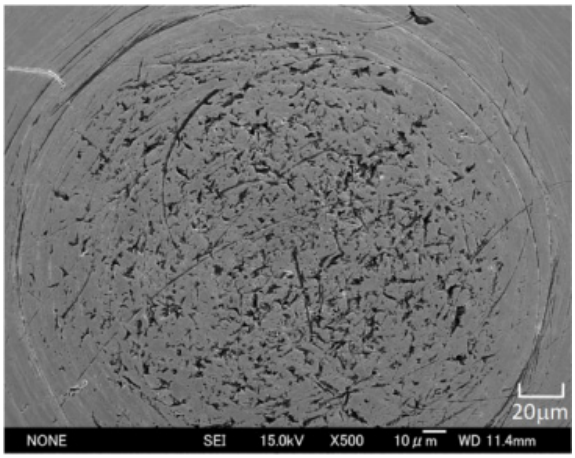

(b)

Fig. 3.5 FE-SEM micrographs of the affected area on the SCM420 pins (a) under different maximum normal impact loads and impact cycles, and (b) as-received.

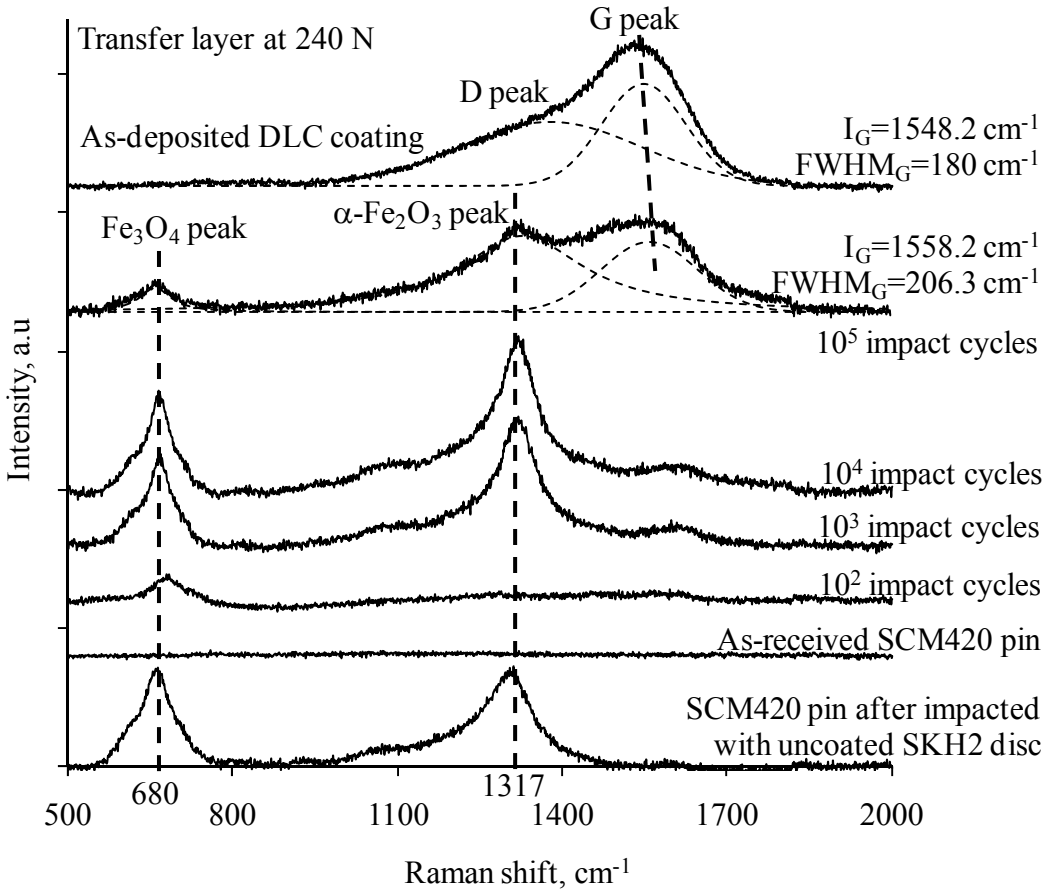

Fig. 3.6 Raman spectra of the transfer layer on the affected area of the SCM420 pins under different impact cycles at a maximum normal impact load of 240 N.

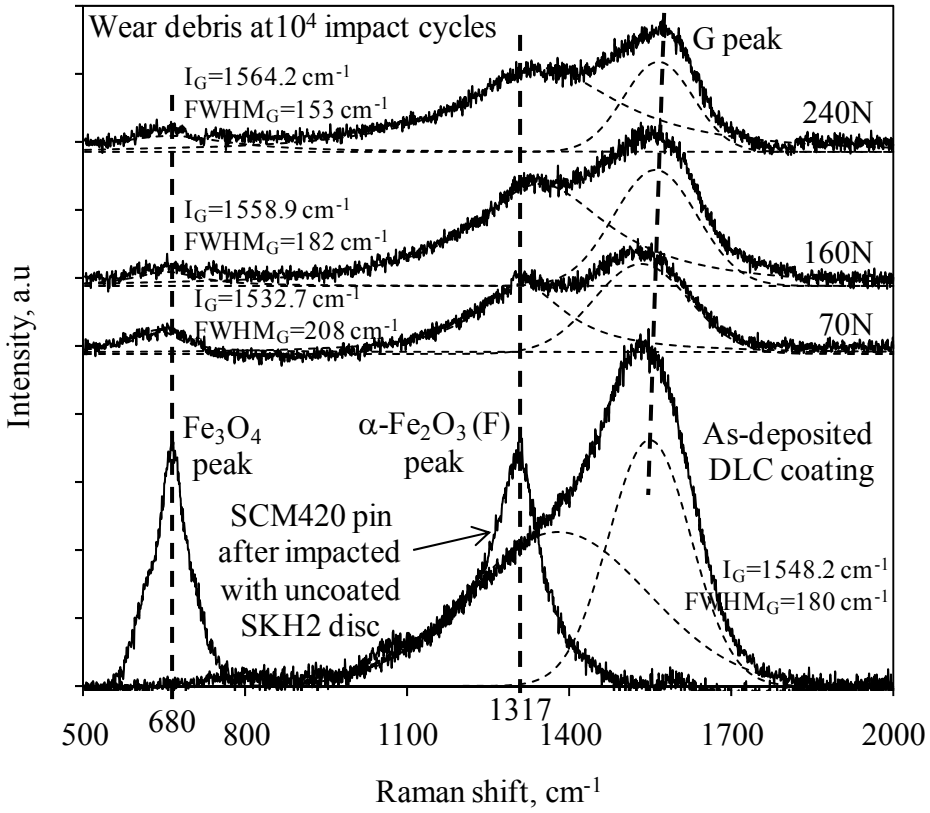

Fig. 3.7 Raman spectra of the wear debris under several maximum normal impact loads after 10^4 impact cycles.

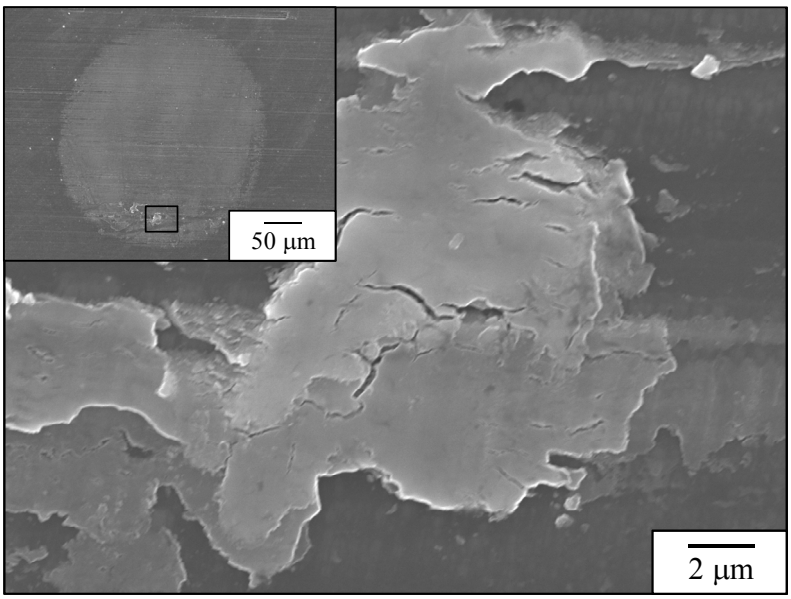

Fig. 3.8 FE-SEM micrograph of the wear debris taken from the edge of impact crater. The top left micrograph is an impact crater.

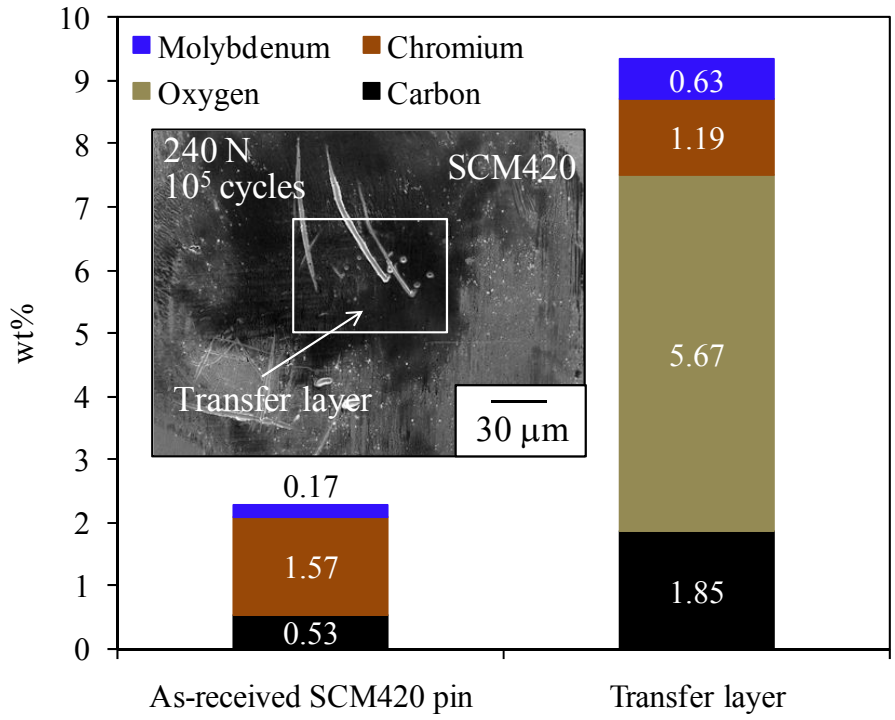

Fig. 3.9 EDS elemental composition (within a small rectangle on the FE-SEM micrograph) of the transfer layer on the affected area of the SCM420 pin after 10^5 impact cycles at 240 N and compared with the as-received.

3.3.3 Oxidation of iron (Fe) in the wear debris and transfer layer

Also noticeable in the Raman spectra of both transfer layer and wear debris (Figs. 3.6 and 3.7) is an additional peak at approximately 680 cm^{-1}. However, a sharp peak at approximately 1317 cm^{-1} of the transfer layer and wear debris is believed not to have come from the disordered graphite (D peak). This is because these two predominant peaks also appeared when the uncoated SKH2 disc, was impacted by the SCM420 pin after several impact cycles. Since the impact test was performed under the atmospheric conditions, these peaks are corresponding to the magnetite (Fe_3O_4) and hematite (α-Fe_2O_3) phases, as described by Lübbe et al. [75].

Firstly, only Fe_3O_4 is formed at low impact cycles and not so much of the DLC phase was detected. However, after several impact cycles, the Raman spectrum shows a mixture of Fe_3O_4 and α-Fe_2O_3 phases and the G peak gradually appeared. Subsequently, the intensity of the Fe_3O_4 and α-Fe_2O_3 peaks is reduced and the spectrum appeared to be similar to that of the DLC phase. This result shows that the oxidation of Fe, either in the wear debris/transfer layer or pin surface, occurred during impacting. Since the impact test was performed under atmospheric conditions, the existence of the oxide phase could be associated with the oxidation of Fe with the environment. It is well known that the oxidation of Fe in wear debris and transfer layer with the environment also takes place during the sliding test [58],[63].

To clarify the existence of an oxide element on the transfer layer, the elemental compositions were analyzed using EDS. The elemental composition data collected for the transfer layer on the affected area of SCM420 pin after 10^5 impact cycles at 240 N and compared with the as-received is shown in Fig. 3.9. The results show that the elemental composition of an oxide element exists in the transfer layer. This is consistent with the Raman analysis, as shown in Fig. 3.6.

3.4 Conclusions

As the maximum normal impact load is increasing, the G peak of the Raman spectra of wear debris, together with the narrowing of its peak width, is shifting towards higher frequencies. This suggests an increasing order and an enlargement of the sp^2 cluster. These structural modifications are induced during the impact test, causing a transformation of the sp^3 sites into sp^2 sites and these are closely related with the graphitization process. As expected, the phase transformation also takes place in the transfer layer since it is mainly coming from the wear debris, where the graphitization occurs. Since the impact test was performed at room temperature, it has been suggested that pressure-induced graphitization.

However, the mechanical impact may destroy and reduce the size of larger sp^2 clusters; therefore, no longer show any breathing modes. This is evidently shown from the Raman spectra of DLC coating on the crater surface, where the I_D/I_G ratio decreases approximately from 0.63 (as-deposited) to 0.47 (after 10^5 impact cycles), accompanied by a widening of $FWHM_G$ (approximately from 179 cm^{-1} to 192 cm^{-1}) with impact cycles. Therefore, the DLC coating on the crater surface tends to have higher sp^3 fractions. Besides, the hardness reaches approximately to 21 GPa, higher than as-deposited (17.14 GPa) after several impact cycles.

Since the impact test was performed under atmospheric conditions, other features observed in the Raman spectra of the transfer layer and wear debris can be attributed to the formation of iron oxides by the oxidation of Fe with the environment after several impact cycles. These peaks approximately centered at 680 cm^{-1} and 1317 cm^{-1} and evidently came from the Fe_3O_4 and α-Fe_2O_3 phases, respectively.

References

[55] J. Robertson, Diamond-like amorphous carbon, Mater. Sci. Eng., R. 37 (2002) 129-281.

[56] J. Robertson, Mechanical properties and coordinations of amorphous carbons, Phys. Rev. Lett. 68 (1992) 220-223.

[57] D. Sheeja, B.K. Tay, S.P. Lau, X. Shi, X. Ding, Structural and tribological characterization of multilayer ta-C films prepared by filtered cathodic vacuum arc with substrate pulse biasing, Surf. Coat. Technol. 132 (2000) 228-232.

[58] S.J. Park, K.R. Lee, D.H. Ko, Tribological behavior of nano-undulated surface of diamond-like carbon films, Diam. Relat. Mater. 14 (2005) 1291-1296.

[59] J.X. Liao, L.F. Xia, M.R. Sun, W.M. Liu, T. Xu, Q.J. Xue, The tribological properties of a gradient layer prepared by plasma-based ion implantation on 2024 aluminum alloy, Surf. Coat.Technol.183 (2004) 157-164.

[60] Y. Liu, A. Erdemir, E.I. Meletis, A study of the wear mechanism of diamond-like carbon films, Surf. Coat. Technol. 82 (1996) 48-56.

[61] Y. Liu, E.I. Meletis, Evidence of graphitization of diamond-like carbon films during sliding wear, J. Mater. Sci. 32 (1997) 3491-3495.

[62] Z.F. Zhou, K.Y. Li, I. Bello, C.S. Lee, S.T. Lee, Study of tribological performance of ECR–CVD diamond-like carbon coatings on steel substrates: Part 2. The analysis of wear mechanism, Wear 258 (2005) 15891599.

[63] J.C. Sánchez-López, A. Erdemir, C. Donnet, T.C. Rojas, Friction-induced structural transformations of diamondlike carbon coatings under various atmospheres, Surf. Coat. Technol. 163–164 (2003) 444-450.

[64] M.A. Tamor, W.C. Vassell, Raman "fingerprinting" of amorphous carbon films, J. Appl. Phys. 76 (1994) 3823-3830.

[65] J. Filik, Raman spectroscopy: A simple, non-destructive way to characterise diamond and diamond-like materials, Spectrosc. Eur. 17 (2005) 10-17.

[66] A.C. Ferrari, J. Robertson, Interpretation of Raman spectra of disordered and amorphous carbon, Phys. Rev. B. 61 (2000) 14095-14107.

[67] S. Prawer, K.W. Nugent, Y. Lifshitz, G.D. Lempert, E. Grossman, J. Kulik, I. Avigal, R. Kalish, Systematic variation of the Raman spectra of DLC films as a function of sp^2:sp^3 composition, Diamond Relat. Mater. 5 (1996) 433-438.

[68] B.K. Tay, X. Shi, H.S. Tan, H.S. Yang, Z. Sun, Raman studies of tetrahedral amorphous carbon films deposited by filtered cathodic vacuum arc, Surf. Coat. Technol. 105 (1998) 155-158.

[69] Q. Jun, L. Jianbin, W. Shinzu, W. Jing, L. Wenzhi, Mechanical and tribological properties of non-hydrogenated DLC films synthesized by IBAD, Surf. Coat. Technol. 128–129 (2000) 324-328.

[70] W.G. Jiang, J.J. Su, X.Q. Feng, Effect of surface roughness on nanoindentation test of thin films, Eng. Fract. Mech. 75 (2008) 4965-4972.

[71] J.T. Jiu, H. Wang, C.B. Cao, H.S. Zhu, Effect of annealing temperature on the structure of diamond-like carbon films by electrodeposition technique, J. Mater. Sci. 34 (1999) 5205-5209.

[72] H. Ronkainen, K. Holmberg, in: C. Donnet, A. Erdemir (Eds.), Tribology of Diamond-like Carbon Film: Fundamentals and Applications, Springer, New York, (2008) 155.

[73] T. Haque, A. Morina, A. Neville, R. Kapadia, S. Arrowsmith, Effect of oil additives on the durability of hydrogenated DLC coating under boundary lubrication conditions, Wear 266 (2009) 147-157.

[74] H. Christensen, The oil film in a closing gap, Proc. R. Soc. Lond. Ser. A. Math. Phys. Sci. 266 (1962) 312-328.

[75] M. Lübbe, A.M. Gigler, R.W. Stark, W. Moritz, Identification of iron oxide phases in thin films grown on Al_2O_3(0 0 0 1) by Raman spectroscopy and X-ray diffraction, Surf. Sci. 604 (2010) 679-685.

Chapter 4

Deformation-wear transition map of DLC coating under cyclic impact loading

4.1 Introduction

The concept of a ‘wear map’ was first discussed by Tabor [76], and was inspired by the pioneering work of Frost [77] on ‘deformation maps’. The development of deformation-wear transition maps is a useful way to study and predict the transition of deformation to wear of one material impacting against another at different operating parameters. Furthermore, the locations of the transition zones within the operating parameters are important, in order to design engineer less component failures occurring prematurely.

Generally, the construction of transition maps follows two routes [78-79]. One is empirical: data from experiments are plotted on suitable axes and identified by wear rate or observation and boundaries are drawn to separate classes of behavior. The other route is that of physical modeling: model-based equations, describing the wear rate caused by each mechanism, are combined to give a map showing the total rate, and the field of dominance of each. However, only the empirical approach is used in this study.

The wear transition maps specific to certain materials, such as ceramics [80], grey cast iron [81], magnesium alloy [82], brass alloy [83], silicon nitride [84], and so on, have been developed extensively for a decade. All the transition maps, which appear in the above studies, were constructed using either a physical modeling or an empirical approach based on the sliding test data. However, in this century, there is still no development of deformation-wear transition map of the DLC coating under cyclic impacts. From the previous results in Chapters 2 the dominant factor that affects the deformation of DLC coating is the maximum normal impact load. Besides, in Chapter 3, it has been suggested that pressure-induced graphitization after repeated impacts. Therefore, the aim of this chapter is to propose a deformation-wear transition map of DLC coating based on variations of maximum normal impact loads

and impact cycles. This empirical-based transition map is intended to graphically distinguish between the plastic deformation and impact wear of DLC coating as well as to predict its transition points for future design purposes. After a short description of the impact test used in this study, the construction of the deformation-wear transition map will be presented using experimental data and observations.

4.2 Experimental method

4.2.1 Impact testing

The impact test was performed using two self-developed impact testers. The horizontal impact tester[§] was used for more than 10^2 impact cycles, with a frequency of 10 Hz; and a drop-weight impact tester was used for low impact cycles as shown in Fig. 4.1.

All materials and impact testing procedures are same as in the Section 2.2, excluding a high speed camera. Several different maximum normal impact loads were applied to the DLC coated disc via a spring system for the horizontal impact tester. Meanwhile, the maximum normal impact load of the drop-weight impact tester could be increased by adding an impactor mass m. It has been reported that the impactor mass does not significantly affect impact performances [43]. This is also in agreement with this study that has been described in Section 2.4.3. The impact test was performed under 1~10^5 impact cycles.

The surface morphology of the affected area on the DLC coating, as well as on the counterpart material, was observed by AFM, FE-SEM, and EDS. In addition, the FIB was used to mill the tested sample, in order to examine the cross section of the DLC coating on the SKH2 substrate. Furthermore, the residual impact crater volume, V_r is determined using Eq. (2.1).

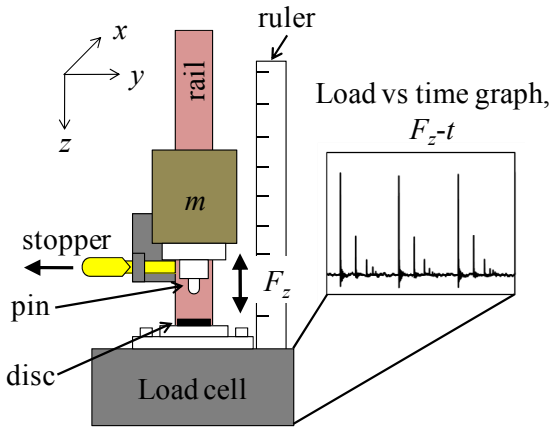

Fig. 4.1 Schematic illustration of the drop-weight impact tester.

[§] The horizontal impact tester is described in Section 2.2.2

4.2.2 Transition of contact pressure

As previously discussed in Section 2.4.2, the mechanical response of the coating system to normal load is controlled by the SKH2 substrate. Besides, it is assumed that the pin has negligible wear such as that no change in its radius takes place. Therefore, mean contact pressure p_{mean} is expressed as [53]:

$$p_{mean} = \frac{2}{3}\left(\frac{6F_z E^2}{R'^2 \pi^3}\right)^{1/3} = \frac{F_z}{\pi a^2} \tag{4.1}$$

where

$$\frac{1}{E} = \frac{1-v_p{}^2}{E_p} + \frac{1-v_d{}^2}{E_d} \tag{4.2}$$

$$\frac{1}{R'} = \frac{1}{R} - \frac{1}{r_r} \tag{4.3}$$

$$a = \left(\frac{3F_z R'}{4E}\right)^{1/3} \tag{4.4}$$

By assuming that contact condition is to be a point contact and by using the major (y) axis and minor (x) axis of the residual contact radius, which obtained experimentally for i impact cycle, the Eq. (4.1) becomes:

$$p_{mean,i} = \frac{F_z}{\pi\left(a_{ry} a_{rx}\right)_i} \tag{4.5}$$

Take note that the above equations are based on the Hertzian model. In reality, however, the response of the SKH2 substrate to impact is elasto-plastic. Therefore, in this study, p_{mean} is an approximation of the contact pressure.

4.2.3 Wear measurements

In this present study, wear can be defined simply as material lost that generates wear debris and/or detaches to the counterpart material by cyclic impact loading. In order to determine the wear depth of the DLC coating, its cross section on the SKH2 substrate was prepared using a FIB and observed by FE-SEM. The tested sample was milled along the centre of the impact crater of the major axis. The difference between the non-impacted and impacted film thickness of the DLC coating is directly measured the wear depth h_w, as shown in Fig. 4.2. From Fig. 4.3, it is assumed that the wear depth is constant throughout the contact surface; and thus:

$$h_p = h_r - h_w \tag{4.6}$$

Where, h_p is the plastic deformation depth and h_r is the residual depth of impact crater.

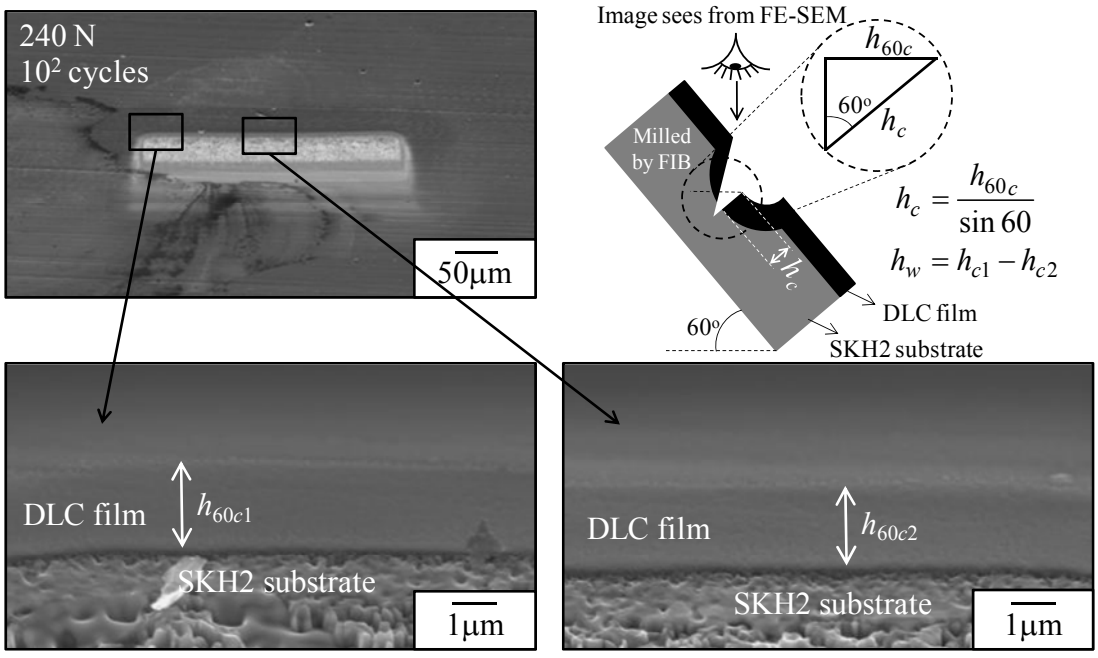

Fig. 4.2 FE-SEM cross-sectional view of the FIB-milled DLC coating on the SKH2 substrate (tilted at 60°); where h_{60c1} is the non-impacted film thickness, and h_{60c2} is the impacted film thickness. The equations at the top right are for the wear depth h_w calculation.

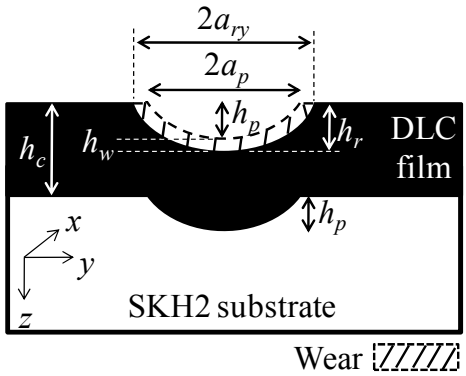

Fig. 4.3 Schematic illustration of the wear depth h_w.

4.2.4 Construction of the deformation-wear transition map

No universal deformation-wear transition map exists, because the controlling variables differ from mechanism to mechanism. Therefore, suitable axes of the map have to be decided. In this study, the appropriate axes are determined to be the maximum normal impact load F_z and the impact cycles N. These independent variables were chosen for two reasons: firstly, they directly determine the residual impact crater volume; and secondly, they are under the control of the operator, and easily measured.

All data points of the residual impact crater volume V_r are plotted as functions of F_z and N, as shown in Fig. 4.4. Some interpolations and extrapolations are needed to obtain an evenly distributed data set. Then, the locations of both load- and impact cycle-dependent deformation-wear transitions, are identified by experimental observations and data trend analysis. Arrows indicate the onset of these variable-dependent deformation-wear transitions. The best fitting curves connecting all of the transition points are then traced and illustrated in the graph of F_z vs. N, as shown in Fig. 4.5. These curves represent the deformation-wear transition boundary of the impacted DLC coating.

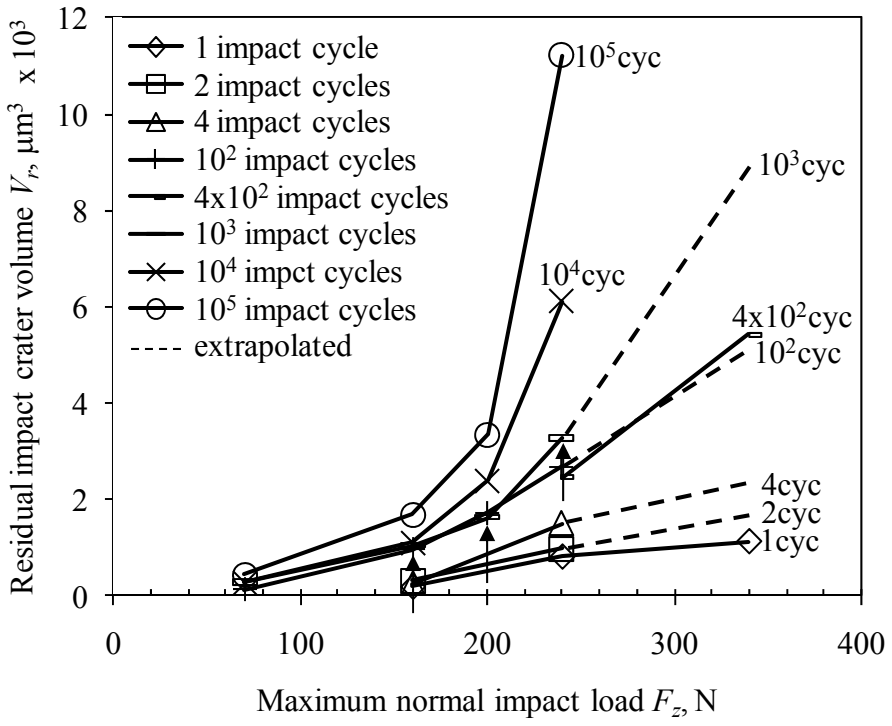

(a)

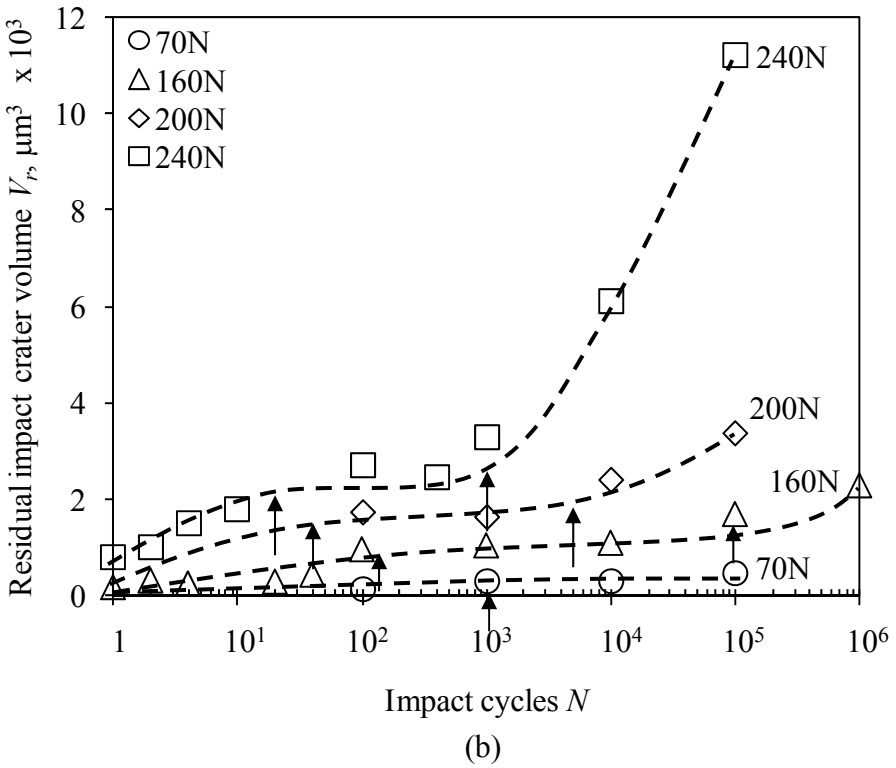

(b)

Fig. 4.4 Residual impact crater volume of the impacted DLC coating, plotted as a function of (a) maximum normal impact load, and (b) impact cycles.
(Arrows indicate the onset of load/cycle-dependent deformation-wear transitions)

4.3 Results and discussion

4.3.1 Deformation-wear transition map

The maximum normal impact load and impact cycles are both important parameters and either variable can induce a transition from deformation to wear of DLC coating, as shown in Fig. 4.4. Therefore, a deformation-wear transition map was generated for the DLC coating by simultaneously varying the maximum normal impact load and impact cycles, which revealed this transition very well.

From Fig. 4.5, three main transition zones that graphically distinguish between the plastic deformation and impact wear of DLC coating were identified: (i) Plastic deformation of the substrate, (ii) suppression of plastic deformation of the substrate and (iii) wear of the DLC coating.

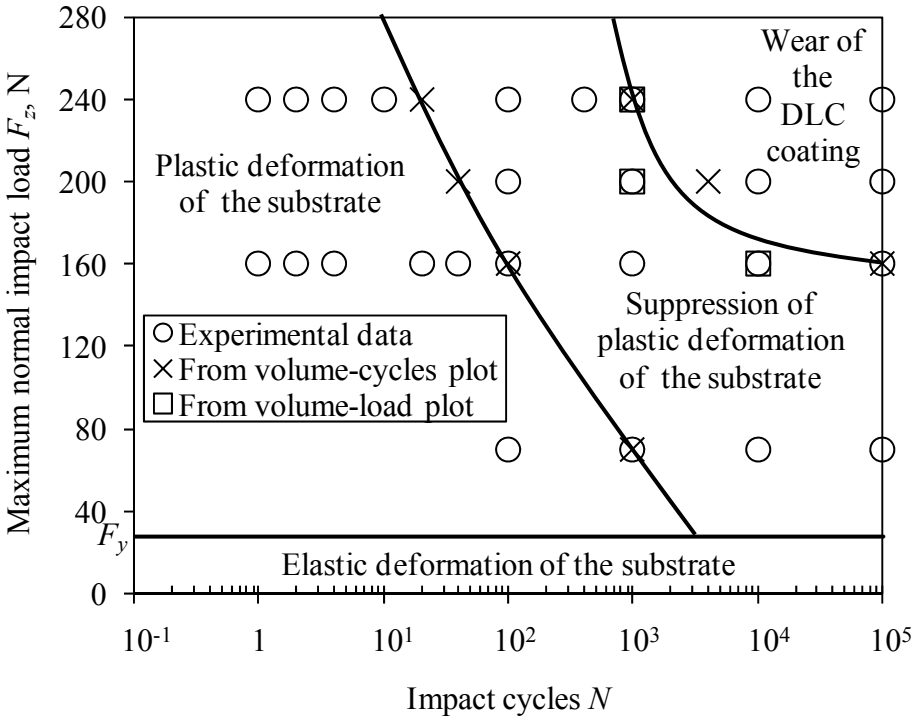

Fig. 4.5 Deformation-wear transition map of DLC coating under cyclic impact loading.

4.3.1.1 Plastic deformation of the substrate zone

The definition of plastic deformation of the substrate zone is the region beyond the elastic zone associated with crater formation, where the residual impact crater volume changes with the maximum normal impact load and impact cycles, as shown in Fig. 4.4. As demonstrated in previous experiment in Section 2.4.2, the deformation of an elastic-perfect plastic substrate should not be altered by the presence of a thin film, which itself simply follows the deformation of the substrate at the interface. The strain in the film is governed by the surface strain of the substrate. Furthermore, Fig. 4.6 clearly shows that almost no wear of DLC coating is observed at 70 N and 160 N of the maximum normal impact load. In addition, the wear depth is almost zero at 200 N and 240 N under low impact cycles. This therefore reveals that only plastic deformation of the substrate has occurred.

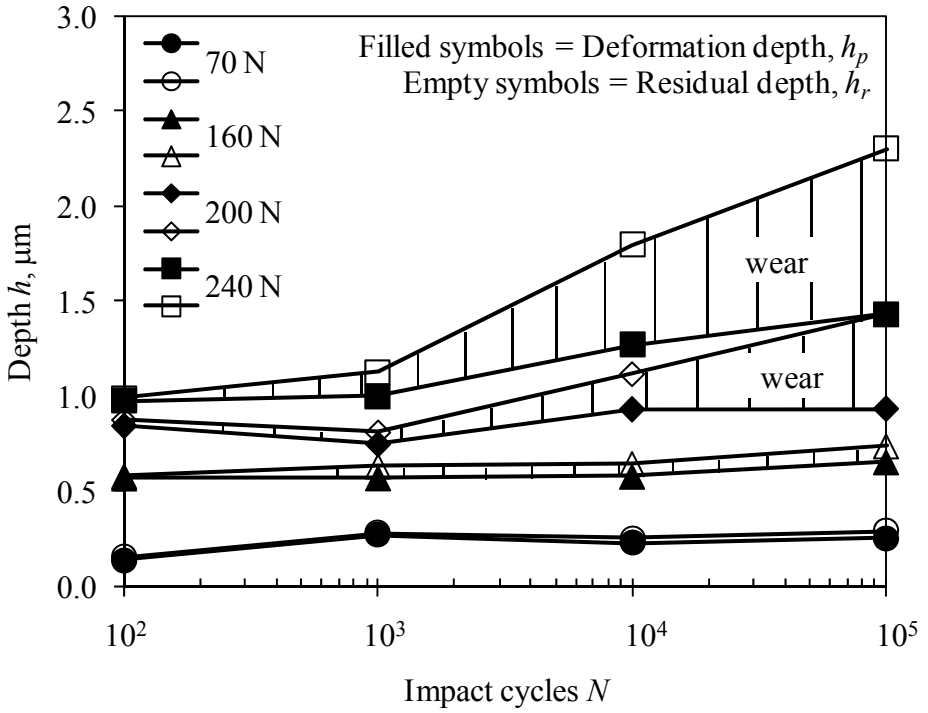

Fig. 4.6 Comparison of the residual depth of the impact crater h_r and the plastic deformation depth h_p as a function of the impact cycles. The difference between both curves (patterned in vertical lines) gives the approximate wear depth of the DLC coating.

4.3.1.2 Suppression of plastic deformation of the substrate zone

The suppression of plastic deformation of the substrate occurs when the residual impact crater volume remains constant with the impact cycles, as shown in Fig. 4.4. This is due to the decreasing contact pressure with impact cycles to the yield point, as shown in Fig. 4.7. As the number of impact cycles is increased, the contact area spreads. Additionally, this experiment was under the constant maximum normal impact load for each impact cycle, and therefore, the contact pressure is decreased. In this zone, the deformation of substrate is most likely to undergo an elastic deformation if the contact pressure is almost or below its yield point. From Fig. 4.5, by increasing the maximum normal impact load, the suppression of plastic deformation of the substrate taking place, is faster. At 240 N of maximum normal impact load, the plastic deformation of the substrate is suppressed after 10^1 impact cycles, because the contact pressure starts to approach the yield point, as shown in Fig. 4.7. However, the plastic deformation of the substrate at 160 N starts to suppress after 10^2 impact cycles for the same reason.

In this zone, the hardness of the DLC coating on the crater surface is harder than as-deposited. This is due to the higher sp^3 content after numerous impacts as previously discussed in Section 3.3.1. Besides, almost no wear of DLC coating is observed, as shown in Fig. 4.6.

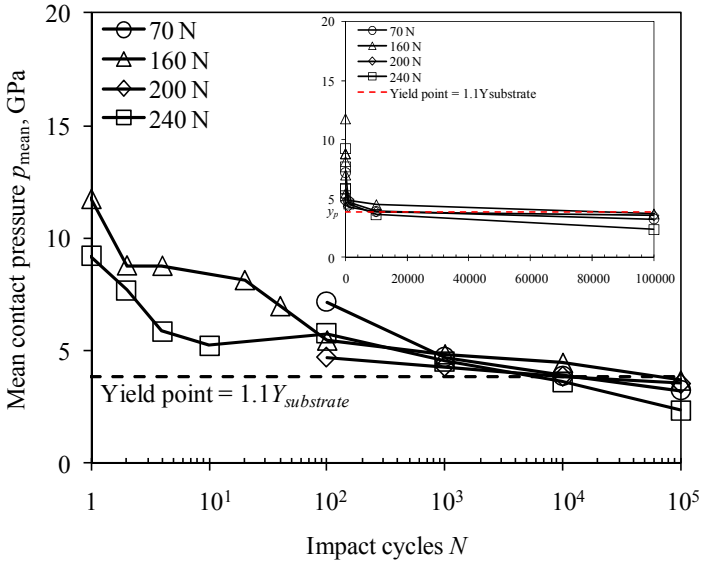

Fig. 4.7 Relationship between mean contact pressure and impact cycles.

4.3.1.3 Wear of the DLC coating zone

Wear transition of the DLC coating begins when the residual impact crater volume increases rapidly/radically with the maximum normal impact load and impact cycles, as shown in Fig. 4.4. According to the previous researches [1],[39], the endurance limit of the DLC coating depending on the normal impact load. This is in accordance with this study, where a critical maximum normal impact load and a critical impact cycle exist that will precipitate the wear transition of the DLC coating. Moreover, at those critical impact loads and impact cycles, wear gradually rises as material is worn away. This can be verified by a wear depth data collection, as shown in Fig. 4.6. No wear occurs if the maximum normal impact load is very small but a wear transition occurs (due to the impact cycles) when the maximum normal impact load reaches above 160 N, as shown in Fig. 4.5. The DLC coating on SKH2 substrate achieves extremely high resistance to impact loading (F_z > 240N) at a low number of impacts ($N < 10^3$).

Generally, a significant temperature rise during impact may result at the contact point due to the energy lost. The graphitization would be expected to be found at a temperature greater than a graphitization temperature of DLC approximately 300^{o}C [72]. Then, some of this graphitic material, which was produced as wear debris, transfers to the counterpart materials as a transfer layer and may ascribe to the adhesive wear. This type of degradation were also observed experimentally in this zone even though the hardness of the DLC coating on the crater surface is harder than as-deposited after numerous impacts, as previously discussed in Section 3.3.1. The graphitization of transfer layer, as well as the wear debris, was confirmed by the Raman spectroscopy study. Besides, the existence of carbon element on the affected area of the SCM420 pin was verified by EDS maps[**], as shown in Fig. 4.8. From Fig. 4.9, the G peak of the transfer layer and wear debris shifted to a higher frequency compared to the as-deposited DLC coating. Therefore, this means that the sp^2 bonding fraction increases, partial tetrahedral bonds have been broken, and have transformed into trigonal bonds [71]. The decrease in the $FWHM_G$ indicated the removal of a bond angle disorder and the increasing dominance of crystallites [71]. From the analysis above, the sp^2 coordinated carbon becomes

[**] The EDS elemental composition can be found in Fig. 3.9

gradually dominant and causes phase transformation from sp^3 to sp^2, which would induce graphitization. However, in this study, the rise of temperature is believes not as high as a graphitization temperature of DLC since the impact test was performed at room temperature. According to Zhou et al. [62] and Haque et al. [73], the graphitization temperature decreases when contact pressure increases. The contact pressure exerted by the counter body on the DLC coating is not just only corresponding to the applied maximum normal impact load. A high contact pressure may also be developed by the presence of oil lubricant on the contact surface of the DLC coating. It was shown both theoretically and experimentally by Christensen [74] that the maximum contact pressure was significantly larger than the corresponding ones produced under Hertzian, dry contact impacts. A small increase in load will produce a large increase in maximum pressure. For this reason, it has been suggested that pressure-induced graphitization during impact.

In addition, as the thin hard coating fully transmits the impact generated stress field to the ductile substrate, the substrate undergoes a large plastic deformation (large indent depth) that the coating cannot accommodate other than by developing a network of cracks. Radial cracks can therefore be observed in the DLC film, as shown in Fig. 4.10. This micrograph has been taken after 10^4 impact cycles at 240 N, using FE-SEM. Radial cracking is observed in the coating below the impaction, which initiates from the coating/substrate interface and propagates upwards into the coating. The radial cracks observed in this study have also been identified in a study on indentation and scratching [85]. Tensile radial stresses (σ_{yyt}) concentrations at the coating/substrate interface during loading have been identified as a driving force that causes this type of crack [86-87], as illustrated in Fig. 4.11.

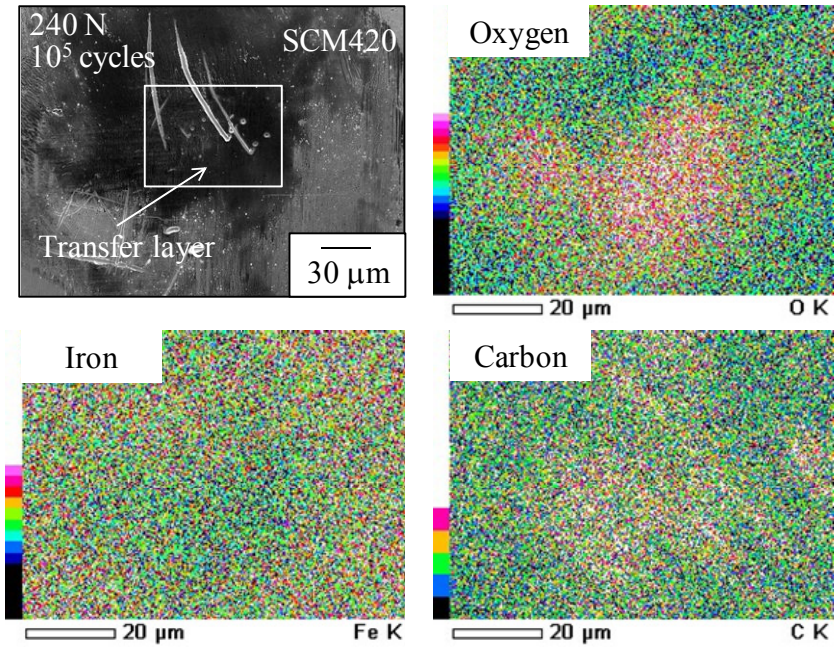

Fig. 4.8 The EDS maps (within a small rectangle in the FE-SEM micrograph) of the transfer layer on the affected area of the SCM420 pin

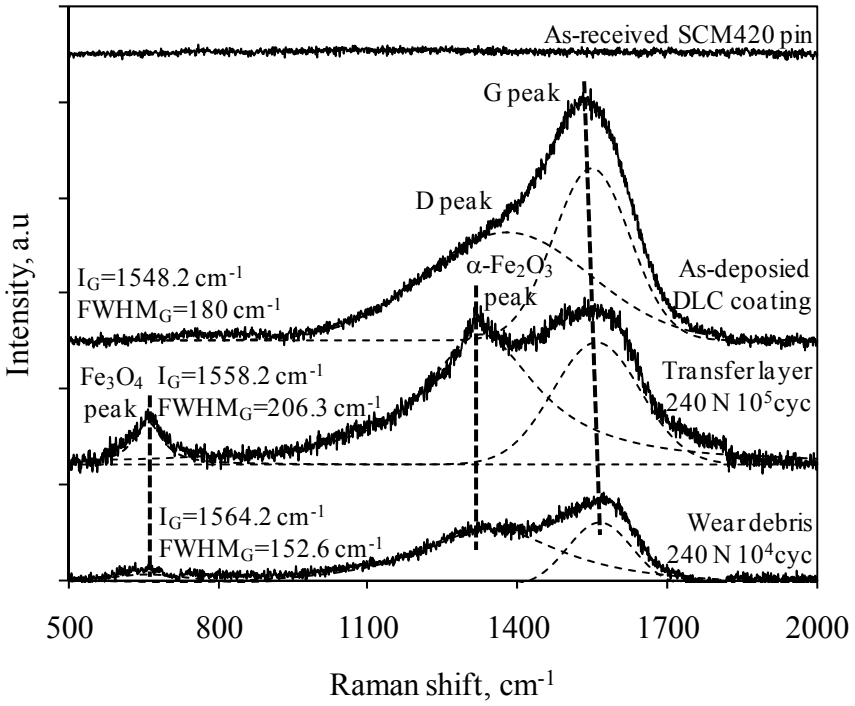

Fig. 4.9 Raman spectrum of the wear debris and transfer layer after 10^4 and 10^5 impact cycles at 240 N, respectively. The Raman spectrum of the as-received SCM420 pin and the as-deposited DLC coating are for comparison.

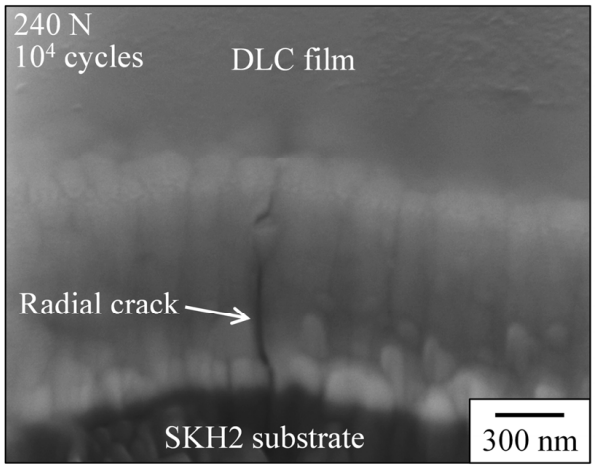

Fig. 4.10 The FE-SEM cross-sectional view of the FIB-milled DLC coating on the SKH2 substrate shows radial crack formation in the impacted area of the DLC film after 10^4 impact cycles at 240 N.

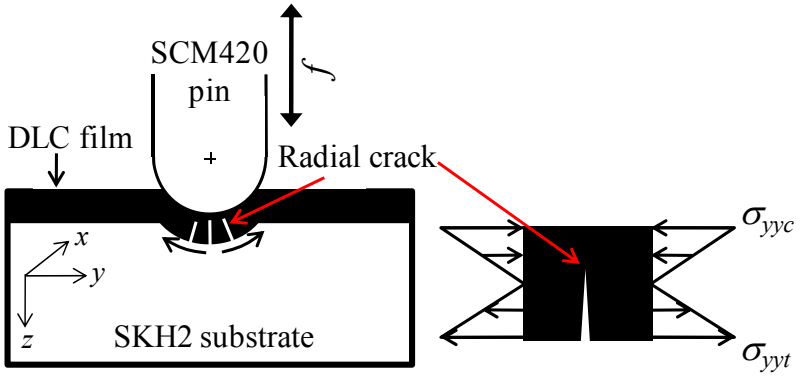

Fig. 4.11 Illustration of the formation of radial crack.

4.3.2 Future developments of deformation-wear transition map

The transition map in this study is originally developed in an attempt to distinguish more clearly between the plastic deformation and impact wear of DLC coating as well as to predict its transition points under the controlled variables such as pin radius, coating thickness, substrate material, environmental conditions and etc. So far, the present goal has been successfully met to fully map out the material transitions under different maximum normal impact loads and impact cycles.

A single universal parameter to fit all the data has been demonstrated to be unrealistic. But one may ask if such a parameter(s) exists in each transition zone. This question will remain unanswered. In the case of normal impact, besides the maximum normal impact load, there are still a lot of parameters that would induce to the material loss.

One of the promising parameters is the contact pressure. Fig. 4.12 shows the comparison of residual depth of crater obtained at all three loads used in this study with two different pin radii. The applied loads of 70, 160, and 240 N correspond to the nominal mean Hertzian contact pressure p_{mean} of 3.9, 5.1, and 5.9 GPa, respectively for pin radius of 1.5 mm. However, for pin radius of 1 mm, the p_{mean} reaches to 5.1, 6.7, and 7.7 GPa, respectively. This parameter is based on the Hertzian model for an ideal ball-on-flat contact geometry. However, the loading conditions beyond the elastic limit and Hertzian model is not strictly applicable. Therefore, in this study, p_{mean} is an approximation of the contact pressure. It is obvious that the residual depth of crater increases more rapidly with increasing contact pressure. Besides, the surface of impact crater with a smooth depth profile is formed the higher contact pressure with the same maximum normal impact load. This is due to the fact that when two surfaces are in normal impact, peaks of some of asperities are worn and some asperities are flattened down. Furthermore, more transfer layer is observed on the pin radius of 1.0 mm than that on the pin radius of 1.5 mm, though at the same maximum normal impact load, as shown in Fig. 4.13. These preliminary observations indicate that more DLC coating is lost under high contact pressure and some of it adheres to a counterpart material as a transfer layer. In future, in order to represent this transition map in a more usable form, the maximum normal impact may be will be replaced by the nominal mean Hertzian

contact pressure since the present study is only considering a normal stress and no tangential stress is involves. More experimental data is needed for this future work to be realized.

A possible high or low impact velocity, which directly affects the strain rate deformation, may also influence on the wear of DLC coating. In addition, high strain rate deformation also results in a significant rise in temperature due to the adiabatic conditions [88]. This can strongly induces the phase transformation of DLC to a graphite-like phase by a sp^3 to sp^2 phase transition at a temperature greater than a graphitization temperature of DLC approximately 300^{o}C [72]. As a result, DLC coating will easy to wear and produces wear debris, while some of it adheres to a counterpart material as a transfer layer. From the micrograph observations as shown in Fig. 4.14 (a), more transfer layer is observed at the higher impact velocity, though at the same maximum normal impact load. Adherent DLC coating on the SCM420 pin was confirmed from the EDS map, as shown in Fig. 4.14 (b). This transfer layer comes from the phase transformation of DLC (indicates by the shifting of the G peak position toward higher frequency, as shown in Fig. 4.15), where the graphite-like structure takes place, as previously described in Section 3.3.2. However, the rise of temperature is believes not as high as a graphitization temperature of DLC since the impact test was performed at room temperature and under the same maximum normal impact load. This suggests that the transition of DLC into a graphite-like phase will be accelerated by the higher energy dissipation from impacts between asperities at the tip-coating interface at high velocities based on these preliminary results.

Other promising parameter such as temperature effects will also demand attention. So, a lot of possible other parameters may influence deformation-wear transition of the DLC coating and there are many areas need to be explored. How this can be incorporated into the existing testing scheme is a topic that requires extensive research. In order to accelerate the progress, if such a testing scheme and methodology are adopted by many researchers, then future progress can be accelerated.

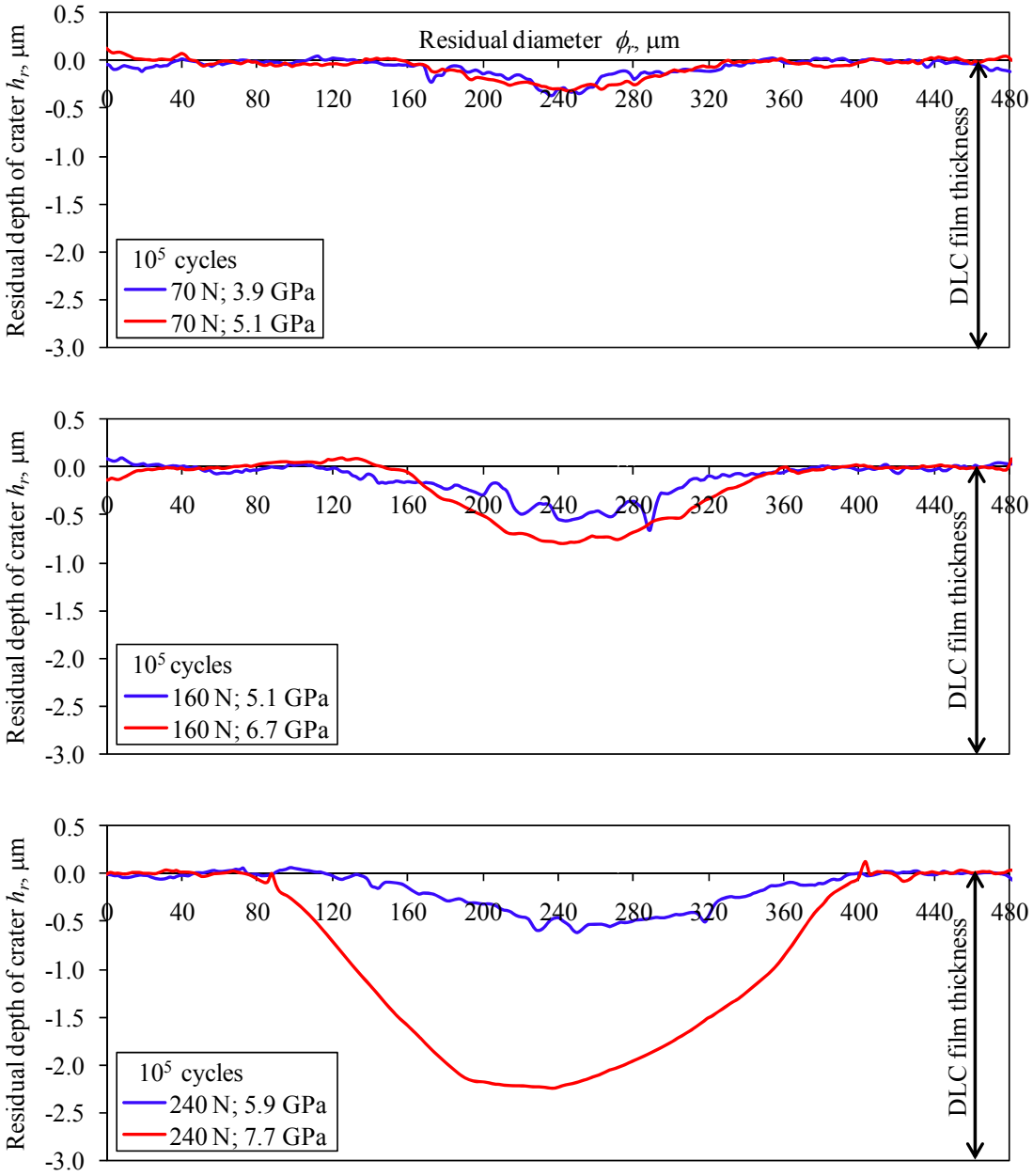

Fig. 4.12 Residual depth of crater for DLC coating on SKH2 substrate impacted by two different SCM420 pin radii. Blue line for pin radius of 1.5 mm and red line for pin radius of 1 mm.

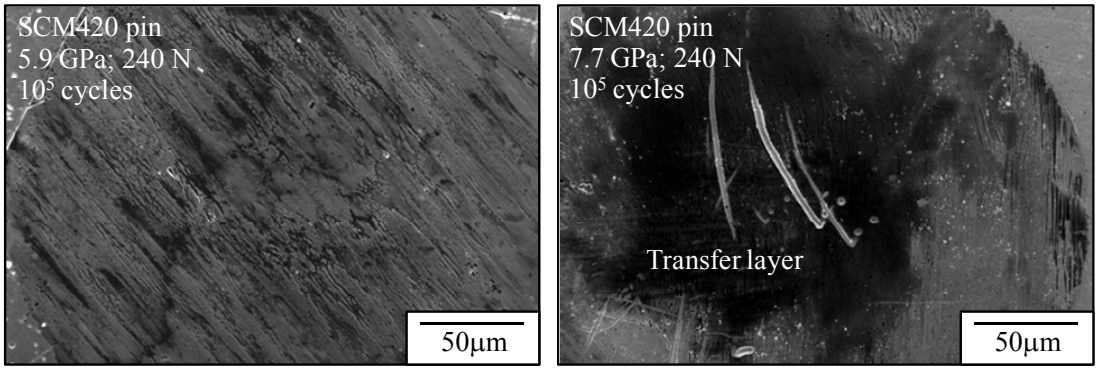

Fig. 4.13 Transfer layer on the SCM420 pin impacted at the same maximum normal impact load with different mean contact pressure.

(a)

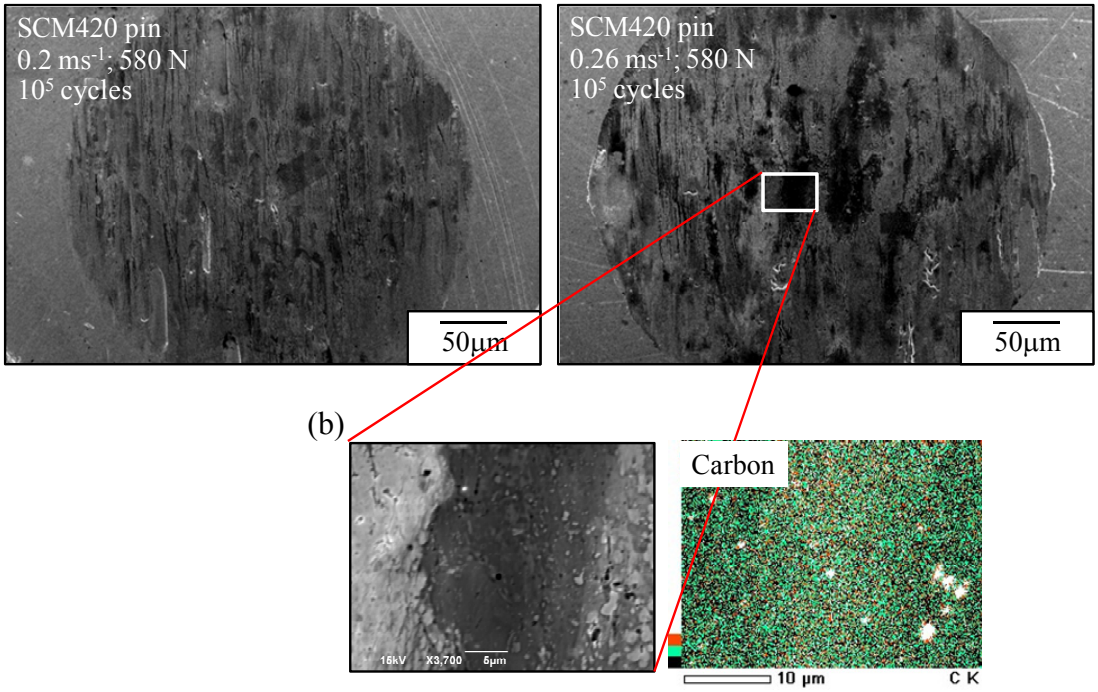

Fig. 4.14 (a) Transfer layer on the SCM420 pin impacted at the same maximum normal impact load with different impact velocity and (b) EDS map of the transfer layer on the SCM420 pin.

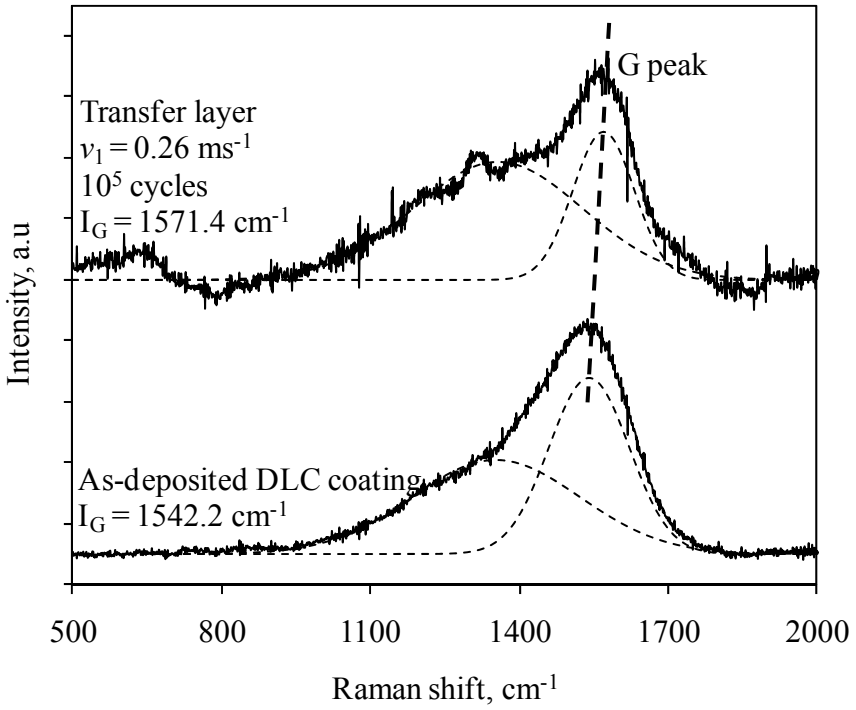

Fig. 4.15 Raman spectrum of the transfer layer at the higher impact velocity compared to as-deposited DLC coating.

4.3 Conclusions

A deformation-wear transition map has been proposed using an empirical approach. This empirical-based transition map is intended to graphically distinguish between the plastic deformation and impact wear of DLC coating as well as to predict its transition points over a range of operating parameters. This transition map reveals the simultaneous dependence on maximum normal impact load and impact cycles.

Three main transition zones were identified as follows:

(a) The plastic deformation of the substrate zone: the residual impact crater volume increases with the maximum normal impact load and impact cycles. Only the substrate is plastically deformed. In addition, wear has not been observed in this zone.

(b) Suppression of plastic deformation of the substrate zone: the residual impact crater volume remains constant with the impact cycles and plastic deformation of the substrate no longer appears. This is due to the decreasing contact pressure with impact cycles to the yield point. By increasing the maximum normal impact load, the suppression of plastic deformation of the substrate taking place, is faster. In this zone, the hardness of the DLC coating on the crater surface is harder than as-deposited and wear has not been observed.

(c) Wear of the DLC coating zone: the residual impact crater volume increases rapidly/radically with the maximum normal impact load and impact cycles, due to material loss. The DLC coating appears to approach a high degree of wear when the critical limit of maximum normal impact load and impact cycles is exceeded and can be verified by a wear depth data collection. This wear is associated with some degradation of the DLC coating, such as phase transformation of the wear debris/transfer layer and the propagation of radial cracks in the DLC film. In addition, formation of a transfer layer on the counterpart material that has been observed experimentally in this zone may attribute to the adhesive wear.

References

[76] D. Tabor, Status and direction of tribology as a science in the 80s: understanding and prediction, Proc. Int. Conf. Tribol. 80s, 1 (1984) 1-17.

[77] H.J. Frost, M.F. Ashby, Deformation Mechanism Maps: The plasticity and creep of metals and ceramics, first ed., Pergamon Press, Oxford, New York, (1982).

[78] S.C. Lim, M.F. Ashby, Wear-mechanism maps, Acta Metall. 35 (1987) 1-24.

[79] M.F. Ashby, S.C. Lim, Wear-mechanism maps, Scr. Metall. 24 (1990) 805-810.

[80] S.M. Hsu, M.C. Shen, Ceramic wear maps, Wear, 200 (1996) 154-175.

[81] A.R. Riahi, A.T. Alpas, Wear map for grey cast iron, Wear, 255 (2003) 401-409.

[82] H. Chen, A.T. Alpas, Sliding wear map for the magnesium alloy Mg-9Al-0.9 Zn (AZ91), Wear, 246 (2000) 106-116.

[83] K. Elleuch, R. Elleuch, R. Mnif, V. Fridrici, P. Kapsa, Sliding wear transition for the CW614 brass alloy, Tribol. Int. 39 (2006) 290-296.

[84] J.R. Gomes, A.S. Miranda, J.M. Vieira, R.F. Silva, Sliding speed-temperature wear transition maps for Si_3N_4/iron alloy couples, Wear, 250 (2001) 293-298.

[85] Z.H. Xie, R. Singh, A. Bendavid, P.J. Martin, P.R. Munroe, M. Hoffman, Contact damage evolution in a diamond-like carbon (DLC) coating on a stainless steel substrate, Thin Solid Films, 515 (2007) 3196-3201.

[86] A. Abdul-Baqi, E. Van der Giessen, Numerical analysis of indentation-induced cracking of brittle coatings on ductile substrates, Int. J. Solid Struct. 39 (2002) 1427–1442.

[87] R.K. Singh, M.T. Tilbrook, Z.H. Xie, Contact damage evolution in diamond-like carbon coatings on ductile substrates, J. Mater. Res. 23 (2008) 27-36.

[88] R.J. Anton, G. Subhash, Dynamic Vickers indentation of brittle materials, Wear, 239 (2000) 27-35.

Chapter 5

Conclusions

For the past decade, impact wear mechanisms of the DLC coating are concerned with the fracture process in the coating due to the crack propagation under severe wear conditions. Besides, nobody will use the DLC under this condition that may lead to a catastrophic failure and should be avoided in most industrial cases. However, no reports discuss about how the impact wear mechanisms of the DLC coating acts under mild wear conditions. Under impact, it is well known that plastic deformation should occur prior to the impact wear. So, the first objective of this study is to identify the most significant impact parameter that controls the deformation of DLC coating. After cyclic impacts, though under mild wear conditions, it believes that impact wear should be occurring by the phase transformation of DLC coating. Therefore, the second objective is to clarify the impact wear mechanisms of DLC coating based on its phase transformation. Finally, in order to distinguish more clearly between the plastic deformation and impact wear of DLC coating as well as to predict its transition point, a deformation-wear transition map has been proposed.

The major findings of this work and their context in current research can be concluded as follows:

(a) In order to identify the most important impact parameter from the viewpoint of mechanical aspects that affects the deformation of DLC coating during impact, an experimental approach is employed. The coefficient of determination R^2 from regression analysis is an indicator of how good is the relationship. There is no unique relationship between the residual impact crater volume/depth of DLC coating and contact impulse. This means that the contact impulse did not have a significant effect on the residual impact crater volume/depth of DLC coating. However, the residual impact crater volume/depth of DLC coating is dependent on maximum normal impact load and absorbed energy, regardless of impactor mass. Even though a good agreement is obtained from the

responses of maximum normal impact load and absorbed energy, both R^2 (for the V_r and h_r) from the response of maximum normal impact load (R^2_{hr} = 0.9362 and R^2_{Vr} = 0.9076) is higher than that from the response of absorbed energy (R^2_{hr} = 0.7945 and R^2_{Vr} = 0.8779). Besides, there is an experimental error in the case of absorbed energy due to the microslip effect. Furthermore, the impact phenomenon in this study can be considered as the quasi-static indentation, where load is a governing parameter, because the impact velocity is very low. By comparing with the analytical solutions, it is easier to predict the residual impact crater volume/depth by static indentation analysis. Therefore, from the above reasons, it can be concluded that the residual impact crater volume/depth is more affected by maximum normal impact load than absorbed energy.

(b) The phase transformation of DLC coating during cyclic impact loading is investigated by Raman spectroscopy analysis. It has been suggested that pressure-induced graphitization since the impact testing was performed at room temperature. Larger volumes of sp^2, which was produced as wear debris, were combined to oil and pushed to the side of the impact crater. Some of the sp^2 phase was adhered to the pin surface as a transfer layer. However, the mechanical impact may destroy and reduce the size of larger sp^2 clusters; therefore, no longer show any breathing modes. As a result, the DLC coating on the crater surface tends to have higher sp^3 fractions as it is evidently shown by decreasing I_D/I_G ratio approximately from 0.63 (as-deposited) to 0.47 (after 10^5 impact cycles), accompanied by a widening of $FWHM_G$ (approximately from 179 cm^{-1} to 192 cm^{-1}) with impact cycles. Besides, the hardness reaches approximately to 21 GPa, higher than as-deposited (17.14 GPa) after several impact cycles. Since the impact test was performed under atmospheric conditions, oxidation of Fe with the environment is also occurred in the wear debris and transfer layer, where two predominant peaks of Fe_3O_4 and α-Fe_2O_3 were observed from its Raman spectrum.

(c) For a given material and controlled variables (pin radius, coating thickness, substrate material, environmental conditions and etc.), the proposed deformation-wear transition map of DLC coating apparently shows that the maximum normal impact load and impact cycles influence this transition. This empirical-based transition map, which presents deformation and wear data in a graphical manner, is able to provide a more global picture of how DLC coating behaves under cyclic impacts systematically. Three main transition zones that graphically distinguish between the plastic deformation and impact wear of DLC coating were identified. Beyond the elastic limit, the DLC coating only follows the plastic deformation of the substrate until several impact cycles. Then, a suppression of plastic deformation of the substrate is taking place due to the decreasing contact pressure with impact cycles to the yield point. The hardness of the DLC coating on the crater surface is also increases after numerous impacts and no wear has been observed within these two zones. Wear of the DLC coating becomes dominant when the critical limit of maximum normal impact load and impact cycles is exceeded. Experimental observations show that this wear is associated with some degradation of the DLC coating. This includes the phase transformation of the wear debris/transfer layer and propagation of radial cracks in the DLC film as well as the formation of transfer layer on the counterpart material, which may attribute to the adhesive wear.

List of publications

International journals

[1] **M.F.B. Abdollah**, Y. Yamaguchi, T. Akao, N. Inayoshi, N. Umehara, T. Tokoroyama, Phase transformation studies on the a-C coating under repetitive impacts, Surface and Coatings Technology, 205 (2010), 625-631.

[2] **M.F.B. Abdollah**, Y. Yamaguchi, T. Akao, N. Inayoshi, T. Tokoroyama, N. Umehara, The effect of maximum normal impact load, absorbed energy and contact impulse on the impact crater volume/depth of DLC coating under impact, Tribology online (2011) - Article in press.

[3] **M.F.B. Abdollah**, Y. Yamaguchi, T. Akao, N. Inayoshi, N. Miyamoto, T. Tokoroyama, N. Umehara, Deformation-wear transition map of DLC coating under cyclic impact loading, Wear (2011) – Under review

International conferences/symposiums/workshops

[1] **M.F.B. Abdollah**, N. Umehara, Preliminary study of impact wears behavior under large impact cycles, Proceedings of the 4th Nagoya University-UCLA International Symposium, Kona, Hawaii, USA, September 6-7, 2009.

[2] **M.F.B. Abdollah**, Y. Yamaguchi, T. Akao, N. Inayoshi, T. Tokoroyama, N. Umehara, The effect of maximum normal impact load, absorbed energy and contact impulse on the impact craters volume/depth of DLC coating under repetitive impacts, Proceedings of JAST Tribology Conference 2010, Fukui, JAPAN, September 14-17, 2010.

[3] **M.F.B. Abdollah**, Y. Yamaguchi, T. Akao, N. Inayoshi, N. Umehara, T. Tokoroyama, Raman spectroscopy study of impacted DLC coatings, Extended abstract of The Tribology Congress in Australia ASIATRIB 2010 "Frontiers in tribology - knowledge & friendship", Perth, WESTERN AUSTRALIA, December 5-9, 2010.

[4] UCLA-Nagoya University GCOE Workshop, Los Angeles, USA, February 28-March 6, 2011. (Participant)

[5] Y. Yamaguchi, **M.F.B. Abdollah**, T. Tokoroyama, N. Umehara, N. Inayoshi, T.Akao, N. Miyamoto, Impact wear mechanisms of DLC, Proceedings of The 4th International Conference on Manufacturing, Machine Design and Tribology 2011, Gamagori, Aichi, JAPAN, April 24-27, 2011.

[6] Y. Yamaguchi, **M.F.B. Abdollah**, T. Tokoroyama, N. Umehara, N. Inayoshi, T.Akao, N. Miyamoto, Observation of cross-sectional images impacted DLC films, Proceedings of JAST Conference 2011, Tokyo, JAPAN, September 11-14, 2011. (In Japanese)

[7] **M.F.B. Abdollah**, Y. Yamaguchi, T. Akao, N. Inayoshi, N. Miyamoto, T. Tokoroyama, N. Umehara, Deformation and wear map of DLC coating under cyclic impacts, Extended abstract of International Tribology Conference 2011, Hiroshima, JAPAN, October 30-November 3, 2011.

Award

[1] **Scholarship award under academic training scheme**, Universiti Teknikal Malaysia Melaka, December 2008-present.